



RADAR SYSTEM CHARACTERIZATION EXTENDED TO HARDWARE-IN-THE-LOOP
SIMULATION FOR THE LAB-VOLTTM TRAINING SYSTEM

THESIS

Oscar C. Mayhew, Second Lieutenant, USAF

AFIT/GE/ENG/07-29

DEPARTMENT OF THE AIR FORCE
AIR UNIVERSITY

AIR FORCE INSTITUTE OF TECHNOLOGY

Wright-Patterson Air Force Base, Ohio

APPROVED FOR PUBLIC RELEASE; DISTRIBUTION UNLIMITED.

The views expressed in this thesis are those of the author and do not reflect the official policy or position of the United States Air Force, Department of Defense, or the U.S. Government

RADAR SYSTEM CHARACTERIZATION EXTENDED TO
HARDWARE-IN-THE-LOOP SIMULATION FOR THE LAB-VOLTTM
TRAINING SYSTEM

THESIS

Presented to the Faculty
Department of Electrical and Computer Engineering
Graduate School of Engineering and Management
Air Force Institute of Technology
Air University
Air Education and Training Command
In Partial Fulfillment of the Requirements for the
Degree of Master of Science in Electrical Engineering

Oscar C. Mayhew, B.S.E.E.
Second Lieutenant, USAF

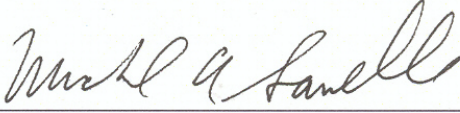
September 2007

APPROVED FOR PUBLIC RELEASE; DISTRIBUTION UNLIMITED.

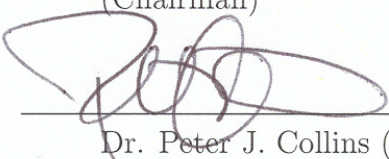
RADAR SYSTEM CHARACTERIZATION EXTENDED TO
HARDWARE-IN-THE-LOOP SIMULATION FOR THE LAB-VOLT™
TRAINING SYSTEM

Oscar C. Mayhew, B.S.E.E.
Second Lieutenant, USAF


Approved:



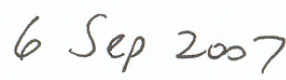
Major Michael A. Saville, PhD
(Chairman)



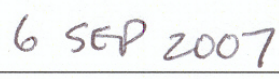
Dr. Peter J. Collins (Member)



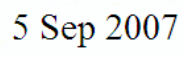
Dr. Randy Jost (Member)



date



date



date

Abstract

Modeling RADAR signals in software allows the testing of potential electronic counter measures and electronic counter counter measures without the associated RADAR hardware and test facilities. Performing a characterization process on a real world RADAR system reveals all imperfections within the system. The Lab-VoltTM RADAR system served as the characterized real world RADAR system. The characterization process consisted of measurements at selected front panel locations on the Lab-VoltTM transmitter module, antenna pedestal, receiver module, and dual channel sampler module. Due to the overwhelming influence of antenna parameters on a received signal, the characterization process also attempted to derive an antenna transfer function that described how the antenna filters a signal that is passed through it. The characterization process also determined the manner in which different adjustments influenced the signal. A MatLab simulation modeled the Lab-VoltTM system operating under ideal conditions. Comparing measurements from the characterization process and the MatLab simulation placed numerical values on the imperfections in the Lab-VoltTM system. Finally, integration of the Lab-VoltTM system explored an elementary hardware-in-the-loop configuration.

Acknowledgements

First and foremost, I wish to thank my thesis advisor Major Michael Saville (AFIT/ENG) for cracking the whip early in the winter quarter. His continual persistence for small consistent deliverables even when I felt overwhelmed by classes helped lay the foundation for my tight schedule. This work could not be completed without its sponsors Dr. Sang Hong (AFRL/SNRA) and those at AFOSR. To the professors that pushed me throughout my undergraduate education, Dr. Randy Musselman and Lieutenant Colonel George York, thank you for peaking my interest in electromagnetics, RADAR, and signal processing. Mr. Greg Taylor's (AFIT/SOCHE) devotion to learning the new wideband lab equipment was invaluable to paving the way for my research. Greg's assistance allowed me to focus on my research instead of being bogged down with the details of learning new equipment. Charlie McNeely's (AFIT/ENG) understanding of the AFIT anechoic chamber and the associated support software was vital. Captain James Townsend's (AFIT/ENG) teamwork was invaluable to delving into the specifics of the Lab-VoltTM system: two heads/bars are better than one. Special thanks to Miss Elise Thomasson of the University of Hawaii for volunteering her grammatical expertise to edit this gargantuan document. Finally, I would like to thank the employees of Kava House, Starbucks, and Waffle House. Their never ending supply of caffeinated products made the creation of this work possible.

Oscar C. Mayhew

Table of Contents

	Page
Abstract	iv
Acknowledgements	v
List of Figures	viii
List of Tables	xii
List of Abbreviations	xiv
 I. Introduction	 1
1.1 Motivation	1
1.2 Research Goal	2
1.3 Organization	2
 II. Background and Literature Review	 3
2.1 RADAR Theory	3
2.1.1 RADAR and Modulation Basics	3
2.1.2 Signal Flow Throughout Radar System	7
2.2 TASRAN	9
2.3 Real Time RADAR Signal Simulator	10
2.4 RAGCLEM	11
2.5 RASER	12
2.6 Automotive Applications of Obstacle Avoidance RADARs.	13
2.7 Guiding the RADAR Characterization Process	14
2.8 Simulator for Advanced Fighter RADAR EPM Develop-	15
ment	15
2.9 ECM-GA Technique Generation	16
2.10 Advanced RADAR Simulator	17
 III. Lab-Volt System Characterization	 19
3.1 RADAR System Background and Comparison	19
3.1.1 General Radar System	19
3.1.2 Lab-Volt System	21
3.1.3 Comparison with a Real World RADAR System.	29
3.2 Methodology	31
3.2.1 Assumptions and Characterization Instrumenta-	32
tion	32
3.2.2 Transmitter Module Characterizations	33

	Page
3.2.3 Antenna Characterization	36
3.2.4 Receiver Module Characterization	41
3.2.5 DCS Module Characterization	42
3.3 Results	43
3.3.1 Transmitter Module Characterization	43
3.3.2 Antenna Characterization	49
3.3.3 Receiver Module	52
3.3.4 DCS Characterization	52
IV. Extension of Lab-Volt TM System Characterization to Simulation .	57
4.1 Chapter Overview	57
4.2 Assumptions	57
4.2.1 Modeling Assumptions	57
4.2.2 Operational Assumptions	58
4.3 Simulation Overview	58
4.3.1 Simulation Initialization	60
4.3.2 Lab-Volt Simulation	63
4.4 Results	67
4.4.1 Comparison of Lab-Volt Simulation and Characterization Measurements	67
4.4.2 Integration of Antenna Characterization into Lab-Volt Simulation	72
V. Extension of Lab-Volt Characterization to Hardware in the Loop Simulation	79
5.1 Methodology	79
5.1.1 Equipment	79
5.1.2 Unsuccessful Attempts At HILS Configuration	79
5.2 Successful HILS Configuration	88
VI. Conclusion and Future Extent to this Work	91
6.1 Lab-Volt Characterization	91
6.1.1 Transmitter Module	92
6.1.2 Antenna Transfer Function	92
6.2 Lab-Volt Simulation	93
6.3 HILS Configuration	93
Appendix A. Matlab Code	95
Appendix B. Lab-Volt Characterization	147
Bibliography	178

List of Figures

Figure		Page
2.1.	PAM Signal.	3
2.2.	PAM Signal in Frequency Domain.	5
2.3.	CW Signal with the Application of LFM.	6
2.4.	Basic Radar Block Diagram.	7
2.5.	RAGCLEM RF RADAR hardware and software simulation interface.	11
3.1.	General RADAR transmitter block diagram.	20
3.2.	General RADAR receiver block diagram.	21
3.3.	Lab-Volt transmitter module.	23
3.4.	Lab-Volt antenna pedestal module.	25
3.5.	Lab-Volt receiver module.	27
3.6.	Dual channel sampler front panel.	29
3.7.	DELFT atmospheric research RADAR.	30
3.8.	Phase measurement setup.	39
3.9.	Travel distances within and around anechoic chamber.	40
3.10.	Rise and fall time of 1-ns pulse.	44
3.11.	Pulse width adjustment characterization curve.	45
3.12.	Carrier frequency adjustment characterization curve.	46
3.13.	Modulating frequency adjustment characterization curve.	47
3.14.	Frequency deviation adjustment characterization curve.	48
3.15.	Uncalibrated signal prior to transmit antenna.	49
3.16.	Calibrated signal prior to transmit antenna.	50
3.17.	Signal post transmit antenna with gain and phase correction.	51
3.18.	Lab-Volt dual channel sampler I-Channel RF output at 9.4-GHz carrier frequency.	52
3.19.	DCS gain adjustment characterization.	53

Figure		Page
3.20.	DCS offset adjustment characterization.	54
4.1.	Lab-Volt simulation architecture.	59
4.2.	Lab-Volt simulation file overview.	59
4.3.	Lab-Volt simulation initialization overview.	60
4.4.	Universal_Initialize.m block diagram.	62
4.5.	Controller.m block diagram.	63
4.6.	Transmitter.m block diagram.	64
4.7.	\Space Environment block diagram.	66
4.8.	Receiver.m block diagram.	67
4.9.	Comparison of simulation and measured data at CW output on Lab-Volt transmitter.	68
4.10.	Comparison of simulation and measured signal at LO output of transmitter.	69
4.11.	Comparison of simulated and measured signal at RF PAM output of transmitter.	70
4.12.	Comparison of simulated and measured signal RF output of an- tenna pedestal.	70
4.13.	Comparison of simulated and measured signal at PAM output of receiver.	71
4.14.	Signal prior to transmit antenna.	73
4.15.	Signal after transmit antenna.	74
4.16.	After reflection time domain.	75
4.17.	Time domain signal after receiver antenna.	76
4.18.	Signal after demodulation.	77
4.19.	Signal in time domain after wideband amplifier.	78
5.1.	Horn antenna setup.	80
5.2.	Various carrier signals out of the AWG.	81
5.3.	Unfiltered 4.30625-GHz CW LO signal.	83
5.4.	BPF response.	83

Figure		Page
5.5.	Filtered 4.30625-GHz CW LO signal.	84
5.6.	Unfiltered 4.30625-GHz PAM transmitted signal.	85
5.7.	LPF response.	86
5.8.	Filtered 4.30625-GHz PAM transmitted signal.	87
5.9.	Lab-Volt integration into a HILS configuration	88
5.10.	PAM signal following amplifier and LPF.	89
5.11.	PAM signal following receive horn antenna.	89
5.12.	Received signal at PAM output of receiver module.	90
B.1.	Lab-Volt Transmitter CW Output.	148
B.2.	Lab-Volt Transmitter LO Output.	149
B.3.	Lab-Volt Transmitter Pulse Generator Output	150
B.4.	Lab-Volt Transmitter Pulsed RF Output at 8-GHz Carrier Fre- quency.	151
B.5.	Lab-Volt Transmitter Pulsed RF Output at 9.4-GHz Carrier Fre- quency.	152
B.6.	Lab-Volt Transmitter Pulsed RF Output at 10-GHz Carrier Fre- quency.	153
B.7.	Antenna Pedestal RF Output at 8-GHz Carrier Frequency. . .	154
B.8.	Antenna Pedestal RF Output at 9.4-GHz Carrier Frequency. .	155
B.9.	Antenna Pedestal RF Output at 10-GHz Carrier Frequency. . .	156
B.10.	Lab-Volt Receiver I-Channel Pulsed RF Output at 8-GHz Carrier Frequency.	157
B.11.	Lab-Volt Receiver I-Channel RF Output at 9.4-GHz Carrier Fre- quency.	158
B.12.	Lab-Volt Receiver I-Channel RF Output at 10-GHz Carrier Fre- quency.	159
B.13.	Lab-Volt Receiver Q-Channel RF Output at 8-GHz Carrier Fre- quency.	160
B.14.	Lab-Volt Receiver Q-Channel RF Output at 9.4-GHz Carrier Fre- quency.	161

Figure		Page
B.15.	Lab-Volt Receiver Q-Channel RF Output at 10-GHz Carrier Frequency.	162
B.16.	Lab-Volt Dual Channel Sampler I-Channel RF Output at 8-GHz Carrier Frequency.	163
B.17.	Lab-Volt Dual Channel Sampler I-Channel RF Output at a 10-GHz Carrier Frequency.	164
B.18.	Dual Channel Sampler Q-Channel 8-GHz Carrier Frequency.	165
B.19.	Dual Channel Sampler Q-Channel 9.4-GHz Carrier Frequency.	166
B.20.	Dual Channel Sampler Q-Channel at 10-GHz Carrier Frequency.	167
B.21.	Pulse Generator Output at $\tau = 1$ -ns.	168
B.22.	Pulse Generator Output at $\tau = 2$ -ns.	169
B.23.	Pulse Generator Output at $\tau = 5$ -ns.	170
B.24.	Pulse Integration at Pulse Generator Output, $\tau = 1$ -ns.	171
B.25.	Carrier Frequency Adjustment Characterization.	172
B.26.	Pulse Width Adjustment Characterization.	173
B.27.	Modulating Frequency Characterization.	174
B.28.	Frequency Deviation Characterization.	175
B.29.	Dual Channel Sampler Gain Adjustment Characterization.	176
B.30.	Offset Adjustment Characterization.	177

List of Tables

Table		Page
2.1.	Significance of RADAR Parameters on a Received Signal. . . .	15
3.1.	Test Matrix for Signals Captured at RF Pulsed Output of Lab-Volt Transmitter.	34
3.2.	Test Matrix for Pulse Width Adjustment Characterization. . .	35
3.3.	Test Matrix for Carrier Frequency Adjustment Characterization.	35
3.4.	Test Matrix for Modulating Frequency Adjustment Characterization.	35
3.5.	Test Matrix for Frequency Deviation Adjustment Characterization.	36
3.6.	Test Matrix for the Lab-Volt Antenna Output Characterization.	37
3.7.	Path from Transmit Antenna to Antenna Under Test.	40
3.8.	Test Matrix for the Lab-Volt Receiver Characterization.	41
3.9.	Test Matrix for the Lab-Volt DCS.	42
3.10.	Test Matrix for DCS Gain and Offset Adjustment Characterization.	42
3.11.	Confidence Interval for Pulse Width Adjustment Characterization.	45
3.12.	Confidence Interval for Carrier Frequency Adjustment Characterization.	46
3.13.	Confidence Interval for Modulating Frequency Adjustment Characterization.	47
3.14.	Confidence Interval for Frequency Deviation Adjustment Characterization.	48
3.15.	Confidence Interval for I-Channel Gain Adjustment Characterization.	55
3.16.	Confidence Interval for Q-Channel Gain Adjustment Characterization.	55

Table		Page
3.17.	Confidence Interval for I-Channel Offset Adjustment Characterization.	56
3.18.	Confidence Interval for Q-Channel Offset Adjustment Characterization.	56

List of Abbreviations

Abbreviation		Page
ECM	Electronic Counter Measures	1
ECCM	Electronic Counter Counter Measures	1
EW	Electronic Warfare	1
HILS	Hardware-in-the-Loop Simulation	2
RF	Radio Frequencies	3
CW	Continuous Wave	3
PAM	Pulse Amplitude Modulated	3
PRI	Pulse Repetition Interval	3
PRF	Pulse Repetition Frequency	3
FM	Frequency Modulation	5
LFM	Linear Frequency Modulation	5
RGPO	Range Gate Pull Off	16
AWG	Arbitrary Waveform Generator	17
VCO	Voltage Controlled Oscillator	19
IF	Intermediate Frequency	19
LNA	Low Noise Amplifier	21
COHO	Coherent Oscillator	21
LPF	Low Pass Filter	28
HPF	High Pass Filter	28
DCS	Dual Channel Sampler	29
STALO	Stable Local Oscillator	31
CI	Confidence Interval	46

RADAR SYSTEM CHARACTERIZATION EXTENDED TO HARDWARE-IN-THE-LOOP SIMULATION FOR THE LAB-VOLTTM TRAINING SYSTEM

I. Introduction

RADAR was developed in World War II to warn against enemy aircraft prior to an attack. RADAR stands for radiation detection and ranging and consists of the transmission and collection of reflected electromagnetic waves. Since its invention, RADAR remains a crucial tool in detecting aircraft in both civilian and military aviation. Civilian aviation uses RADAR for weather detection, collision avoidance, and instrument landing aids. With the introduction of electronic counter measures (ECM) and electronic counter counter measure (ECCM), RADAR in military aviation becomes considerably more involved. Power and antenna constraints limit ECM and ECCM abilities. Electronic warfare (EW) is the on going battle between adversaries to overcome one another's electronic defenses. An opponent's ECM or ECCM can be defeated by changing one's modulation technique, operating frequency, power levels, polarization, line of sight, or orientation. EW often boils down to adversaries' attempts to quickly adapt to one another's modulation techniques. The quicker a system can adapt to an opponent's ECM or ECCM the quicker the opponent can be defeated.

1.1 Motivation

Within the research community there exists a desire to produce accurate RADAR signals in software. Producing such signals in software allows realistic testing of potential ECM techniques. In this application, RADAR signal creation goes beyond simple software simulations. A real world RADAR system must be characterized such that signal errors and imperfections within the system are reproducible. The

Lab-Volt^{TM1} system is a low power active RADAR system that serves as a teaching aid for basic RADAR principles. Ultimately it is desired to have a large simulation fidelity to the point that the simulation could be interfaced with RADAR hardware without any system change. This configuration is often referred to as hardware in the loop simulation (HILS) [9]. HILS offers lower development cost and provides extensive in-depth engineering in development and product improvement.

1.2 Research Goal

Ultimately this research strives to lay a solid foundation for future work by creating a thorough literature review, characterizing the recently acquired Lab-Volt system, and breaking ground on HILS with the Lab-Volt simulation. Due to the influence of the antenna on the received signal, experimental antenna characterization is also presented.

1.3 Organization

This thesis presents the characterization process and its integration into the hardware-in-the-loop simulation. Chapter II presents recent relative research in RADAR simulations and characterization. Chapter II presents the process used to characterize the antenna and the results obtained. Chapter IV presents the Lab-Volt characterization process and its application to the Lab-Volt simulation. Chapter V presents research in integrating the Lab-Volt system into the simulation to form a HILS configuration. Chapter VI concludes this work and presents possible directions in which to take future research. Appendix A contains the code for the Lab-Volt simulation and software block diagrams that show how the different software blocks interact. Appendix B contains all measurements taken during the characterization process.

¹Lab-Volt is a registered trademark of ComLab, Inc. The trademark superscript is suppressed for convenience.

II. Background and Literature Review

2.1 RADAR Theory

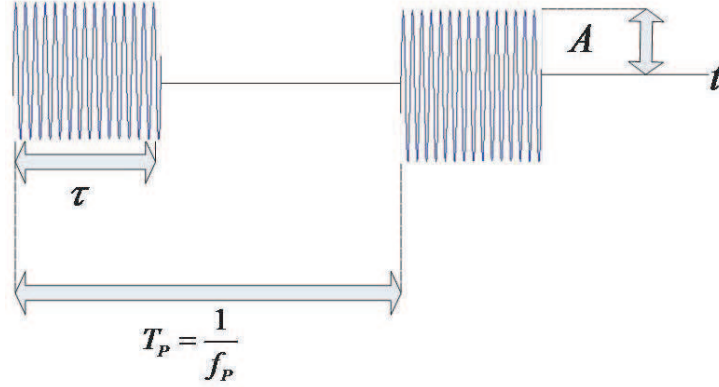


Figure 2.1: PAM Signal.

2.1.1 RADAR and Modulation Basics. A RADAR transmits a basic sinusoidal signal at radio frequencies (RF) ranging from 3-MHz for HF bands to 300-GHz for millimeter waves [20]. If a RADAR continually transmits an RF signal, it is known as a continuous wave (CW) RADAR. Turning the carrier signal off and on forms a pulsed amplitude modulated (PAM) signal. Figure 2.1 shows a PAM signal where τ is the width of the transmitted pulse in time, or pulse width, T_p is the time between pulses, or the pulse repetition interval (PRI), and f_p is the rate at which pulses are transmitted, or the pulse repetition frequency (PRF). Mathematically a PAM signal is

$$p(t) = \begin{cases} \cos(2\pi f_c t), & nT_p \leq t \leq nT_p + \tau, n = 0, 1, 2, \dots, \\ 0, & \text{otherwise.} \end{cases} \quad (2.1)$$

RADAR signals are electromagnetic waves and travel at the speed of light. Assuming the transmit and receive antennas are collocated, the distance a received RADAR pulse travels, and hence, the range to the reflecting target, is calculated from the time difference between when the signal is transmitted and received, T_R , through

$$R_{un} = \frac{cT_R}{2}. \quad (2.2)$$

Similarly the maximum unambiguous range is dependent on the PRF and is

$$R = \frac{c}{2PRF}. \quad (2.3)$$

Range resolution is a RADAR system's ability to distinguish objects closely spaced in its line of sight and is defined as

$$R_{\text{Resolution}} = \frac{\tau c}{2}. \quad (2.4)$$

From Equation (2.4), range resolution is based on the physical span of the RF pulse spans. The factor of two accounts for the two-way path to the target just as in Equation (2.2). Objects spaced closer than half of a pulse width cannot be resolved. Range resolution is an important consideration when attempting to identify targets based on observed reflections.

Figure 2.2 shows a PAM signal with a pulse width of 1-ns and a carrier frequency of 9.4-GHz. Understanding of the transmitted pulse in the frequency domain provides an additional tool in which to analyze how the pulse may vary throughout the RADAR system. Figure 2.2 shows the PAM signal disseminates about the carrier frequency in the frequency domain. Nulls occur at integer frequency spacings away from the carrier frequency. The frequency spacing is equal to the inverse of the pulse width. Based on the radial velocity of a target relative to the RADAR, return pulses may also be shifted in frequency due to the doppler effect as described by Stimson [21]. If the received signal's frequency is different than the transmitted signal's frequency it is important to understand what parameters within the RADAR system would make these differences unmeasurable. Nyquist theory specifies that for a function sampled in time, the maximum frequency that can be recreated without aliasing is half the sampling frequency [21]. Mathematically the maximum frequency is

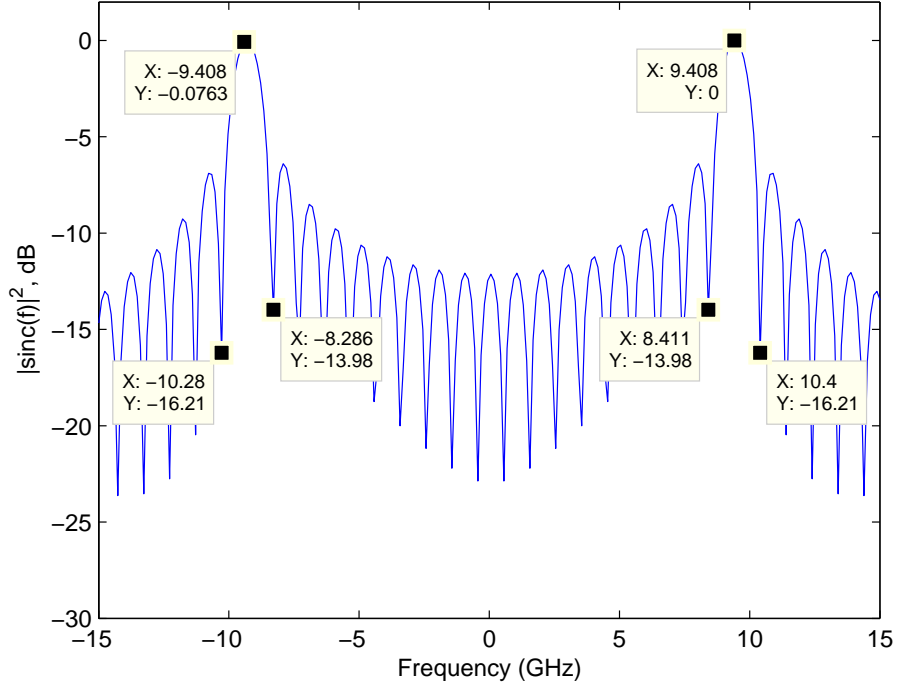


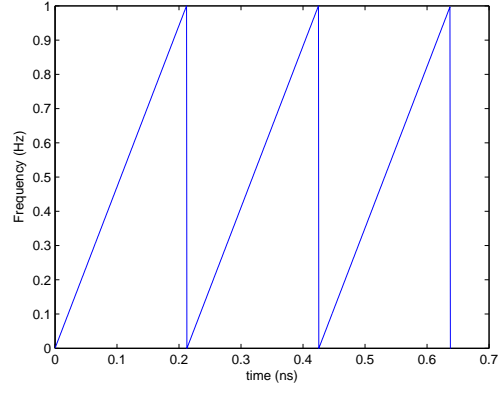
Figure 2.2: PAM Signal in Frequency Domain.

$$f_{\max} = \frac{f_s}{2} = \frac{1}{2T_{\text{step}}}, \quad (2.5)$$

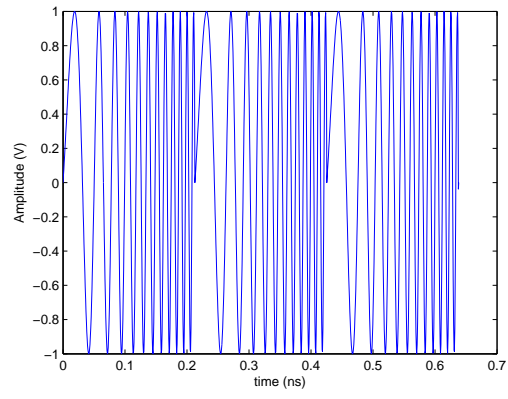
where f_s is the sampling frequency and T_{step} is the time step between samples. The frequency resolution is based on the record length, N , through

$$f_{\text{res}} = \frac{f_{\max}}{N - 1}. \quad (2.6)$$

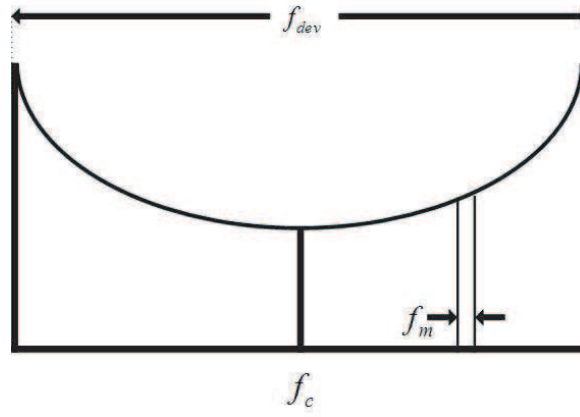
CW signals are useful for determining a target's doppler frequency, but because transmission never ceases range cannot be determined in the same manner as a PAM signal. To overcome this problem, the transmitted carrier frequency is modulated with another signal seen in Figure 2.3(a). This is known as a frequency modulation (FM). Figure 2.3(b) shows a linear frequency modulation (LFM) signal. Because the received signal's frequency corresponds to time at which the signal was transmitted,



(a) Modulating Signal.



(b) FM-CW Signal in Time Domain.



(c) Typical FM-CW Signal in Frequency Domain as Presented by Stremler [23].

Figure 2.3: CW Signal with the Application of LFM.

employing an FM scheme enables range detection. Figure 2.3(c) shows an FM signal in the frequency domain. The modulating frequency determines the spacing between individual spikes. The frequency deviation, or the maximum displacement from the carrier frequency, determines the bandwidth of the signal. For any FM scheme, the modulating signal, $f(t)$ and modulated signals, $s(t)$, become

$$s(t) = \sin \left(2\pi f_c t + \int_0^t f(\tau) d\tau \right), \quad (2.7)$$

where f_c is the carrier frequency.

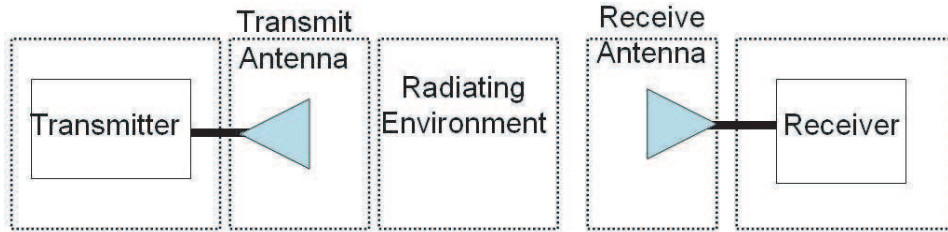


Figure 2.4: Basic Radar Block Diagram.

2.1.2 Signal Flow Throughout Radar System. A basic RADAR system consists of a transmitter, transmit antenna, radiating environment, receive antenna, and a receiver [21]. Figure 2.4 shows the basic block diagram of a generic radar system and the placement of each unit within the overall system.

As the signal leaves the transmitter and travels towards the target, the power density decays proportionally to the area of a sphere with radius equal to the range [20]. The power density reaching the target is

$$P_{D,Target} = \frac{P_T G}{4\pi R^2}, \quad (2.8)$$

where G is the antenna gain and P_T is the transmitted power, and R is the one way range to target.

The radar cross section (RCS) determines the power reflected by the target. Physically, RCS is the electrical size of the object from the perspective of the RADAR. According to [21] the monostatic RCS is

$$\begin{aligned}
\sigma &= A \times R \times D, \\
&= A \times \frac{P_{\text{Scatter}}}{AP_{\text{Incident}}} \times \frac{P_{\text{Backscatter}}}{\frac{1}{4\pi}P_{\text{Scatter}}}, \\
&= \frac{4\pi P_{\text{Backscatter}}}{P_{\text{Incident}}}, \tag{2.9}
\end{aligned}$$

where A is the cross sectional area, R is the reflectivity, D is the directivity. Reflectivity is the ratio of the power reflecting off the target to the power striking the target. Directivity is the ratio of the power scattered back in the direction of the radar receiver to the isotropically scattered power. The electromagnetic wave reflecting off a target can have a different phase than the electromagnetic signal striking the target. For this reason it is possible for RCS to be complex.

A large target can be made up of several smaller individual scattering objects. It is possible to combine these smaller individual targets with a single equivalent reflecting point. As expressed in [20], the process for combining the RCS of each reflecting point is

$$\sigma_{\text{Total}} = \sum_{n=1}^N \sigma_n e^{-j\alpha} \delta \left(t - \frac{2R_0}{c} \right), \tag{2.10}$$

where σ_n is the RCS for each scatterer, $e^{-j\alpha}$ relates how the radial spacing of the scatters effects the phase, and $\delta \left(t - \frac{2R_0}{c} \right)$ relates how the scatterer is a point excitation or impulse in time with reference of the target centroid, R_0 .

In the time domain, convoluting the transmitted signal at the target and the RCS gives the signal reflected off the target. Mathematically this is

$$TX_{\text{PostReflection}} = TX_{\text{PreReflection}} * \sigma_{\text{Total}}. \quad (2.11)$$

In Equation (2.9), if the incident power is viewed as the power density and the backscattered power is viewed as the power reflected back to the receiver, rearranging the equation allows the power reflected back to the receiver to become

$$P_{\text{D,Reflect}} = \sigma P_{\text{D,Target}}. \quad (2.12)$$

As with the transmitted signal in Equation (2.8), the reflected signal will experience spacial decay proportional to the square of the distance from the target to the receiver. The power density at the receiver is

$$P_{\text{D,Receive}} = \frac{P_{\text{D,Reflect}} A_e}{4\pi R^2} \quad (2.13)$$

Multiplying Equation (2.8), (2.12), (2.13), and using the relation $G_r = \frac{4\pi A_e}{\lambda^2}$ gives the power at the receiver for a given power transmitted. According to [20], this product is known as the RADAR range equation and is mathematically expressed as

$$P_r = \frac{P_t G_{\text{Transmit}} G_{\text{Receive}} \sigma \lambda^2}{(4\pi)^3 R^4}, \quad (2.14)$$

where P_t is the transmit power, G_{Transmit} is the gain of the transmit antenna, and G_{Receive} is the gain of the receive antenna.

2.2 *TASRAN*

A simulation for evaluating netted tactical air surveillance systems was presented in [27] and is known as the tactical air surveillance RADAR netting (TASRAN). Similar to HILS, TASRAN goes beyond simple simulation. TASRAN accepts RADAR measurements and tracks messages and processes them alongside simulated measurements and simulated tracks. TASRAN is a tool for the exploration of RADAR netting

functions, self-survey, and multi-sensor target identification. On a large scale, beyond the RADAR system level, TASRAN models user-defined, ground-based RADAR networks and tests these networks against simulated hostile and friendly aircraft on various flight paths.

TASRAN simulates two classes of RADAR: track while scan (TWS) and stationary phased-array RADAR. Parameters such as power, antenna beamwidth, gain, losses, noise figure, and scan rate can be modified. Position and orientation citing errors are also incorporated. The addition of pseudo-random noise better models a real world environment. The more accurately each RADAR system is recreated in software the better the overall simulation will model a real world scenario. Unfortunately, TASRAN simulates few details at the RADAR subsystem level and therefore offers little guidance for this research. TASRAN focuses on RADAR operation on a large scale or system level, but important to future work, TASRAN shows the potential HILS offers when incorporated with ECM and ECCM techniques.

2.3 Real Time RADAR Signal Simulator

Bankui et al. [10] reported a real time RADAR signal simulator at video frequency for injection into a RADAR receiver. From signal injection, moving target detection (MTD), constant false alarm rate (CFAR), and detection methods can be tested. The real time simulation in [10] differs from HILS in that there is no RADAR hardware. The only RADAR component present is the processor at video frequencies. An infinitesimally narrow transmitted pulse and point target govern the simulated RADAR return. Swerling models govern fluctuations of RCS. In contrast to TASRAN and of significance to the path taken with HILS in this research, [10] focuses on RADAR operation at the signal level.

This RADAR signal simulator is developed from a computer science approach as opposed to an engineering approach. The RADAR simulation is divided into four basic processes: data base generation, on-line preprocessing, signal generation, and real time output. To decrease the computational burden and aid in real time performance,

target and clutter environment as well as RADAR characteristics are stored in a data base. It can be inferred that this feature only allows for predetermined signals to be fed into the RADAR processor. Dynamic performance is therefore impossible. This is contrary to the goal of HILS. Furthermore, a RADAR system is not characterized for signal imperfections. Though at the signal level as opposed to the large scale RADAR system level as in TASRAN, this RADAR simulation lacks the necessary fidelity and dynamic operation desired by HILS.

2.4 RAGCLEM

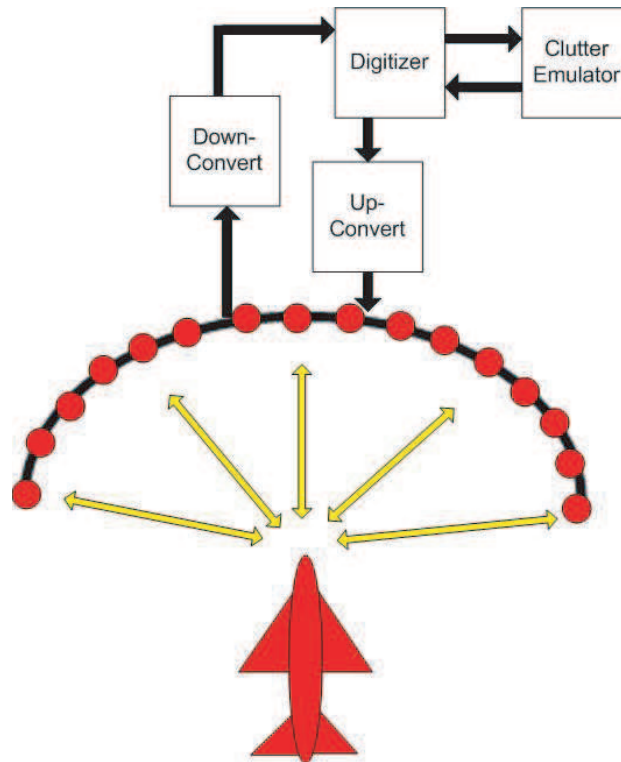


Figure 2.5: RAGCLEM RF RADAR hardware and software simulation reproduced from [7].

Space time adaptive processing (STAP) algorithms minimize interference such as jamming and clutter that compete with a desired signal. Algorithm complexity makes simulation and analysis difficult while jamming signals are easily represented. Ground clutter is dependent upon aircraft speed, antenna beam width, and antenna

look angle and is therefore difficult to reproduce. In order to accurately test STAP algorithms, clutter signals must be realistically represented. Lefevre et al. [7] produced a RADAR ground clutter emulator (RAGCLEM) in support of STAP algorithm tests.

RAGCLEM closely resembles HILS in that it integrates signal modification with actual RF hardware. Sixteen equally spaced antennas are placed in the far field of a transmit antenna at different azimuth angles. Upon reception, the sixteen signals are down-converted, digitized, and sent to the emulator for convolution with the complex valued range profiles for each azimuth angle. Time-varying clutter profiles produced by validated clutter modeling software are loaded in memory and applied to the signals. After convolution, the signal is up converted to RF and transmitted from each of the sixteen antennas to the original transmit antenna where interface with the RAGCLEM system begins. Figure 2.5 shows this setup.

The clutter model is based upon spatial, spectral, and temporal characteristics. Clutter information in azimuth is modeled with the placement of the sixteen antennas in the cross range dimension. Clutter information in range is modeled using stored range profiles. Due to the integration of RADAR hardware and signal modification in software, RAGCLEM is pertinent to beginning research in HILS that is conducted in this thesis. RAGCLEM is too dependent on predetermined data. Long term research would desire a HILS model that can modify or adapt transmitted RADAR signals so as to overcome ECM or clutter aspects. Research techniques presented by RAGCLEM offer a foundation in which to build upon.

2.5 RASER

Huddleston, Walker, and Trott [5] developed the research and seeker emulator RADAR (RASER) to analyze data from sensors employed by smart munitions. RASER can perform RADAR and seeker concepts, evaluate and optimize seeker algorithms, generate and evaluate signal processing techniques, advanced waveforms, and tracking processes, produce clutter and target data under dynamic conditions, and implement HILS with generated RADAR target and clutter returns.

RASER works in conjunction with the associated RADAR front end hardware that operates from 2-GHz to 300-GHz. RADAR hardware supports noncoherent, coherent-on-receive, and fully coherent transmit and receive hardware. RASER has versatile operating modes including pulse, monopulse, FMCW, and a combination of all three. RASER can produce polarization versus range profiles, target doppler signatures, tracking versus range profile, target simulator, and ECM/ECCM. RASER can process and modify (if desired) received waveforms, and re-radiate in real-time. From this description, RASER performs similar to HILS. Compared to other methods discussed, RASER is most significant to this research because it incorporates RADAR hardware in a dynamic environment. RASER does not account, compensate, or characterize errors or imperfections introduced by the RF hardware.

2.6 Automotive Applications of Obstacle Avoidance RADARs.

Obstacle Avoidance RADAR (OAR's) systems are under development to keep cars at safe distances from one another. Due to safety concerns, such RADAR system's behavior under all road conditions must be fully understood prior to implementation. Some road conditions necessary for testing may be difficult or hazardous to set up. RADAR simulations test the RADAR system's behavior under such conditions so as to increase the probability of success during real world implementation [22].

Due to the automobile application, OAR does not vary in elevation. Only targets that vary in azimuth are of concern to OAR. The RADAR simulation focuses on the postprocessing stages after detection so as to determine the RADAR's performance in the presence of obstacles. Processing complexity and anomalous responses arise in the post processing stages. OAR does not interface with RADAR hardware; it is purely a computer simulation. As with RASER, without transmission into the surrounding environment fidelity in the RADAR simulation is lost. The basic RADAR range equation determined received signal strength. Two constants controlled antenna gain and system noise level. These constants were either pre-calculated or obtained

from measurements. Reflectivities of fluctuating targets are assumed to be Rayleigh-distributed and completely uncorrelated between one frame and the next.

The scenario in which the simulation was tested contained cars on both sides of a two lane road. A barrier occupied the right side of the road while lamp posts were spaced between the two traffic lanes. This simulation ran with detection thresholds of -10 dBm, -20 dBm, -30 dBm, and -55 dBm. Detection increased as the threshold decreased; however, output saturation was common at -55 dBm and target spacing could not be determined. At some points the simulation could not accurately detect the barrier due to the shadowing of the cars.

This RADAR simulation focuses on the post processing software stages of the receiver, but does not address hardware characterization within a RADAR system. If this simulation was integrated in a HILS configuration it would exhibit true potential for a real world system and would be more significant to this research.

2.7 Guiding the RADAR Characterization Process

Knowing the degree to which RADAR system parameters influence a received signal will guide the RADAR characterization process. The approach in [28] incorporates response surface methodology to prioritize RADAR parameters influence on a received signal. Confidence factors are assigned to parameters whose accuracy is suspect. Combining the results of response surface methodology and the confidence factors, will identify which parameters must be estimated more accurately.

By determining which RADAR parameters degrade a received signal the most, [28] intended to adjust RADAR parameters so as to maximize its performance while minimizing the system cost. It is the intent of this thesis to apply the same prioritization of RADAR parameter influence to the characterization process.

Table 2.1 shows the order of significance for each RADAR parameter as yielded by the response surface methodology. No information is given for the degree of significance for each factor. True, Krile, and Bauer [28] found that as the inaccuracy of

Table 2.1: Significance of RADAR Parameters on a Received Signal Ordered From Most Significant to Least Significant, Modified from [28].

RADAR Parameter
Transmit Antenna Gain
Receive Antenna Gain
Probability of Detection
Power
Probability of False Alarm
RADAR Cross Section
Pulses Incoherently Integrated
Frequency
Noise Figure

estimation increases, the received signal is degraded in gain, frequency, noise figure, bandwidth, losses, and power. As inaccuracies in estimation increase, probability of detection, probability of false alarm, RADAR cross section, and number of pulses integrated become less important. Overall, antenna gain has the most influence on a received signal and therefore must be characterized with the most accuracy.

2.8 Simulator for Advanced Fighter RADAR EPM Development

Due to RADAR complexity and ECM sophistication, it is difficult to model an active RADAR environment through analysis alone. The associated cost of laboratory equipment and jamming hardware limit the complexity of a scenario. Di-Filippo, Currie, and Geling [4] proposed a flexible high-fidelity simulation capable of modeling an airborne intercept RADAR in an ECM environment known as the Simulator for Advance Fighter RADAR EPM Development (SAFIRE). ECM effects on RADAR operation usually need to be observed over tens of seconds. SAFIRE can easily accommodate a dynamic scenario of long duration. ECM modeling in the SAFIRE system focuses on jammer techniques only and does not address specific jammer hardware. SAFIRE models the following ECM techniques: velocity gate pull-off

(VGPO), range gate pull-off (RGPO), smart noise, and multiple pulse repeat. Results presented by [4] analyze the effectiveness of the ECM techniques to verify simulation performance. Though SAFIRE is versatile, computationally efficient, and explores many of the ECM techniques pertinent to the application of HILS in this research, SAFIRE does not characterize a real world system or attempt to incorporate actual RADAR hardware. The analysis of ECM effectiveness will prove useful to later research once the Lab-Volt simulation has been effectively integrated with associated RADAR hardware.

2.9 ECM-GA Technique Generation

Hong et al. [19] give a thorough overview of the ultimate goal of the research presented in this thesis. The use of genetic algorithms in ECM development introduces the potential for optimized performance against various RADAR systems. Specifically, [19] addresses the application of genetic algorithms to range gate pull off (RGPO) techniques. Characterization and simulation of Lab-Volt RADAR and ECM signals are analyzed. Finally, [19] addresses the method in which to integrate the Lab-Volt simulation into a HILS configuration.

The basic RGPO signal is defined by

$$s(t) = p(t - \tau) \quad (2.15)$$

where the time delay, τ , is $\tau(t) = \frac{|t - T_0|^f}{T_{\max}}$. The delay within the RGPO signal is the basis for implementing the genetic algorithm. If the delay is too fast, the track RADAR may detect the RGPO signal and trigger ECCM; however, if the delay is too slow then the track RADAR is unaffected. The genetic algorithm attempts to optimize the ECM signal through the fitness function parameters. The specifics of genetic algorithms are beyond the scope of this paper. For more information on fitness functions, Coello et al. [2], Back et al. [26] [26], gives more information on genetic algorithms. The more accurate the fitness function, the more efficient the RGPO

signal. In HILS, it is not critical to characterize the tracking RADAR because the closed-loop simulation will immediately adjust the ECM signals for imperfections; however, RADAR characterization is necessary for RGPO optimization.

Though beyond the scope of this research, [19] discusses how the Lab-Volt RADAR and an arbitrary waveform generator (AWG) are configured in HILS. The time required for the RGPO signal to make the Lab-Volt RADAR break lock is the criteria used to evaluate the fitness function parameters. With the modified fitness function, the genetic algorithm passes the new signal to the AWG to repeat the process.

2.10 Advanced RADAR Simulator

The advanced RADAR simulator (ARS) models a large scale RADAR scenario ensuring the physical structure and operation of the simulation reflects a typical RADAR system. The simulation allows the application of various ECM and ECCM techniques. Because a real world RADAR has a bandwidth on the order of megahertz and may last for several hours, a resulting data set could be unrealistically large. To limit the memory requirements, ARS relies on representing returns on a pulse-to-pulse basis [17].

The major contribution of ARS is the approach taken in developing the simulation architecture. The ARS simulation is centered around the interface file. The interface file contains all variable declarations for the entire model and links all blocks together. This architecture allows easy addition of processing blocks. The value of parameters passed between processing blocks represents realistic voltage and power levels. ARS allows any processing block to be replaced with a real processing unit provided the appropriate analog-to-digital interfaces [17]. Processing blocks are subdivided into smaller blocks such that the blocks at the lowest level consist of simple calculations capable of being performed by a simple calculator.

Processing blocks within ARS are organized such that after initialization the `Transmitter` processing block is called. The `Transmitter` processing block is made of the transmitter and transmit antenna. The transmitter portion of the `Transmitter` processing block determines the frequency, phase, and amplitude of the transmitted signal while the transmit antenna portion applies the appropriate gain based on the targets location in reference to the antennas boresight direction. The `Propagation` processing block follows and is called twice to model the two way propagation of signals sent from the RADAR to the target and back. `Propagation` applies the appropriate phase, amplitude, and time stamp of each pulse according to the range of the target. `Reflectivity` determines the power reflected by the target by multiplying the RCS and the power density after the one way trip from RADAR to the target as determined in `Propagation`. ECM is applied after calling `Reflectivity` but prior to calling `Propagation` for a second time. `Receiver` is the final subroutine to be called and applies the receive antenna gain, receiver noise, and sorts pulses according to their time of arrival.

Significant to this research, ARS shows how to best organize the architecture of the Lab-Volt simulation that will ultimately be integrated with RADAR hardware in HILS. Yet, ARS is deficient to this research in that it does not integrate RADAR hardware. All data generated in ARS is completely theoretical. Additionally, ARS presents no characterization of a real RADAR system.

III. Lab-Volt System Characterization

The first section of this chapter analyzes the components of a general RADAR system, the Lab-Volt RADAR system, and a real world RADAR system in order to understand how the characterization process would differ between the three systems. The second section of this chapter discusses the process used to characterize the Lab-Volt system. The final section presents the selected results of the characterization process. The results of the remainder of the Lab-Volt system are presented in the following chapter where the captured and simulated signals are compared to one another.

3.1 *RADAR System Background and Comparison*

The ultimate goal of this research is to apply the same methodology used to characterize and simulate the Lab-Volt system to a large-scale, real world RADAR system. The first subsection analyzes a general RADAR transmitter, antenna, and receiver. The second subsection analyzes the Lab-Volt RADAR system to show how modifications from the general RADAR system allow for the specific application of the Lab-Volt system. Specifically, the Lab-Volt RADAR synchronizer and antenna controller, transmitter, parabolic antenna, receiver, and dual channel sampler module are presented in detail. The final subsection analyzes a real world RADAR system to understand the differences between a real world system and the Lab-Volt system. Due to limited technical literature, only the transmitter and receiver of a real world system are analyzed.

3.1.1 *General Radar System.*

3.1.1.1 *Transmitter.* A general RADAR transmitter begins with a voltage controlled oscillator (VCO) at an intermediate frequency (IF) on the order of KiloHertz. The VCO's input signal allows the application of frequency modulation. As discussed in Section 2.1.1, frequency modulation introduces a method in which to determine a target's range and doppler frequency. The output of the VCO is a CW signal. Modulating the CW signal with a local oscillator, *LO*, shifts the signal to RF.

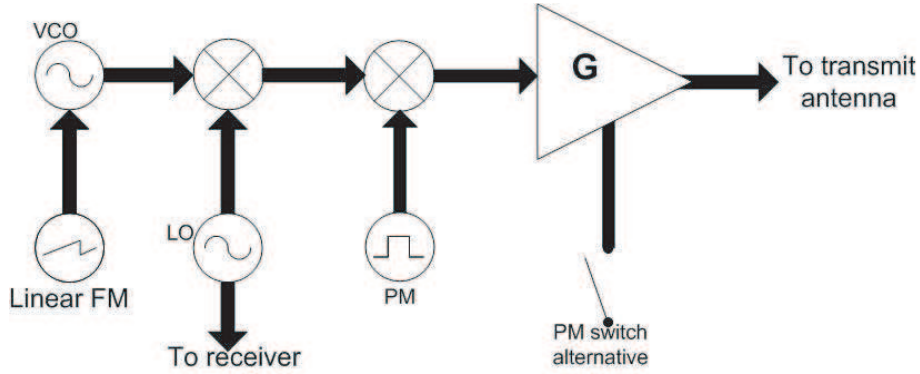


Figure 3.1: General RADAR transmitter block diagram. The source, VCO, is mixed to RF and PAM at the LO and pulsed signal respectively. FM and gain are applied as needed. Pulse modulation is alternately applied by turning the amplifier off and on.

The *LO* signal is also sent to the receiver as a reference signal in which to demodulate the received signal. Modulating the signal out of the VCO with a pulse train produces a PAM signal. A gain stage follows to achieve the power necessary for transmission. PAM is alternately achieved by turning the amplifier off and on. Figure 3.1 shows a generic RADAR transmitter block diagram. The specific arrangement of components within a RADAR transmitter varies with operational specifications.

Two options exist to produce high power levels in a real world RADAR systems. The first option places amplifiers following the RF oscillator. Employing amplifiers is noisy and may require cascading to generate sufficient power [20]. The second option to generate high power levels is to replace RF oscillators and amplifiers with microwave devices such as klystrons, magnetrons, and traveling wave tubes. These microwave devices produce high power levels but may have limited bandwidths [20].

3.1.1.2 Antenna. A RADAR system whose transmit and receive antenna are collocated is referred to as a monostatic RADAR. A RADAR system whose transmit and receive antennas are not collocated is referred to as a bistatic RADAR. An antenna is much like a filter in that it operates across a specific bandwidth. If a signal's bandwidth exceeds the antenna's bandwidth signal attenuation will result. The Lab-Volt antenna characterization process will explore this effect.

The equipment inside the receiver of a real world RADAR system is extremely sensitive and is easily damaged if exposed to high RF power levels. For this reason, it is imperative to insure that transmitted power does not find its way to the receiver. To accomplish this, a real world RADAR system employs a duplexer. A duplexer is device that alternates signal direction from the transmitter to the antenna on transmit, and from the antenna to the receiver on receive. In a general RADAR system, a duplexer connects in series with the plumbing between the transmitter, antenna, and receiver. An ideal duplexer is lossless [20].

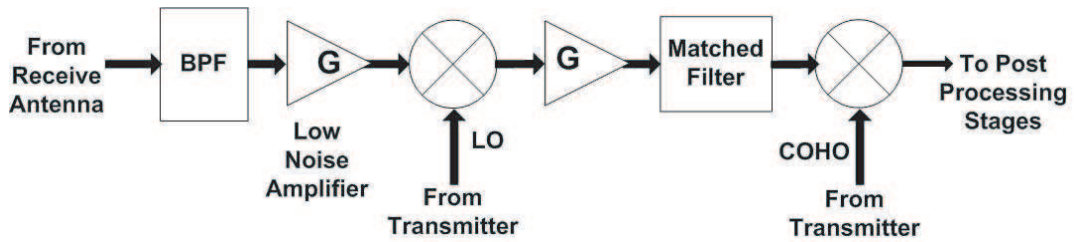


Figure 3.2: General RADAR receiver block diagram.

3.1.1.3 Receiver. Microwave plumbing feeds the received signal from the receive antenna to the receiver. To avoid amplifying noise, an initial low noise amplifier (LNA) eliminates noise outside the signal's envelope and amplifies the signal. The low noise amplifier essentially boosts the signal to noise ratio. After the LNA, modulating the filtered signal with the LO returns the signal to IF. Additional amplification or filtering is applied depending on receiver specifications. A matched filter maximizes the energy of the signal captured. A detailed discussion on matched filters is presented by [20]. A coherent oscillator (COHO) returns the signal to baseband where advanced processing occurs.

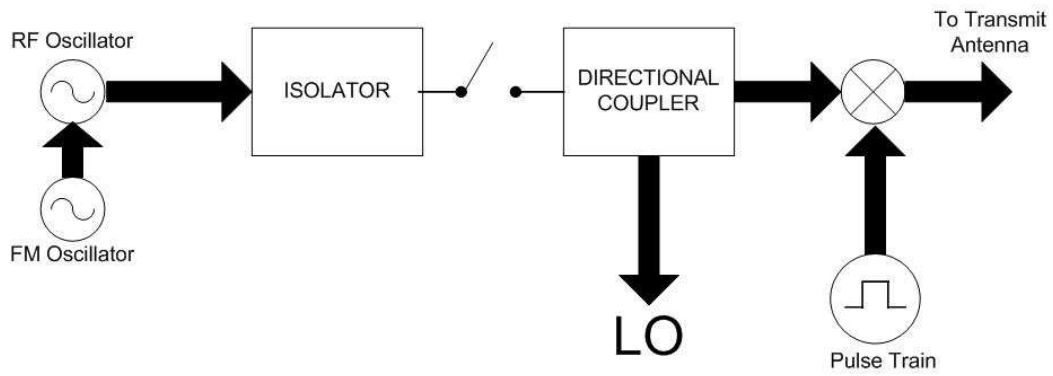
3.1.2 Lab-Volt System. As discussed, the Lab-Volt system is the foundation in which to develop the RADAR characterization process. Analysis of each module and subsystem within the Lab-Volt system is presented and analyzed so as to provide a foundation for the characterization techniques later developed.

3.1.2.1 Radar Synchronizer and Antenna Controller. As its name suggests the Lab-Volt RADAR Synchronizer and Antenna Controller module is divided into two parts. The RADAR Synchronizer generates the PRF signal. The PRF MODE button allows the selection of a single or staggered PRF. The PRF is set to 12, 18, 144, 216, or 288-Hz. To allow for measurements on common oscilloscopes, the actual PRF is set 1024 times the displayed amount. Through Equation (2.3), the different PRF settings correspond to a maximum unambiguous range of 12.5-km, 8.3-km, 1.04-km, 694.44-m, and 520.83-m respectively. From the scale of the Lab-Volt set up, no secondary returns will occur. A staggered PRF alternates between the selected PRF and three-fourths of the selected PRF [12]. It was concluded that no further details of the Lab-Volt RADAR Synchronizer are relevant to this research.

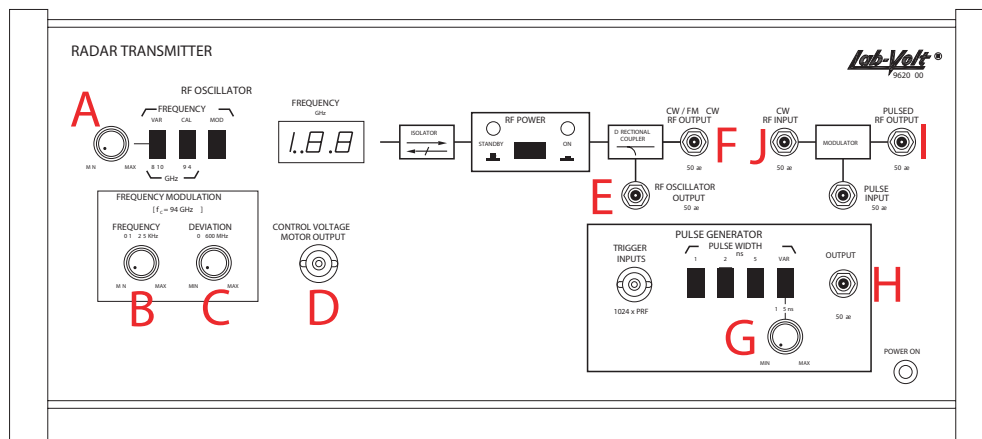
3.1.2.2 Transmitter. The Lab-Volt RADAR transmitter generates the RF signal and waveform sent to the transmit antenna for release into the radiating environment. Figure 3.3(a) shows the components of the Lab-Volt transmitter module. Figure 3.3(b) shows the front panel of the Lab-Volt transmitter module; various locations are marked for reference in the characterization and simulation process.

Specifications of power levels and frequency ranges that will be verified throughout the characterization process are given in [15]. The RF oscillator sets the carrier frequency between 8 and 10-GHz. According to [15], the RF oscillator produces power levels between 8 and 12-dBm; however, only a maximum of 3-dBm reaches the transmit antenna. For FM, the carrier frequency is 9.4-GHz and the modulation frequency is manually selected between 0.1 and 2.5-kHz. The frequency deviation is manually selected between 0 and 600-MHz.

An isolator follows the RF oscillator and prevents RF power from returning to and possibly damaging the source. An isolator is a two-port microwave ferrite device. Because it only allows power flow in one direction, an isolator has unidirectional transmission characteristics. Pozar [18] states that an ideal isolator is lossless. The isolator within the Lab-Volt transmitter is not accessible without taking the module



(a) Block diagram.



(b) Front panel obtained from [15].

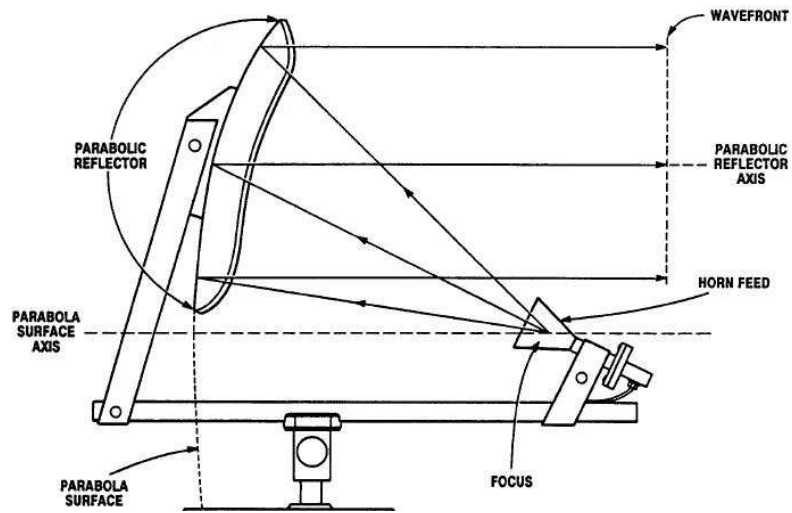
Figure 3.3: Lab-Volt transmitter module.

apart and will therefore be assumed lossless. The RF power switch follows the isolator and controls when the system is transmitting into the surrounding environment. Based on this configuration, the RF oscillator is not turned off by the RF power switch; the RF power switch only disrupts the path between the oscillator and the transmit antenna.

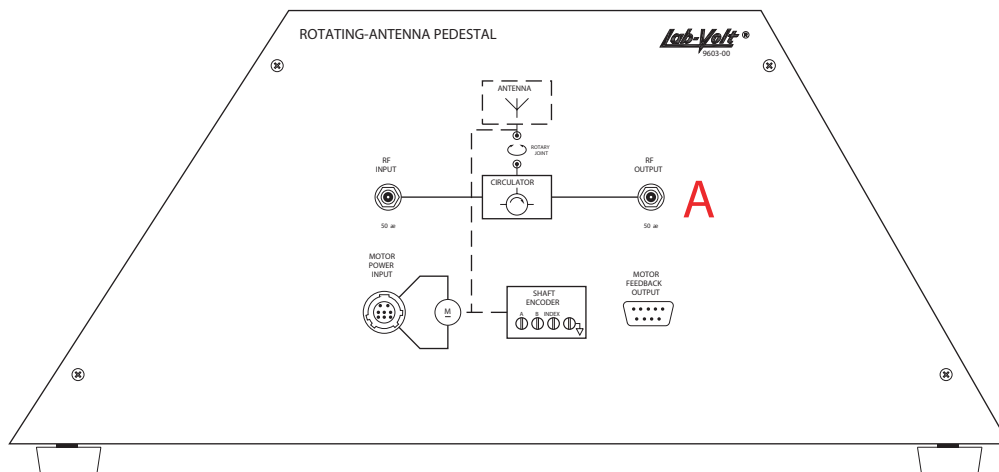
A directional coupler follows the RF power switch and splits power between the LO and the remainder of the transmit system. The technical manual for the Lab-Volt transmitter states the power out of the directional coupler towards the transmit antenna ranges from -1.5 to 2.5-dBm [15]. The characterization process will determine the ratio in which the directional coupler splits power between the RF oscillator and the LO.

The output of the directional coupler is sent to the transmit antenna as a CW signal or continues to the pulse generator to produce a PAM signal. The pulse generator produces a pulse width ranging between 1 and 5-ns. The pulse generator receives an input pulse in the form of the PRF from the RADAR synchronizer module telling it when to activate the pulse. The technical manual for the Lab-Volt transmitter states the output power of the pulse generator is between -1.5 and 2.5-dBm [15].

3.1.2.3 Parabolic Antenna and Pedestal. The dish antenna consists of a horn antenna and a parabolic reflector. The dish antenna connects to a pedestal through a rotary joint. The horn antenna transmits microwave power toward the parabolic reflector. The parabolic reflector culminates the waves into a narrow beam parallel to the parabola surface. Due to the curvature of the parabolic reflector, the waves originating from the horn feed are converted into a plane wavefront of uniform phase. The arrows in Figure 3.4(a) show how the parabolic reflector changes the transmitted microwave energy from the horn antenna into a uniform plane wave. The parabolic antenna has a 27-dB gain and a bandwidth spanning 46.5-GHz. The technical manual for the Lab-Volt antenna states the half-power beamwidth is 6 degrees in azimuth and 8 degrees in elevation [13]. Figure 3.4(b) shows the front panel of the



(a) Parabolic dish antenna obtained from [13].



(b) Antenna pedestal front panel obtained from [13].

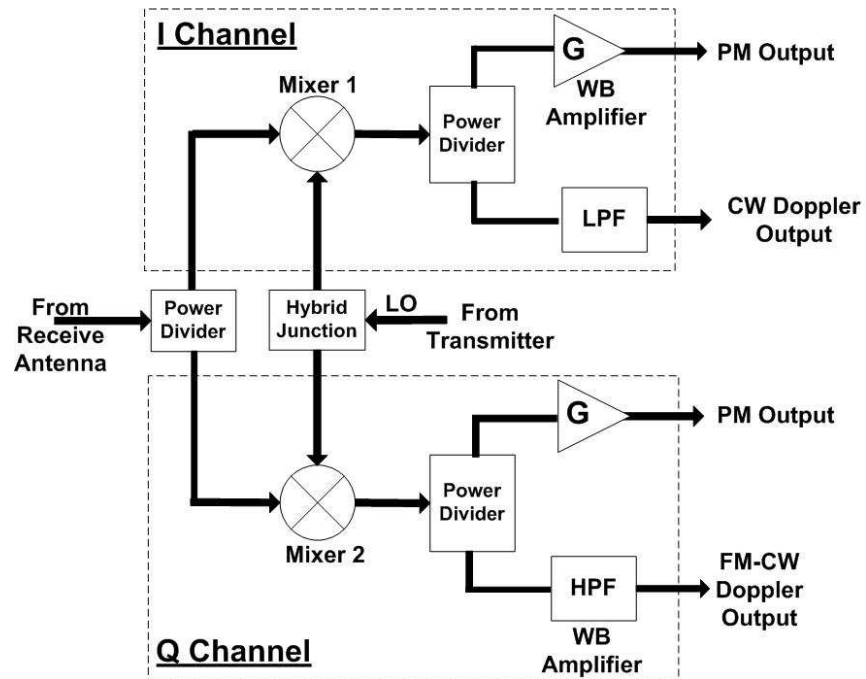
Figure 3.4: Lab-Volt antenna pedestal module.

antenna pedestal and is marked for reference in the characterization and simulation process.

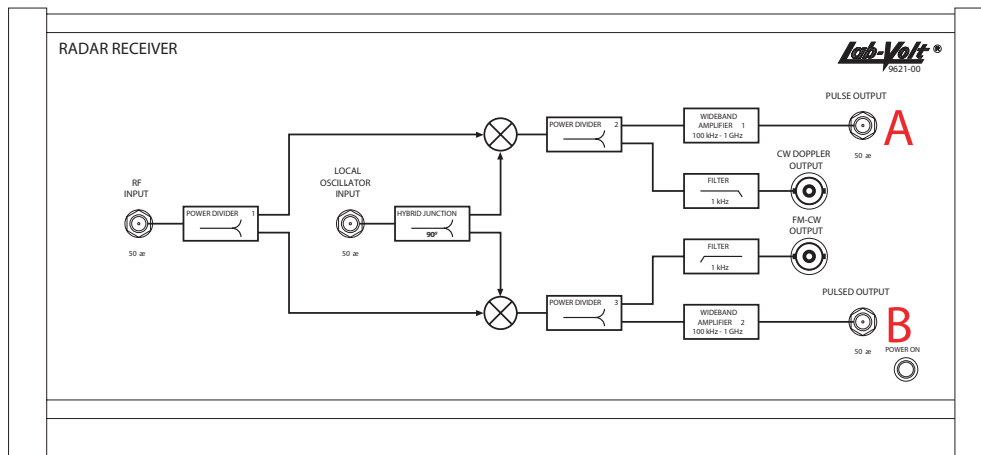
The Lab-Volt system also provides a tracking antenna. The tracking antenna is more relevant so as to support the overarching goal of HILS for ECM and ECCM techniques; however, no operating parameters are specified for the tracking antenna. For this reason, the tracking antenna pattern and frequency response must be determined. The characterization process will verify the bandwidth and beamwidth for the tracking antenna.

To allow the antenna to function simultaneously on transmission and reception, the Lab-Volt system employs a circulator as opposed to a duplexer often used in a real world RADAR system. Pozar [18] describes a circulator as a three port device that is nonreciprocal and has matched inputs. The antenna pedestal connects the Lab-Volt transmitter and receiver by introducing and collecting RF energy into the surrounding environment as shown in Figure 2.1. The antenna pedestal contains the antenna drive motor used to control antenna rotation. An incremental optical shaft encoder encodes the angular position of the motor shaft. Motor voltage and current levels are sent from the antenna pedestal as feedback signals. Angular position and voltage and current feedback signals determine antenna position and control rotation speed of the tracking antenna during tracking and scan modes. RF coupling allows the antenna to rotate without breaking transmission.

3.1.2.4 Receiver. The Lab-Volt system incorporates a homodyne receiver because the received RF signal is converted directly to baseband without an IF stage. The LO from the transmitter module serves as the reference signal to demodulate the received signal. Based on this configuration any difference in phase between the reference signal and the received signal is due to target parameters. Because the receiver preserves phase differences, the Lab-Volt receiver module can be viewed as a coherent system. Figure 3.5(a) shows a block diagram of the Lab-Volt receiver module. Figure 3.5(b) shows the front panel of the Lab-Volt receiver module



(a) Block diagram.



(b) Front panel obtained from [14].

Figure 3.5: Lab-Volt receiver module.

and serves as a reference for the I- and Q-channel PAM outputs used extensively in the characterization process.

The first power divider divides the received RF signal into the I and Q channel prior to *MIXERs 1* and *2*. The LO reference signal from the transmitter module is divided at the *HYBRID JUNCTION* into two reference signals separated by 90 degrees in phase. To avoid taking apart the receiver module, it is assumed that each reference signal is of equal power. Mixing these reference signals at *MIXERs 1* and *2* with the outputs of the first power divider converts the received RF signal to baseband. *Mixer 1* and *Mixer 2* outputs are referred to as the in-phase and quadrature channel or the I and Q channels, respectively.

Power dividers following *Mixer 1* and *Mixer 2* divide the I and Q channels into various outputs. For PAM mode, I-and Q-channel baseband signals are amplified by a wideband amplifier after the mixer and prior to the pulsed output. According to [14], the wideband amplifiers have a gain of 45-dB and a bandwidth of 1-GHz. If the Lab-Volt system is set up as a CW RADAR, a 1-kHz low pass filter (LPF) is applied to the baseband of the I-channel signal prior to the *CW DOPPLER OUTPUT*. The LPF preserves the doppler frequency components by removing unwanted higher frequency components to include harmonic by product of the mixer. If the Lab-Volt is set up as a CW RADAR, a baseband Q-channel signal is passed through a 1-kHz high pass filter (HPF) prior to the FM-CW OUTPUT. Removing low frequencies causes the baseband signal to have uniform amplitude and thus facilitates measurements in frequency. In an FM-CW configuration, accurate measurements in frequency are important to determining the range of an observed target [14].

3.1.2.5 Dual-Channel Sampler. After exiting the receiver module, the received signal is at baseband and pulses occur at 1024 times the PRF. The relationship established between pulse width and bandwidth as outlined in Section 2.1.1 and Figure 2.1, states that a pulse width on the order of nanoseconds has a bandwidth on the order of gigahertz. This signal is unobservable with inexpensive,

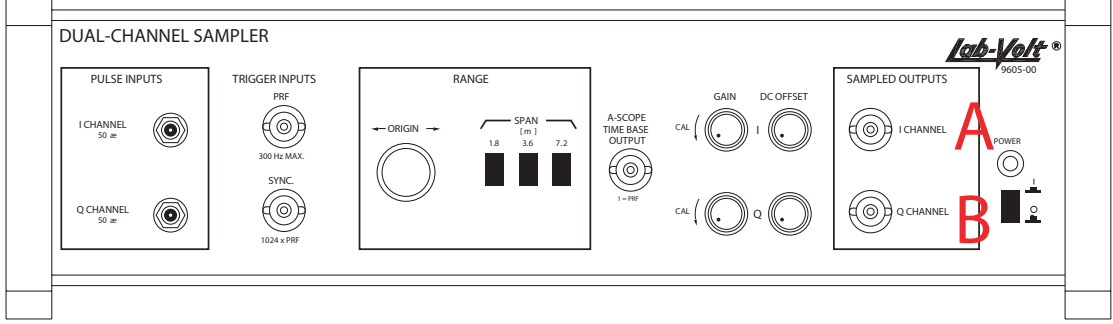
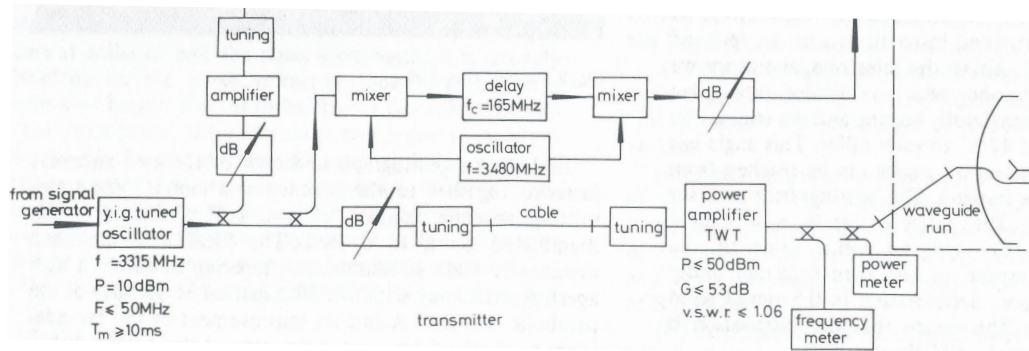


Figure 3.6: Dual channel sampler front panel obtained from [11].

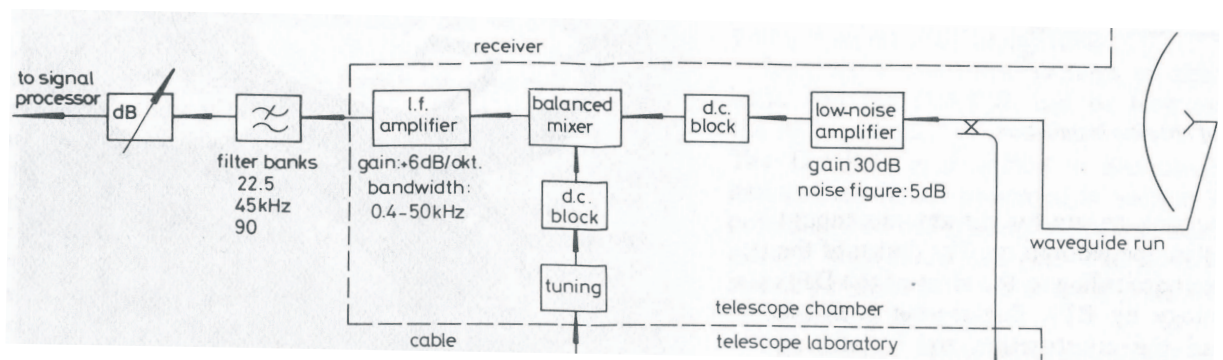
low-bandwidth oscilloscopes found in a typical academic environment. To solve this dilemma the Dual Channel Sampler (DCS) module samples the received signal on the I and Q channel in time and delays each sample so as to stretch the signal on the order of microseconds. Stretching these signals in time reduces the bandwidth and allows less complex and costly equipment to be used for further processing.

The DCS's sampling period is slightly larger than the PRI. The overlap between the sampling period and PRI causes received pulses to be sampled at different points. Samples are held for an extended period of time so as to increase the time between samples and effectively stretch the signal in time. It should be noted that the DCS does not slow the rate at which pulses occur; the PRI remains unchanged. The range origin control delays the SYNC signal so as to control the time range within the PRI (and hence radial distance from the antenna) that is sampled. The samples captured by the DCS span 1.8, 3.6, or 7.2-meters in range. It should be noted that stretching the signal in time increases the pulse width and seemingly increases the signal's duty cycle [11].

3.1.3 Comparison with a Real World RADAR System. The ultimate goal of this research is to show the Lab-Volt RADAR characterization process can be extended to a real world system. For this reason it is important to note the differences between a real world RADAR system and the Lab-Volt system. The FM-CW Delft



(a) Transmitter.



(b) Receiver.

Figure 3.7: DELFT atmospheric research obtained from [3].

Atmospheric Research RADAR will serve as the reference RADAR system. Figure 3.7(a) and 3.7(b) show the Delft’s transmitter and receiver respectively [3].

The first major difference between the Delft and Lab-Volt transmitter is that the Delft transmitter is strictly a CW system while the Lab-Volt system allows for PAM. Immediately following the *y.i.g. tuned oscillator*, a power divider splits the RF signal to produce a COHO just as in the Lab-Volt transmitter. The first power divider produces a COHO because it has the same phase as the transmitted signal and after demodulation, any resulting phase differences are due to target parameters. The Delft transmitter splits the signal a second time to produce a stable local oscillator (STALO). Mixing the split signal with a 3480 MHz signal twice, decreases the variations in signal frequency and thus produces a LO. The Delft system implements a traveling wave tube (TWT) to produce high power. Various tuners are found throughout the Delft system so the Delft system is expected to have a significantly more stable signal. The Lab-Volt system does not use any amplification; therefore, if the Lab-Volt characterization process were extended to the Delft system, the noise introduced by the amplifier would need to be included.

After the receive antenna, the Delft system intermediately incorporates the STALO to bring the received signal to baseband. A low-noise amplifier, not found in the Lab-Volt receiver, follows the demodulator. The Lab-Volt system lacks a low noise amplifier. If the Delft system were to be characterized, care must be taken to incorporate the noise figure of the low noise amplifier. The *d.c. block* prevents undesired biasing of the solid state mixer. The signal is then demodulated to baseband with the COHO. Finally an IF amplifier is applied. With the primary differences noted, the Lab-Volt characterization process is much simpler than characterizing the Delft system.

3.2 Methodology

The characterization process explores the Lab-Volt transmitter module, tracking antenna, parabolic antenna, receiver module, and DCS module. Prior to delving into

the Lab-Volt characterization process, target and signal parameters are presented. Equipment used to complete the characterization process is presented along with the instrument's limitations. The characterization process consists of capturing signals at various outputs, understanding antenna influences on signals, and characterizing adjustment settings on the transmitter and DCS module.

3.2.1 Assumptions and Characterization Instrumentation. The three-inch by three-inch metal plate target provided with the Lab-Volt system was used for the characterization of return signals obtained from antenna pedestal, PAM output of the receiver module, and DCS module. Unless otherwise stated, all received signal measurements are conducted with PAM signals. To characterize the various adjustments several trials were conducted in an attempt remove randomness between trials. Six trials were conducted at each rotational position. Trials were separated by 1-hour in which the Lab-Volt system was powered down. Prior to taking measurements, the Lab-Volt system was allowed to warm up for twenty minutes as specified by the Lab-Volt operating manuals.

The Agilent E4407B ESA-E Spectrum Analyzer captured all signals in the frequency domain. This spectrum analyzer has a bandwidth spanning 9-kHz to 26.5-GHz. The Tektronix TDS6124C Oscilloscope captured the signals in the time domain. This oscilloscope has a bandwidth of 12-GHz and is capable of capturing 40-giga-samples per second. The 12-GHz bandwidth is sufficient for capturing 10-GHz carrier signals, the maximum carrier frequency producible by the Lab-Volt system. If 40-giga-samples per second is interpreted as a 40-GHz sampling rate, the time between samples and correspondingly the minimum rise and fall time is 25-ps as specified by the oscilloscope operating manual [25]. When contacted, Tektronix officials verified the oscilloscope is capable of measuring a minimum rise and fall time of 25-ps. All measurements were captured with phase-matched, precision microwave cables to reduce pulse dispersion, and time differences due to the measurement.

3.2.2 Transmitter Module Characterizations. The Lab-Volt transmitter module characterization process consisted of capturing signals at various outputs and characterizing the various adjustments. Capturing signals at various outputs consisted of two measurements. The first series of signals captured were out of the CW, LO, pulse generator, and pulsed RF output. In Figure 3.3(b), the CW output, LO output, pulse generator, and pulsed RF output correspond to ports E, F, H, and I respectively. The second series of signals captured analyzed the rise and fall times of a 1, 2, and 5-ns pulse from the pulse generator output. The pulse width, carrier frequency, frequency deviation, and modulating frequency adjustments were characterized to understand how the degree of rotation effects the final output.

3.2.2.1 Captured Signals from Transmitter Module. The first signals captured out of the Lab-Volt transmitter are at the minimum and maximum carrier frequencies, 8-and 10-GHz respectively, as well as the standard 9.4-GHz carrier frequency. Signals were captured at the LO and CW outputs. Signals were captured at the pulse generator output at pulse widths of 1, 2, and 5-ns. At each carrier frequency the pulse width is set to 1, 2, and 5-ns and signals are captured at the pulsed RF output. Table 3.1 shows the test matrix for signals captured out of the Lab-Volt transmitter module.

The second series of tests in the Lab-Volt transmitter characterization process analyzed the rise and fall times of the pulse generator for 1, 2, and 5-ns. The oscilloscope was connected to port H in Figure 3.3(b) and 1 000 000 pulses were averaged to remove noise. Using the oscilloscope's internal measuring features, the rise and fall times from 10% to 90% of the maximum signal values.

3.2.2.2 Transmitter Module Adjustment Characterization. The first series of tests in the Lab-Volt transmitter adjustment characterization process characterized the pulse width adjustment. The pulse width adjustment, knob G in Figure 3.3(b), was increased from 0% to 100% rotation by increments of one-fourth of a rotation while the oscilloscope captured signals from the output of the pulse generator,

Table 3.1: Test Matrix for Signals Captured at RF Pulsed Output of Lab-Volt Transmitter.

Location	Carrier Frequency (GHz)	Pulse Width (ns)
CW Output	8	N/A
CW Output	9.4	N/A
CW Output	10	N/A
LO Output	8	N/A
LO Output	9.4	N/A
LO Output	10	N/A
Pulse Generator Output	N/A	1-ns
Pulse Generator Output	N/A	2-ns
Pulse Generator Output	N/A	5-ns
Pulse RF Output	8	1
Pulse RF Output	9.4	1
Pulse RF Output	10	1
Pulse RF Output	8	2
Pulse RF Output	9.4	2
Pulse RF Output	10	2
Pulse RF Output	8	5
Pulse RF Output	9.4	5
Pulse RF Output	10	5

port H in Figure 3.3(b). Five-thousand pulses were averaged with the oscilloscope’s averaging feature to remove noise. The resulting pulse width for each rotation was measured using the oscilloscope’s internal pulse width measuring function. Table 3.2 shows the test matrix for the pulse width adjustment characterization. Six trials were repeated for each adjustment position.

The second series of tests in the Lab-Volt transmitter adjustment characterization process characterized the carrier frequency adjustment. The carrier frequency adjustment, knob A in Figure 3.3(b), was increased from 0% to 100% rotation by

Table 3.2: Test Matrix for Pulse Width Adjustment Characterization.

Location	Pulse Generator Adjustment (% rotation)
Pulse Generator Output	0
Pulse Generator Output	25
Pulse Generator Output	50
Pulse Generator Output	75
Pulse Generator Output	100

Table 3.3: Test Matrix for Carrier Frequency Adjustment Characterization.

Location	Carrier Frequency Adjustment (% rotation)
CW Output	0
CW Output	25
CW Output	50
CW Output	75
CW Output	100

increments of one-fourth of a rotation while the oscilloscope captured signals from the CW output, port F in Figure 3.3(b). The oscilloscope measured the time between consecutive peaks so as to determine the carrier frequency. Table 3.3 shows the test matrix for the carrier frequency adjustment characterization. Six trials were repeated for each adjustment position.

Table 3.4: Test Matrix for Modulating Frequency Adjustment Characterization.

Location	Modulating Frequency Adjustment (% rotation)
Monitor Output	0
Monitor Output	25
Monitor Output	50
Monitor Output	75
Monitor Output	100

The third series of tests in the Lab-Volt transmitter adjustment characterization process characterized the modulating frequency adjustment. To characterize

the modulating frequency adjustment, knob B in Figure 3.3(b), the frequency deviation setting was held constant at 100% rotation (600-MHz), while the oscilloscope captured signals at port D in Figure 3.3(b). The modulating frequency setting was increased from 0% to 100% rotation in increments of one-fourth of a rotation. Using the oscilloscope's internal measuring features, the frequency of the measured signal corresponded to the modulating frequency. Table 3.4 shows the test matrix for the characterization of the modulating frequency adjustment. Six trials were repeated for each adjustment position.

Table 3.5: Test Matrix for Frequency Deviation Adjustment Characterization.

Location	Frequency Deviation Adjustment (% rotation)
Monitor Output	0
Monitor Output	25
Monitor Output	50
Monitor Output	75
Monitor Output	100

The fourth series of tests in the Lab-Volt transmitter adjustment characterization process characterized the frequency deviation adjustment. To characterize the frequency deviation adjustment, knob C in Figure 3.3(b), the frequency deviation setting was held constant at 100% rotation (600-MHz), while the spectrum analyzer was connected to port F in Figure 3.3(b). The modulating frequency was held constant at 50% (1.25-kHz) while the frequency deviation setting was increased from 0% to 100% rotation in increments of one-fourth of a rotation. Table 3.4 shows the test matrix for the characterization of the frequency deviation adjustment. Six trials were repeated for each adjustment position.

3.2.3 Antenna Characterization. The antenna characterization process consists of two parts. In the first part, the oscilloscope captured signals at the RF output of the antenna pedestal. The second series of measurements, attempted to derive a transfer function that described how the antenna modified a transmitted signal.

Table 3.6: Test Matrix for the Lab-Volt Antenna Output Characterization.

Location	Carrier Frequency (GHz)	Pulse Width (ns)
RF Output	8	1
RF Output	9.4	1
RF Output	10	1
RF Output	8	2
RF Output	9.4	2
RF Output	10	2
RF Output	8	5
RF Output	9.4	5
RF Output	10	5

3.2.3.1 Signals Captured RF Antenna Output. To characterize and understand signal variations that are introduced by the radiating environment, the oscilloscope captured signals at the output of the antenna pedestal, port A in Figure 3.4(b). Table 3.6 shows the test matrix of signals captured.

3.2.3.2 Lab-Volt Antenna Transfer Function Derivation. According to the results derived from response surface methodology [28], antenna parameters have the most influence on a received RADAR signal. For this reason great care was taken to characterize the Lab-Volt monopulse tracking antenna. The parabolic antenna was not characterized. The following tests attempted to characterize the tracking antenna in both phase and magnitude to approximate a transfer function that accurately modeled the manner in which a transmitted signal is modified by the antenna.

3.2.3.3 Assumptions. The receive antenna within the AFIT anechoic chamber is known to operate over a 2 to 18-GHz bandwidth. Lab-Volt specifications only list operating parameters for the parabolic antenna operating at 9.0-GHz; no operating frequency range is specified for the tracking antenna. Based on its physical

dimensions; it is assumed that the tracking antenna only supports X-band frequencies. It is therefore assumed that the gain antenna within the anechoic chamber fully spans the tracking antenna's operating band.

3.2.3.4 Antenna Pattern Transfer Function. This research characterizes the antenna so as to derive a transfer function for all 360° in azimuth. The Lab-Volt system operates at X-Band, 8-12-GHz as specified by [20]. This describes the operational or 3-dB bandwidth. To better capture signal characteristics across the entire X-Band spectrum, all antenna measurements span 6.4 to 14.4-GHz with a spacing of 10-MHz. As described in the background, the Lab-Volt system is capable of a minimum pulse width of 1-ns and will therefore have a maximum spectral mainlobe bandwidth of 2-GHz as shown in Figure 2.2. Additional nulls are spaced at 1-GHz intervals from the mainlobe nulls. With a carrier frequency of 9.4-GHz, the 6.4 to 14.4-GHz bandwidth incorporates two sidelobes on either side of the mainlobe. Signals at the first and second sidelobes are attenuated by 6.3 and 8.5-dB respectively off the mainlobe. All frequencies outside the bandwidth of the antenna pattern measurement will therefore contribute less than 8.5-dB to the overall signal. With such a small contribution, these signals are deemed insignificant.

3.2.3.5 Antenna Transfer Function Derivation. Absolute gain measurements require a calibrated standard gain antenna. Measured data was calibrated according to the gain transfer method presented by Balanis [1]. Mathematically the gain transfer method is

$$G_{T,dB} = G_{S,dB} + 10 \log_{10} (S_{21}), \quad (3.1)$$

where $G_{S,dB}$ is the gain of the standard horn and S_{21} is the measured gain for the Lab-Volt tracking antenna.

An antenna is calibrated in phase through the use of three antennas [1]: the antenna under test, the transmit antenna, and a stationary reference antenna. Figure

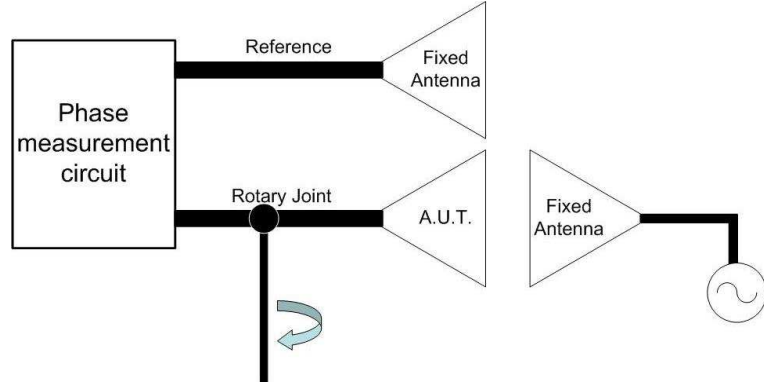


Figure 3.8: Phase measurement setup [1].

3.8 shows this setup. The antenna under test is rotated while the fixed antenna serves as a phase reference. This setup would require two antennas and two network analyzers interfaced with the associated software. The AFIT anechoic chamber does not provide this option. An alternate option is presented for test.

If the distance the wave travels is known, the change in phase from start to finish is calculated for each frequency via

$$\Delta\phi_n = 2\pi \frac{D}{\lambda_n}, \quad n = 1, \dots, N, \quad (3.2)$$

where D represents the measured distance the wave travels and λ_n represents the stepped wavelengths corresponding to the stepped frequencies in which antenna pattern measurements are taken. Once the phase change encountered over the travel path is calculated it is removed from measured antenna data. Any remaining phase changes can be attributed to the Lab-Volt tracking antenna.

The distance a transmitted signal travels is the accumulation of the total lengths of microwave plumbing and the spatial distance between the transmit and receive antenna within the anechoic chamber. Figure 3.9 shows the physical arrangement of various distances that the transmitted signal traverses from Port 1 to Port 2 of the network analyzer.

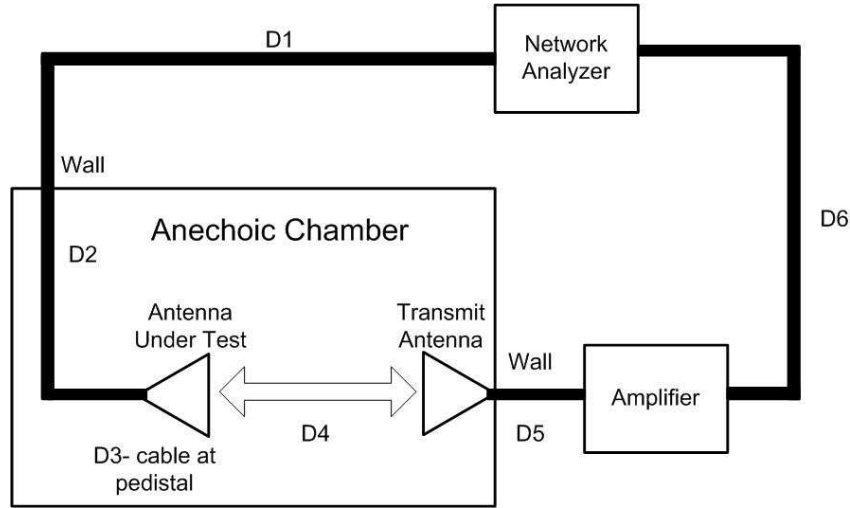


Figure 3.9: Travel distances within and around anechoic chamber.

Table 3.7: Path from Transmit Antenna to Antenna Under Test.

Location	Distance (m)
D1	2.110
D2	2.905
D3	2.530
D4	2.730
D5	1.300
D6	0.670

Table 3.7 lists the measurements of the distances presented in Figure 3.9. All measurements were taken with a standard tape measure with millimeter precision. As shown in Figure 4(a), the distance between the horn and the parabolic reflector is 0.315-m and is included twice to account for the signal traveling from the horn to the reflector and back to the horn prior to traveling into the surrounding anechoic chamber environment. Pictorially the distances are seen in Figure 3.9. Adding this distance to the accumulated distances found in Table 3.7 yields a combined distance of 12.875-m.

Upon closer observation of the lab equipment setup, the exact distance between the transmit and receive antenna cannot be measured with accuracy. The additional

plumbing inside the amplifier is unknown and transmission cable curvature limits measurement accuracy. To remedy this problem, a range of transfer functions with varying phase corrections was created. Using Equation (3.2), the phase correction for each transfer function was defined for a range of distances spanning 12.375-m to 13.375-m. The actual distance is hypothesized to lie in this range. The phases are incremented according to one-eighth the wavelength at 14.4-GHz, the highest frequency and hence shortest wavelength. Using the shortest wavelength as an increment defines the maximum precision in phase. The magnitude of the various transfer functions do not differ. It is hypothesized that the antenna introduces pulse dispersion, and the transfer function will reveal the band limitations imposed by the antenna.

Table 3.8: Test Matrix for the Lab-Volt Receiver Characterization.

Location	Carrier Frequency (GHz)	Pulse Width (ns)
I- and Q-Channel PAM Output	8	1
I- and Q-Channel PAM Output	9.4	1
I- and Q-Channel PAM Output	10	1
I- and Q-Channel PAM Output	8	2
I- and Q-Channel PAM Output	9.4	2
I- and Q-Channel PAM Output	10	2
I- and Q-Channel PAM Output	8	5
I- and Q-Channel PAM Output	9.4	5
I- and Q-Channel PAM Output	10	5

3.2.4 Receiver Module Characterization. To understand and characterization signal imperfections introduced by the Lab-Volt receiver module, the oscilloscope captured signals at the I- and Q-channel PAM output of the receiver module, Ports A and B respectively of Figure 5(b). For simplicity, the FMCW and CW outputs are not characterized. Table 3.6 shows the test matrix for this characterization process. The test matrix was repeated for the I and Q channel.

3.2.5 DCS Module Characterization. The DCS characterization process was broken into two parts. In the first part, signals were captured from the I-and Q-channel outputs using the oscilloscope. The second part of the characterization process characterized the I- and Q-channel gain and offset adjustments.

Table 3.9: Test Matrix for the Lab-Volt the DCS.

Location	Carrier Frequency (GHz)	Pulse Width (ns)
I and Q Channel DCS Output	8	1
I and Q Channel DCS Output	9.4	1
I-and Q-Channel DCS Output	10	1
I-and Q-Channel DCS Output	8	2
I-and Q-Channel DCS Output	9.4	2
I-and Q-Channel DCS Output	10	2
I-and Q-Channel DCS Output	8	5
I-and Q-Channel DCS Output	9.4	5
I-and Q-Channel DCS Output	10	5

3.2.5.1 Captured Signals from the DCS Module. To understand and characterize how the DCS modified the received signal in time and amplitude, the oscilloscope captured signals at the I- and Q-channel output, ports A and B respectively in Figure 3.6. Table 3.9 shows the test matrix for these measurements.

Table 3.10: Test Matrix for DCS Gain and Offset Adjustment Characterization.

Location	DCS Adjustment (% rotation)
DCS Output	0
DCS Output	25
DCS Output	50
DCS Output	75
DCS Output	100

3.2.5.2 DCS Gain and Offset Adjustment Characterization. The first series of measurements in the Lab-Volt DCS adjustment characterization process characterized the gain adjustments for both the I and Q channel. The offset adjustment was held constant at 0% while the gain adjustment was stepped from 0% to 100% rotation in one-fourth increments. The oscilloscope captured the DCS output on port A in Figure 3.6. The maximum signal amplitude for each rotational position was captured using the oscilloscope's internal measuring features. Each measurement at each position was repeated six times. The same process was repeated on the Q channel. Table 3.10 shows the test matrix for the gain adjustment.

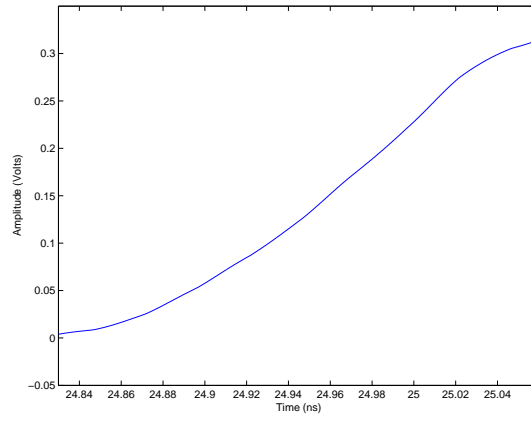
The second series of measurements in the Lab-Volt DCS characterization process characterized the offset adjustments for both the I and Q channel. The gain adjustment was held constant at 0% rotation while the offset adjustment was stepped from 0% to 100% rotation by a quarter of a rotation. The oscilloscope captured the DCS output at port A in Figure 3.6. Utilizing the oscilloscope's internal measuring features, the signal floor was measured for each rotational position. A single value describing the noise floor was generated for each rotational position. This process was repeated six times for each knob position. The same process was repeated on the Q Channel. Table 3.10 shows the test matrix for the offset adjustment.

3.3 Results

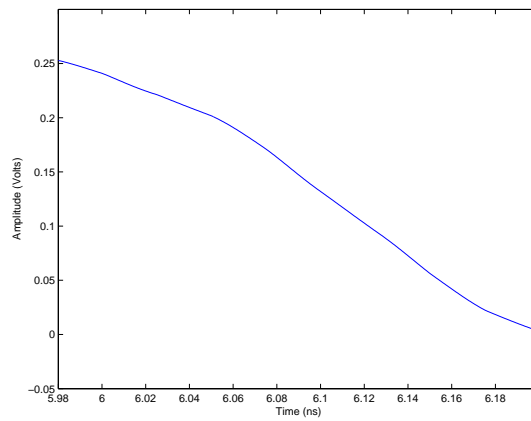
3.3.1 Transmitter Module Characterization.

3.3.1.1 Captured Signals from the Lab-Volt Transmitter Module. The results of the signals captured out of the Lab-Volt transmitter module are compared to the simulated Lab-Volt system presented in the following chapter. Those signals not presented in the following chapter are contained in Appendix B.

Figure 3.10(a) and 3.10(b) show the rise and fall time of a 1-ns pulse respectively. Rise and fall times for 2 and 5-ns pulses can be found in Appendix 3. The oscilloscope measured the rise and fall time of a 1-ns pulse to be 194 and 201-ps respectively. The



(a) Rise time.



(b) Fall time.

Figure 3.10: Rise and fall time of 1-ns pulse.

measured rise and fall time is well within oscilloscope limitations as outlined in the methodology.

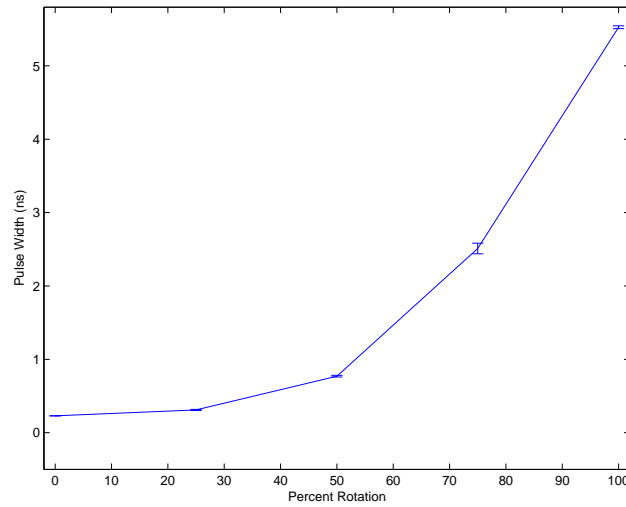


Figure 3.11: Pulse width adjustment characterization curve.

Table 3.11: Confidence Interval for Pulse Width Adjustment Characterization.

Adjustment Position (Percent Rotation %)	Lower CI (ns)	Upper CI (ns)
0	0.2294	0.2306
25	0.2957	0.3245
50	0.7473	0.7933
75	2.3648	2.6562
100	5.4878	5.5642

3.3.1.2 Transmitter Module Adjustment Characterization. Figure 3.11 shows the characterization of the pulse width adjustment as presented in Table 3.2. The pulse width adjustment has a nonlinear, possibly quadratic, influence on the pulse width. At no rotation, the pulse width 230 picoseconds. At full rotation, the pulse width exceeds 5-ns. The error bars are smallest at 0% rotation while they are a maximum at 75% rotation. This is anticipated and is a reoccurring trend across the characterization of all adjustments. Placing the adjustment at 0% or 100% rotation is a consistent location and hence the deviation between trials is significantly less.

The intermediate adjustment positions vary with a degree of human error. Table 3.11 shows the 95% confidence interval (CI) for each adjustment position. The CI and all further CIs were calculated using the t-distribution presented by [6]. The decimal places for each confidence interval is carried out to four places in order to distinguish between the upper and lower limits of the confidence interval at 0% rotation. The confidence intervals for remaining trials and other adjustment characterization curves are carried out to four decimal places for consistency.

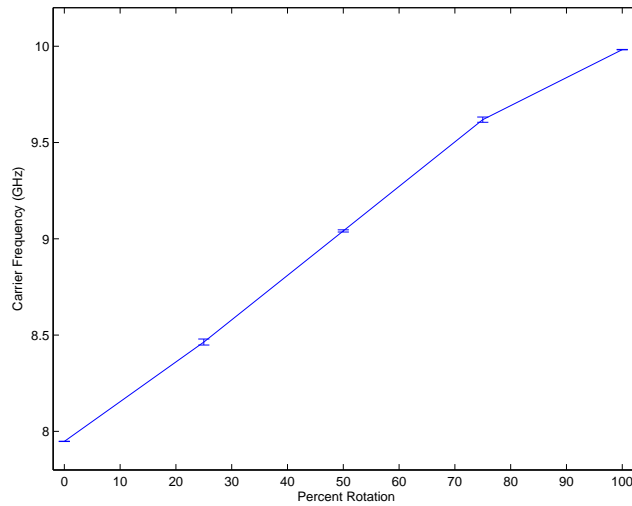


Figure 3.12: Carrier frequency adjustment characterization curve.

Table 3.12: Confidence Interval for Carrier Frequency Adjustment Characterization.

Adjustment Position (Percent Rotation %)	Lower CI (GHz)	Upper CI (GHz)
0	7.9463	7.9497
25	8.4330	8.4950
50	9.0296	9.0524
75	9.5912	9.6458
100	9.9799	9.9841

Figure 3.12 shows the characterization of the carrier frequency adjustment as presented in Table 3.3. The carrier frequency adjustment has a linear effect on the carrier frequency. The error bars are largest at a quarter and three-quarter rotation,

where human placement is susceptible to the most deviation. At no rotation, the pulse width adjustment produces a pulse width of several hundred picoseconds. At full rotation, the pulse width exceeds 5-ns. Table 3.12 shows the 95% CI for each adjustment position.

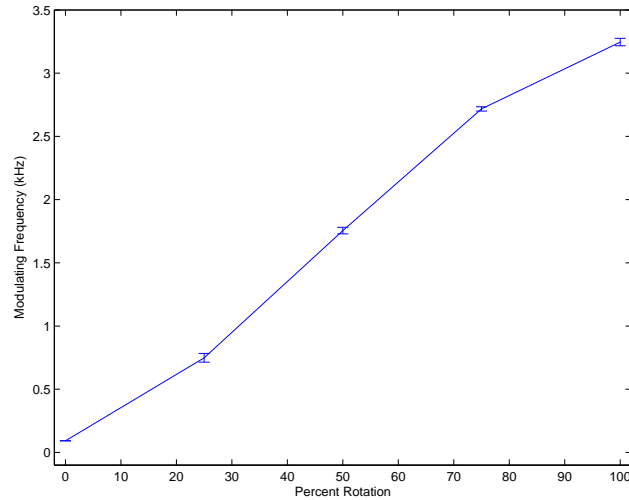


Figure 3.13: Modulating frequency adjustment characterization curve.

Table 3.13: Confidence Interval for Modulating Frequency Adjustment Characterization.

Adjustment Position (Percent Rotation %)	Lower CI (kHz)	Upper CI (kHz)
0	0.0916	0.0929
25	0.6791	0.8178
50	1.7029	1.8066
75	2.6830	2.7517
100	3.1875	3.3042

Figure 3.13 shows the results of characterizing the modulating frequency adjustment as presented in Table 3.4. As the modulating frequency adjustment linearly effects the modulating frequency. Unlike previous adjustment, a large variation between trials exists at 100% rotation. The variation in human adjustment is seen in the middle adjustment placement. The Lab-Volt transmitter manual specifies that the maximum modulating frequency is 2.5-kHz; however, characterization of the modulat-

ing frequency shows that the maximum modulating frequency exceeds 3-kHz. Table 3.13 shows the 95% CI for each adjustment position.

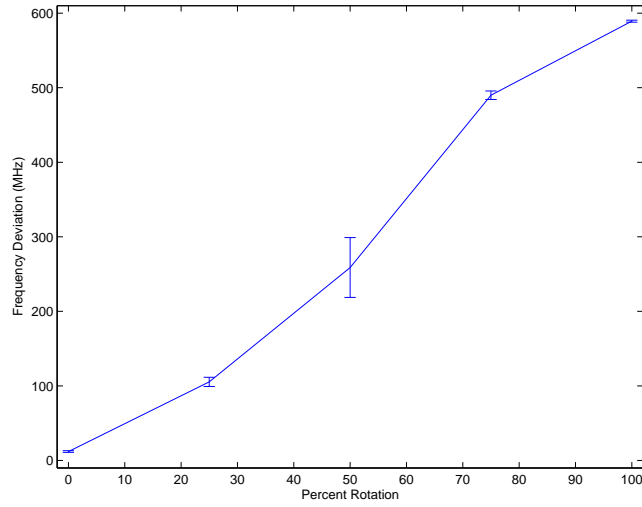


Figure 3.14: Frequency deviation adjustment characterization curve.

Table 3.14: Confidence Interval for Frequency Deviation Adjustment Characterization.

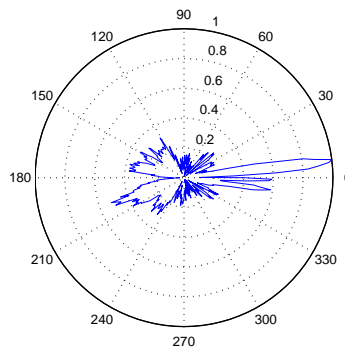
Adjustment Position (Percent Rotation %)	Lower CI (MHz)	Upper CI (MHz)
0	9.81	14.19
25	92.99	117.85
50	178.59	339.08
75	478.38	501.29
100	586.54	591.96

Figure 3.14 shows the results of frequency deviation adjustment characterization presented in Table 3.5. The frequency deviation appears to respond linearly to the frequency adjustment. The error bars are the least at the maximum and minimum rotation as expected; however, the error bar at 50% rotation is much larger than the other error bars. This is attributed to the same exact rotational position being achieved for each trial. Due to the manual placement, there is a degree of ambiguity between trials for the three adjustment positions between the maximum and minimum position. This ambiguity is seen in the increased error bars. Table 3.13 shows the 95%

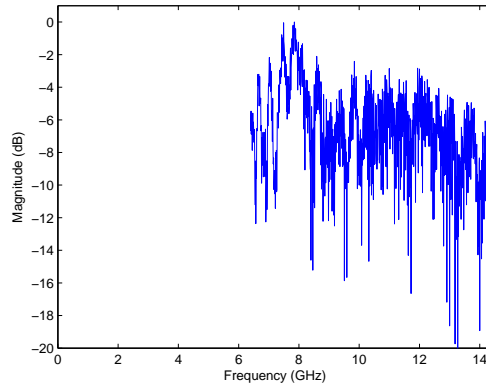
CI for each adjustment position. Table 3.14 shows the 95% CI for each adjustment position.

3.3.2 Antenna Characterization.

3.3.2.1 Signals Captured at RF Antenna Output. The captured 9.4-GHz PAM signal with a 1-ns signal pulse width is presented in the following chapter when it is compared to a simulated signal at the same location in the Lab-Volt system. Other signals captured are presented in Appendix B.



(a) Uncalibrated antenna pattern.

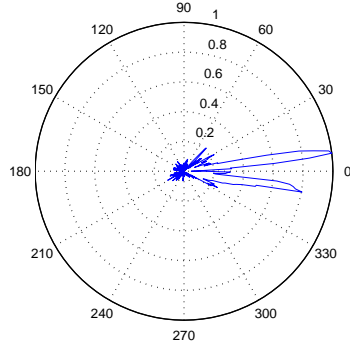


(b) Uncalibrated antenna pattern.

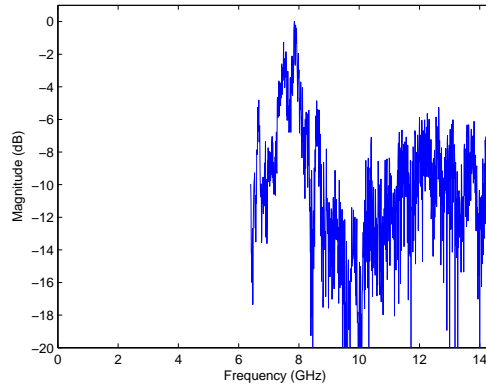
Figure 3.15: Uncalibrated signal prior to transmit antenna.

3.3.2.2 Lab-Volt Antenna Transfer Function Derivation. Figure 3.15(a) and 3.15(b) show the antenna pattern and antenna frequency response respectively for

the tracking antenna as generated from the raw data captured in the AFIT anechoic chamber. As anticipated for a tracking antenna, there are two broadside main lobes in the antenna pattern. The antenna uncalibrated frequency response gives no useful information.



(a) Gain calibrated antenna pattern.



(b) Gain calibrated antenna pattern.

Figure 3.16: Calibrated signal prior to transmit antenna.

Figure 3.16(a) and 3.16(b) show the antenna pattern and antenna frequency response respectively for the tracking antenna measurements calibrated for gain via the gain transfer method presented in Equation (3.1). When compared to Figure 3.15(a), Figure 3.16(a) loses the back lobe. This is highly desirable because a dish antenna would be expected to have a small back lobe. No note worthy differences occur between the calibrated and uncalibrated frequency response.

Antenna pattern and filter response plots are not best for analyzing the effects of phase calibration methods presented in Figure 3.9 because these plots are constructed by taking the magnitude of the data and thus discard the phase. To measure the effects of phase calibration, resulting time domain signal responses are observed.

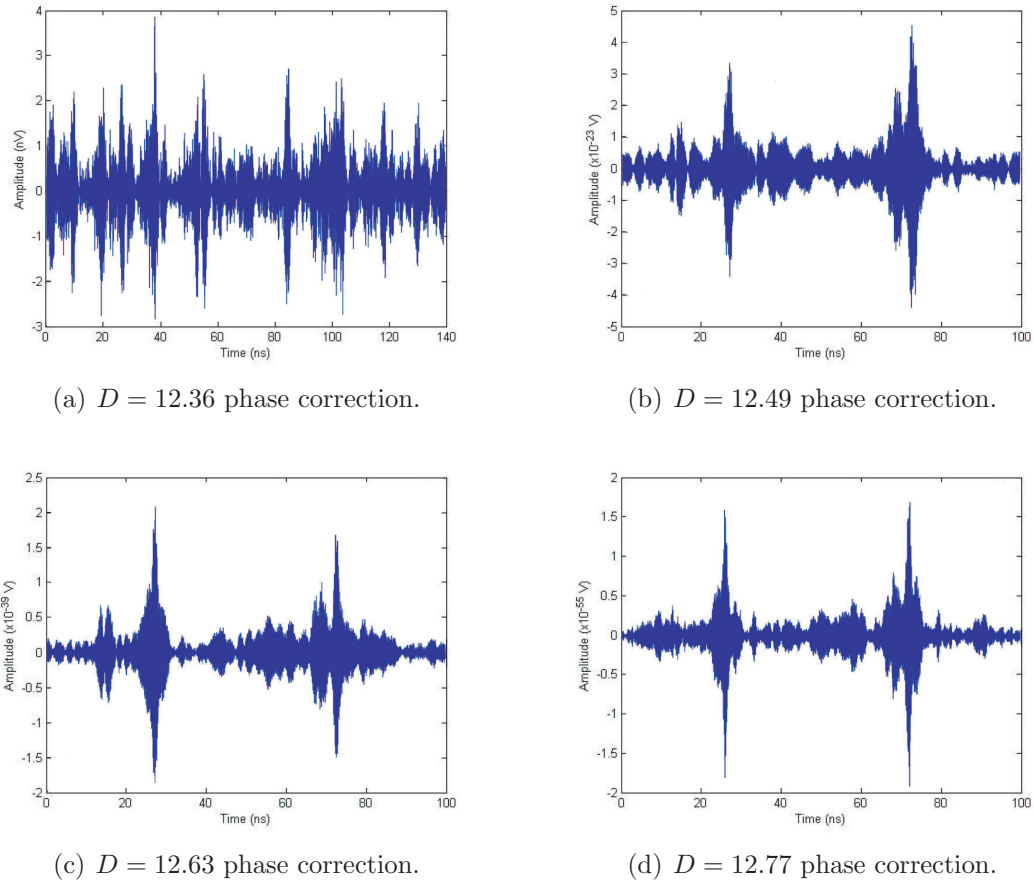


Figure 3.17: Signal post transmit antenna with gain and phase correction.

For phase calibration, antenna transfer functions derived from phase correction methods discussed in the methodology were applied to a signal made up of a 9.4-GHz carrier frequency with a 1-ns pulse width. Resulting time domain signals for four select transfer functions are plotted in Figure 3.17(a) through 3.17(d). With phase correction applied, more accurate signal spreading as governed by the reciprocal spreading theorem [8] is expected; however, anticipated results are not obtained. One distinct widened pulse is not seen. For this reason phase calibration techniques are not

carried to the Lab-Volt simulation. Only gain calibration techniques are implemented in the Lab-Volt simulation.

3.3.3 Receiver Module. The 9.4-GHz PAM signal with a 1-ns pulse width is presented in the following section where it is compared to a simulated signal at the same location in the Lab-Volt system. All other captured signals from Table 3.8 are presented in Appendix B.

3.3.4 DCS Characterization.

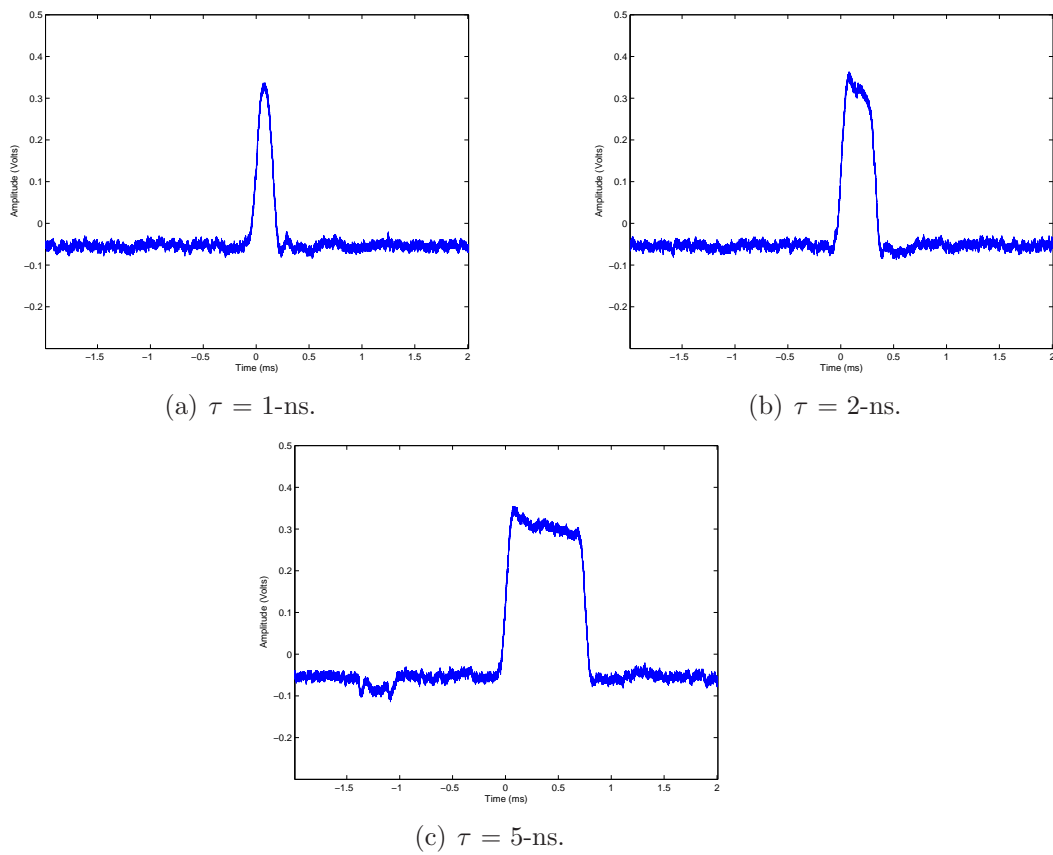
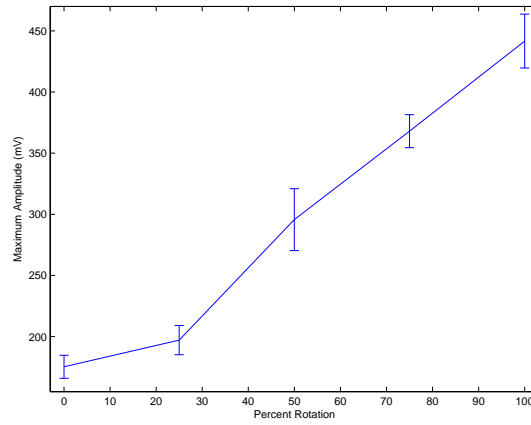


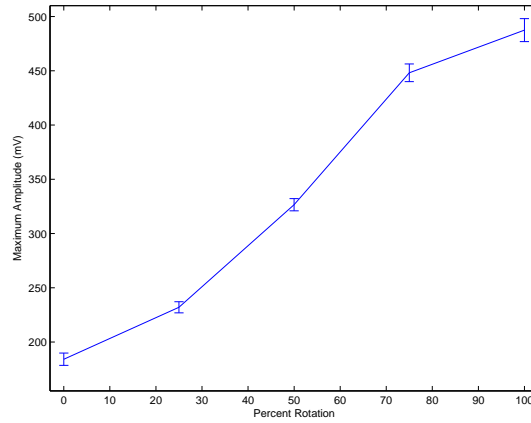
Figure 3.18: Lab-Volt dual channel sampler I-Channel RF output at 9.4-GHz carrier frequency.

3.3.4.1 Captured Signals from DCS Module. Figure 3.18(a), 3.18(b), and 3.18(c) show the I-channel output of the DCS module at 1, 2, and 5-ns pulse widths respectively. The DCS only modified the time interval. The amplitude was

not scaled. Appendix B contains the remainder of the signals captured out of the DCS I and Q channel.



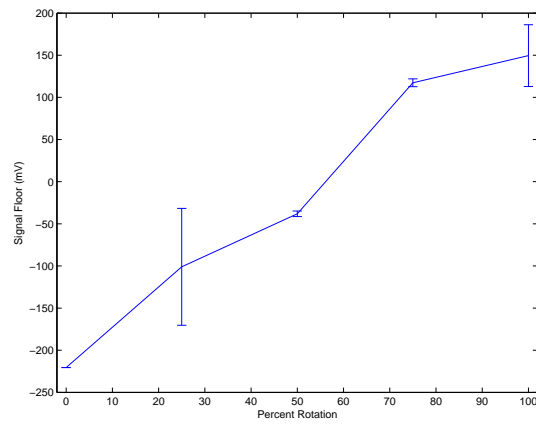
(a) I-Channel characterization curve.



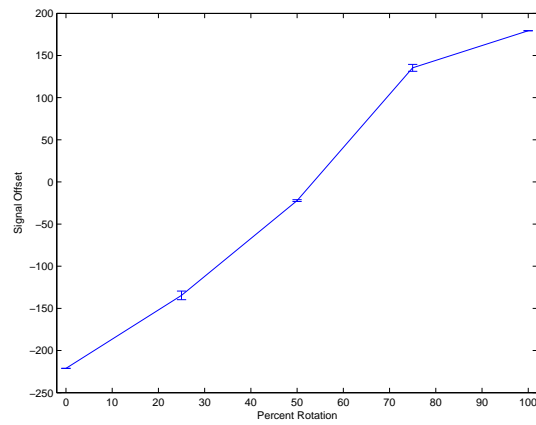
(b) Q-Channel characterization curve.

Figure 3.19: DCS gain adjustment characterization.

3.3.4.2 DCS Gain and Offset Adjustment Characterization. Figure 3.19(a) and 3.19(b) respectively show characterization curves for the I- and Q-channel gain adjustments as presented in Table 3.10. The I- and Q-channel gain adjustments produce linear responses in the DCS output signal. The error bars are tighter for the Q-channel characterization curve than the I-channel characterization curve. It is unsure if this is due to hardware variations or human placement of the gain adjustment. Table 3.15 and 3.16 respectively show the 95% CI for each adjustment position on the I- and Q-channel gain adjustment



(a) I-Channel characterization curve.



(b) Q-Channel characterization curve.

Figure 3.20: DCS offset adjustments characterization.

Table 3.15: Confidence Interval for I-Channel Gain Adjustment Characterization.

Adjustment Position (Percent Rotation %)	Lower CI (mV)	Upper CI (mV)
0	156.58	194.12
25	173.21	221.02
50	245.05	346.18
75	341.01	394.96
100	397.62	485.71

Table 3.16: Confidence Interval for Q-Channel Gain Adjustment Characterization.

Adjustment Position (Percent Rotation %)	Lower CI (mV)	Upper CI (mV)
0	172.81	195.46
25	221.71	242.29
50	315.28	337.73
75	431.81	464.39
100	466.31	508.59

Figure 3.20(a) and 3.20(b) respectively show characterization curves for the I- and Q-channel offset adjustments as presented in Table 3.10. The I- and Q-channel offset adjustments produce linear responses in the DCS output signal. As with the gain adjustment, the error bars are tighter for the Q-channel characterization curve than the I-channel characterization curve. It is unsure if this is due to hardware variations or imprecise human placement of the adjustment. Table 3.17 and 3.18 respectively show the 95% CI for each adjustment position on the I- and Q-channel offset adjustment.

Table 3.17: Confidence Interval for I-Channel Offset Adjustment Characterization.

Adjustment Position (Percent Rotation %)	Lower CI (mV)	Upper CI (mV)
0	-220.60	-220.60
25	-239.59	37.52
50	-44.79	-31.41
75	108.03	126.62
100	76.38	222.79

Table 3.18: Confidence Interval for Q-Channel Offset Adjustment Characterization.

Adjustment Position (Percent Rotation %)	Lower CI (mV)	Upper CI (mV)
0	-221.47	-220.90
25	-144.89	-124.31
50	-24.18	-20.02
75	127.21	143.52
100	179.40	179.40

IV. Extension of Lab-VoltTMSystem Characterization to Simulation

4.1 Chapter Overview

Chapter IV discusses the construction of the Lab-Volt simulation and its comparison to the measurements taken in the characterization process of Chapter III. After presenting the assumptions that govern the Lab-Volt simulation, the construction of the Lab-Volt simulation is presented through the simulation architecture. The initialization process and Lab-Volt simulation are stepped through. Signal comparison between the simulation and the corresponding measurements from the characterization process are made. Finally, the empirical antenna response developed in Chapter III is integrated with the simulation and results are compared to the captured signals in Chapter III.

4.2 Assumptions

4.2.1 Modeling Assumptions. The three-inch by three-inch rectangular plate that comes with the Lab-Volt system serves as the target in this simulation and for simplicity, the target's RCS is approximated by the RCS of a flat plate as defined by [20]. This approximation is

$$\sigma = \frac{4\pi A^2}{\lambda^2}, \quad (4.1)$$

where A is the physical area of the plate and λ is the wavelength of the carrier signal.

The target length is 6.27 wavelengths at a 9.4-GHz carrier frequency. Substituting these values into Equation (4.1) yields an RCS of 123.37-m². The Lab-Volt target is simulated as a point scatter at a range of 1.5-m, 47 wavelengths. It is assumed that the target is a point scatterer and RCS will not vary as a function of azimuth or elevation in this simulation. The parabolic antenna is modeled in this simulation as opposed to the tracking antenna. The parabolic antenna is not characterized so as to derive a transfer function as in Chapter III. Instead a gain of 23-dB as specified by

the Lab-Volt antenna manual [13] is applied to the antenna. Balanis [1] specifies the far-field of an antenna as

$$\frac{2D^2}{\lambda} \tag{4.2}$$

where D is the largest dimension of the antenna. The largest dimension of aperture of the horn antenna is measured to be 5-cm and through Equation (4.2) the far field of the parabolic antenna begins at 15.7-cm away from the aperture. At a range of 1.5-m, the simulated target is in the far field of the parabolic antenna.

4.2.2 Operational Assumptions. The Lab-Volt simulation is not a dynamic simulation. The Lab-Volt simulation is composed of m-files and is therefore a static simulation. The goal of this simulation is to establish a basis for comparison for the signals captured in the characterization process. M-files were relied upon for simplicity. Based on the execution time of the final simulation, 30.8 seconds, the Lab-Volt simulation cannot keep up with the PRF of the Lab-Volt system. For HILS integration, a dynamic simulation is desired.

4.3 Simulation Overview

The basic Lab-Volt simulation constructed in Matlab modeled the transmitter module, parabolic antenna, radiation environment to include the basic flat reflector previously described, and receiver module as seen in Figure 2.4. Each RADAR block presented in Figure 2.4 was given its own directory. Figure 4.1 shows the organization of the individual MatLab files within each directory. Figure 4.2 shows the sequence of events throughout the Lab-Volt simulation. The organization and content of the individual MatLab files was modeled after the process used in ARS [17] as presented in Chapter II. Ideally, each MatLab file has the potential to be integrated in a HILS configuration by replacing it with the corresponding RADAR hardware. With the exception of the antenna transfer function ideal conditions are modeled; noise is

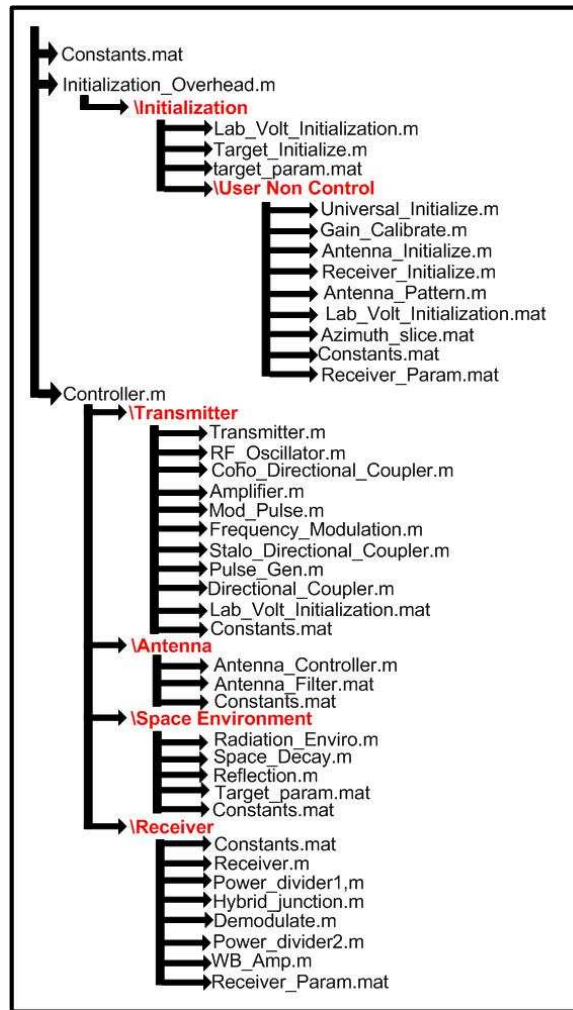


Figure 4.1: Lab-Volt simulation architecture.

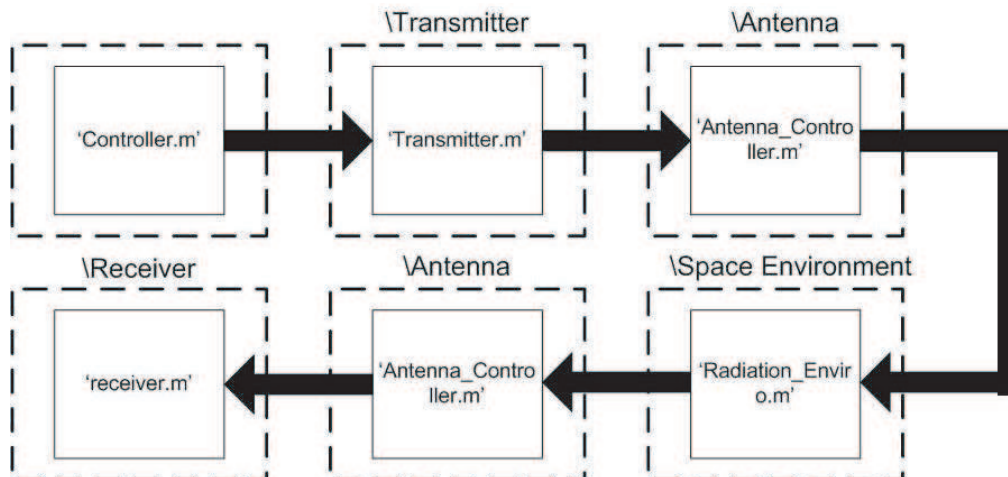


Figure 4.2: Overview of Lab-Volt file overview.

not introduced. As shown in Figure 4.1, the simulation has two hierarchical control modules that reside in the master directory: `Initialization_Overhead.m` and `Controller.m`.

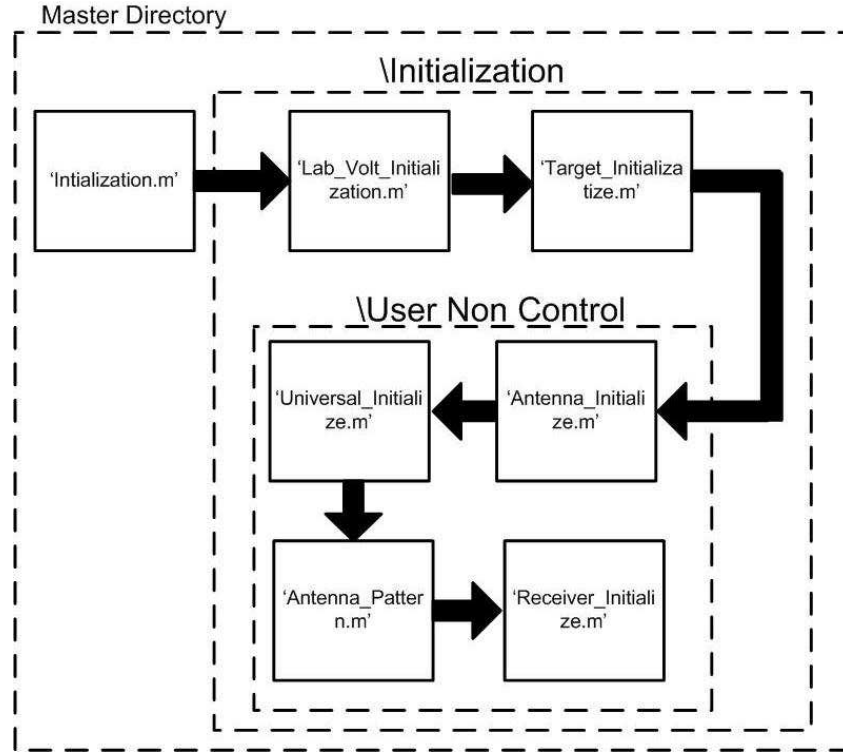


Figure 4.3: Lab-Volt initialization overview.

4.3.1 Simulation Initialization. Before running the simulation, `Initialization_Overhead.m` calls various initialization files located within `\Initialization` to set up the basic parameters of the Lab-Volt system. Figure 4.3 shows a block diagram of the initialization process.

Manipulating parameters within `\Lab_Volt_Initialization.m` controls the various operating options of the simulated Lab-Volt transmitter module to include: carrier frequency, FM frequency deviation and modulating frequency, pulse width, and CW or PM output. A potential addition would be to place a graphical user interface setting over `\Lab_Volt_Initialization.m` so as to allow the user to more conveniently select the various settings. Because this simulation is at the pulse level,

PRF selection is not modeled. For this simulation, the Lab-Volt system operates at a 9.4-GHz carrier frequency with a 1-ns pulse width and no frequency modulation. This operating set up is merely presented for illustration. The pulse width, carrier frequency, modulating frequency, and frequency deviation adjustments are set to a value between one and ten which corresponded to a minimum and maximum rotation respectively. Beyond the adjustment, the pulse width is set to 1, 2, or 5-ns. Lab-Volt operating parameters are saved in the file `Lab_Volt_Param.mat` under `\Transmitter`. `Target_Initialize.m` defines the dimensions and range of the small rectangular target based on the assumption previously discussed. Though equal in a monostatic RADAR model, the range from the target to the transmit antenna and from the target to the receive antenna are set independent of one another to allow for a general bistatic RADAR system. These parameters are saved in `\User Non Control` in the file `Target_Param.mat`.

A second set of initialization files defines aspects of the Lab-Volt simulation in which the user has no control. These files reside in `\User Non Control` within `\Initialization`. From the measured antenna data `Antenna_Initialize.m` determines the minimum, maximum, and frequency step from the raw antenna data. `Antenna_Initialize.m` also combines the upper and lower bandwidths of the raw antenna pattern data. `Antenna_Initialize.m` calls `Antenna_Pattern.m` to generate the azimuth antenna pattern and calls `Gain_Calibrate.m` to calibrate the gain with the standard gain horn data through Equation (3.1). The calibrated antenna pattern data is saved as `Azimuth_Filter.mat` within `\User Non Control` within `\Initialization`.

`Universal_Initialize.m` defines and saves the time vector, frequency vector, and speed of light to `Constants.mat` within `\Transmitter`, `\Receiver`, `\Antenna`, and `\Space Environment`. `Universal_Initialize.m` takes the minimum frequency, maximum frequency, and frequency step from the antenna pattern as inputs. Using Nyquist theory and Equations (2.5) and (2.6), a corresponding time vector is also created. Figure 4.4 shows a software block diagram of

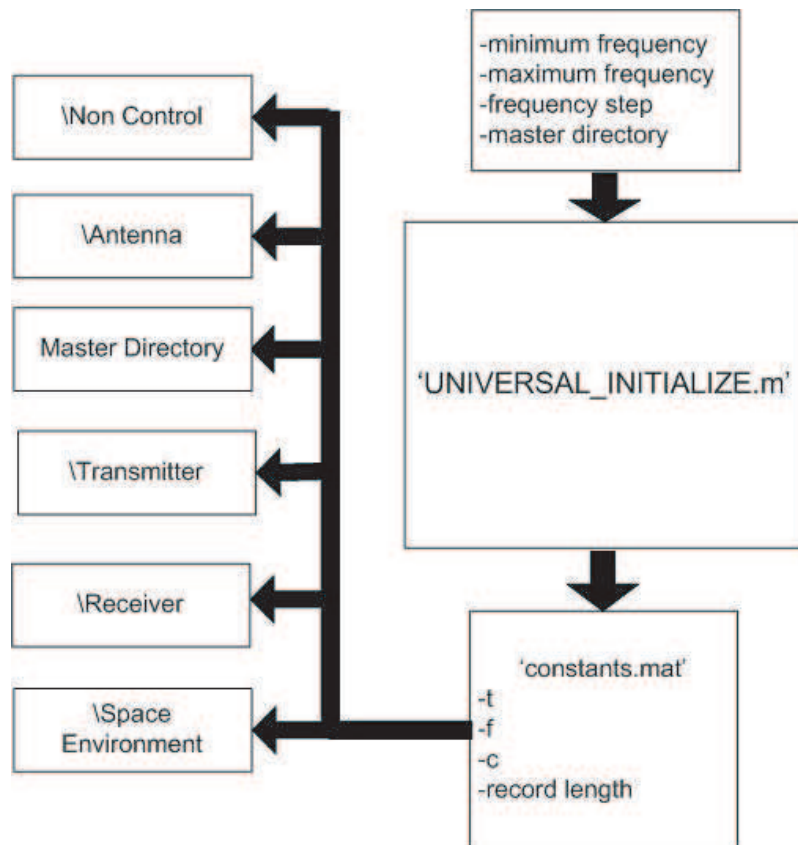


Figure 4.4: `Universal_Initialize.m` block diagram.

`Universal_Initialize.m` and the manner in which it interfaces with the initialization process. `Receiver_Initialize.m` defines the BPF on the PAM outputs of the I and Q channel and saves it within `\Receiver`.

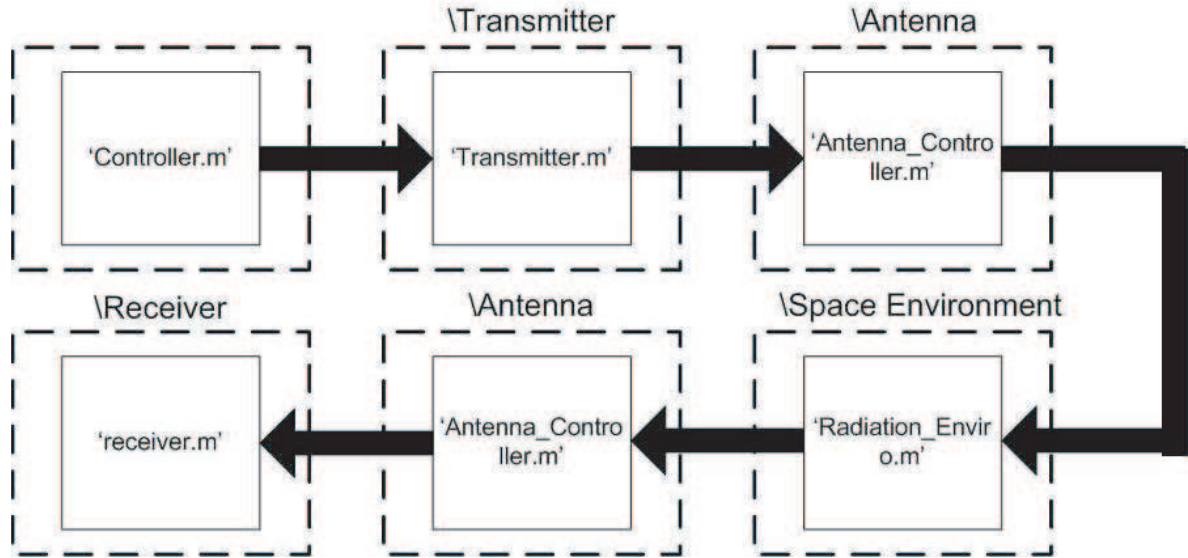


Figure 4.5: `Controller.m` block diagram.

4.3.2 Lab-Volt Simulation. The overhead program, `Controller.m`, coordinates the sequence of events for the major blocks of the RADAR diagram seen in Figure 2.4. In accordance with Figure 2.4 the sequence of functions called are `Transmitter.m`, `Antenna_Controller.m`, `Radiation_Enviro.m`, `Antenna_Controller.m`, and `Receiver.m`. `Controller.m` is located in the top level directory. Figure 4.5 shows a block diagram of `Controller.m` and how it interfaces with other MatLab files in other directories.

`Controller.m` begins a sequential operation that follows the complete signal path from transmit to receive. The first MatLab file called by `Controller.m` is `\Transmitter.m` and is located in `\Transmitter`. As shown in Figure 4.6, `Transmitter.m` coordinates all activities within the Lab-Volt transmitter module. `Transmitter.m` calls `RF_Oscillator.m` to generate the 9.4-GHz CW carrier signal. The manner in which the amplitude of the signal out of the RF os-

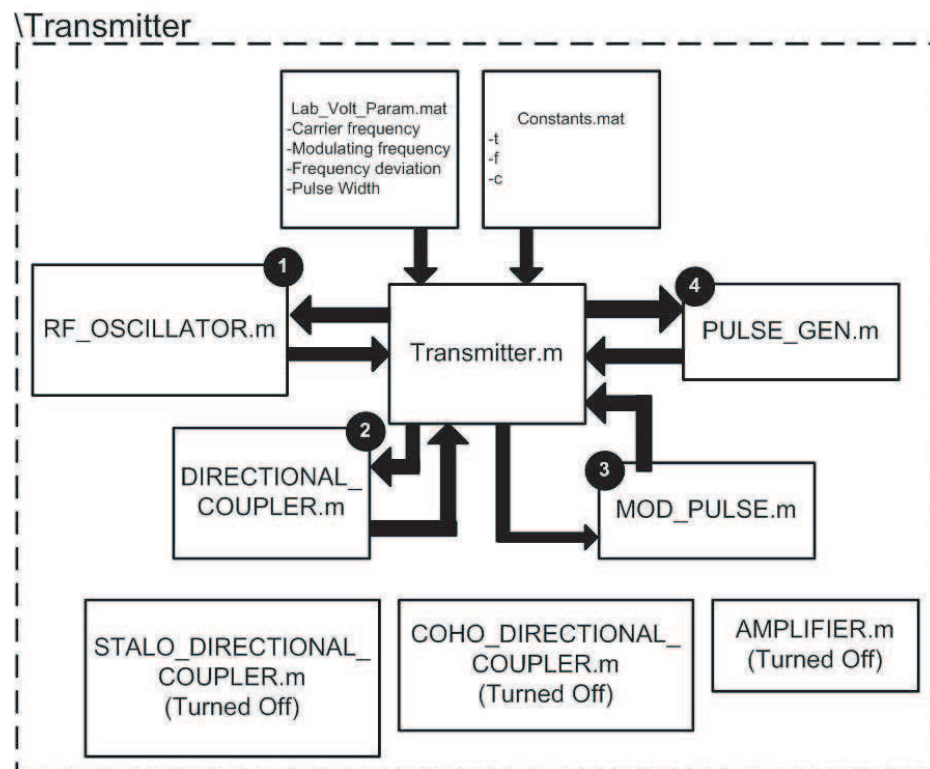


Figure 4.6: Transmitter.m block diagram.

cillator is determined is presented in the following paragraph. `RF_Oscillator.m` calls `Frequency_Modulation.m` to apply the selected modulating frequency and frequency deviation. No frequency modulation is applied for this simulation.

The characterization process conducted in Chapter III determined the ratio in which the directional coupler splits the signal from the RF oscillator between the CW and LO outputs of the Lab-Volt transmitter module. The characterization process also determined the amplitude of the RF oscillator prior to the directional coupler. Using Ohms Law and an assumed unity resistance, the voltage levels measured at the CW and LO outputs on the Lab-Volt transmitter are converted to a power. Assuming the directional coupler is lossless, the power out of the RF oscillator is the sum of the power measured out of the CW and LO outputs. Ratios of power into the directional coupler to power out of the LO and CW outputs are developed. In the Lab-Volt simulation, these power ratios are then applied in `Directional_Coupler.m` to the signal out of the RF oscillator to produce the LO and CW signals.

`Stalo_Directional_Coupler.m` and `Coho_Directional_Coupler.m` divide the signal between the transmitted signal and stable and coherent oscillator respectively. These have no functionality for the Lab-Volt simulation and are included to easily extend the simulation to a more complicated real world system. `Pulse_Gen.m` generates the pulse in which to modulate the CW signal. Based on signals captured in the characterization process, `Pulse_Gen.m` produces a pulse with an amplitude 0.3 V. `Mod_Pulse.m` modulates the pulse and the CW signal to generate the PM signal. `Amplifier.m` allows the Lab-Volt simulation to be easily extended to a high power real world system. It contributes no functionality to the Lab-Volt simulation.

`Antenna_Controller.m` located in `\Antenna` applies the calibrated antenna filter response to the signal. `Radiation_Enviro.m` located in `\Space Environment`, controls the activities that occur once the signal leaves the transmit antenna until it returns to the receive antenna. `Radiation_Enviro.m` calls the `Space_Decay.m` and applies the space decay encountered on the way to the tar-

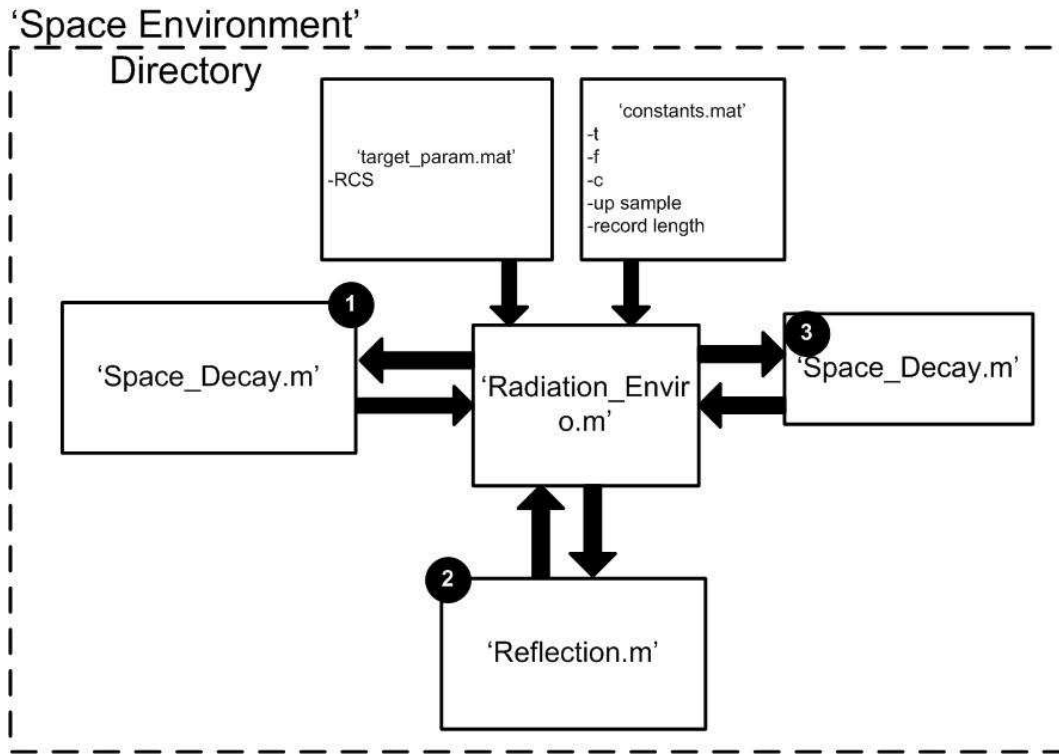


Figure 4.7: \Space Environment block diagram.

get as defined by the Fries transmission equation [1]. `Reflection.m` treats the small rectangular target as a point reflector as stated in the assumptions. `Space_Decay.m` is called a second time to model the signal decay encountered from the target to the receive antenna. To model signal reception at the receive antenna, the antenna filter response is applied to the signal a second time by calling `Antenna_Controller.m`. This process completes the transmitter, transmit antenna, radiating environment, and receive antenna blocks seen in Figure 2.4.

`Receiver.m` is the overhead controller for the simulated Lab-Volt receiver module and is located in `\Receiver`. `Power_Divider1.m` models the first power divider in the receiver and splits the received signal equally between the I and Q channel. `Power_Divider1.m` is ideal and lossless. `Hybrid_Junction.m` splits the LO signal from the transmitter so as to provide the LO for demodulation on the I- and Q-channel signals. Like the power divider, the hybrid junction is assumed ideal and lossless. A 90° phase shift is applied to the LO of the Q channel.

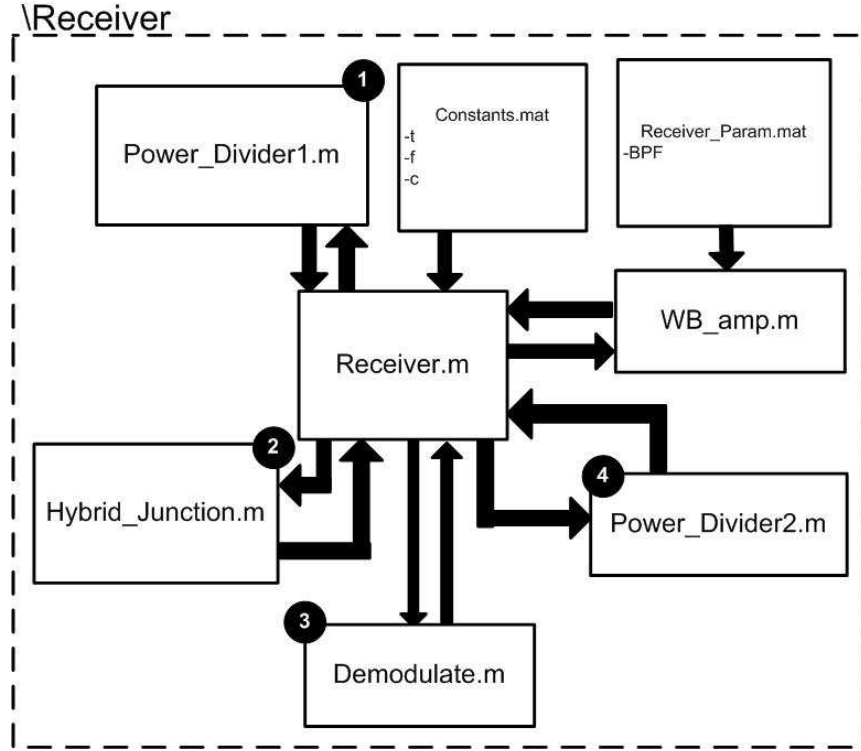


Figure 4.8: Receiver.m block diagram.

Demodulate.m modulates the split LO signals with the respective I- and Q-channel signal. Power_Divider2.m splits the demodulated signal between the PM and CW signal on the I channel and PM and FM CW signal on the Q channel. For simplicity, the LPF for the CW output on the I channel and the HPF for the FM CW signal on the Q channel are not modeled. The ideal wideband amplifier is identical for the I and Q channels.

4.4 Results

4.4.1 Comparison of Lab-Volt Simulation and Characterization Measurements.

4.4.1.1 Transmitter CW Signal. Figure 4.9 shows the measured and simulated signal at the CW output on the Lab-Volt transmitter module. By taking the inverse of the time between peaks, the simulated and measured frequency is 9.433-

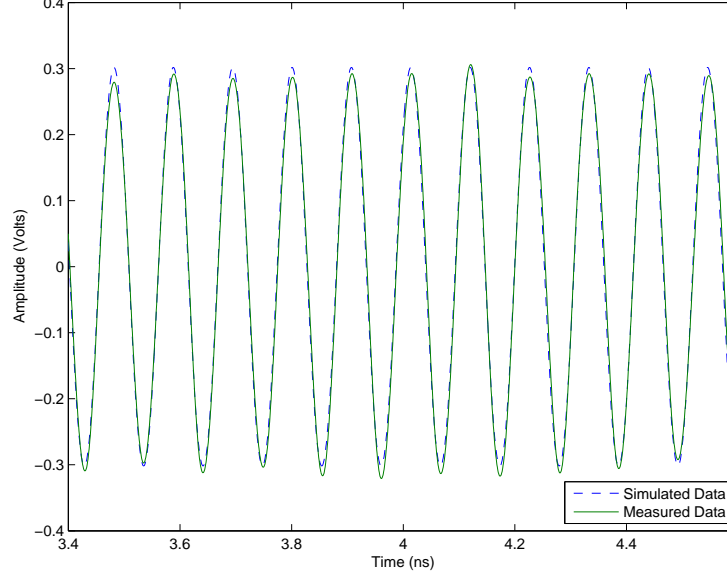


Figure 4.9: Comparison of simulation and measured data at CW output on Lab-Volt transmitter.

GHz and 9.524-GHz respectively. When compared to the ideal 9.400-GHz signal, the simulated and measured signal have an error of 0.36% and 1.31% respectively. The deviation in the simulated signal is attributed to the manner in which the 9.4-GHz signal is sampled in Matlab. The error in the simulated signal is removed if the sampling frequency is made to be an integer multiple of the carrier frequency such that the peaks of the signal fall on a sample as opposed to between samples. As discussed in the Section 4.3.2, the amplitude of the signal out of the RF oscillator is governed by the signal amplitudes measured out of the CW and LO outputs in the Lab-Volt characterization process. The peak-to-peak voltage of the measured and simulated CW output of the Lab-Volt transmitter is 0.62 and 0.60-V respectively. Because the amplitude of the simulated signal is based on the measured signal, the cause of the deviation in measured and simulated amplitudes is unknown. Using the measured signal amplitude as a baseline, the amplitude of the simulated signal has an error of 2.45%.

4.4.1.2 Transmitter LO Signal. Figure 4.10 shows the measured and simulated signal at the LO output of the Lab-Volt transmitter module. Extending

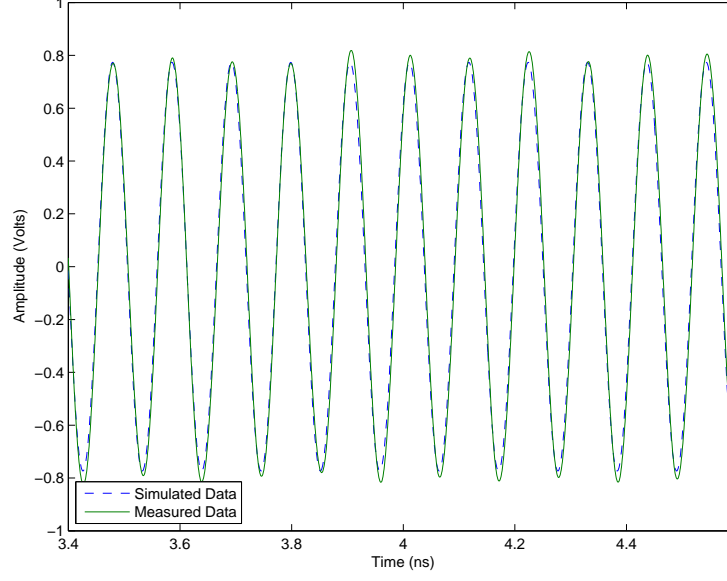


Figure 4.10: Comparison of simulation and measured signal at LO output of transmitter.

the process used with the CW signal, the simulated and measured frequency is 9.346-GHz and 9.434-GHz, respectively. When compared to the ideal 9.400-GHz signal, the simulated and measured signal has an error of 0.577% and 0.361% respectively. The peak to peak voltage of the measured and simulated LO output of the Lab-Volt transmitter is 1.63 and 1.55-V respectively. Using the measured amplitude as the nominal value, the simulated amplitude has an error of 5.39%.

4.4.1.3 Transmitter Module PAM Output. Figure 4.11 shows the simulated and measured PAM output of the Lab-Volt transmitter module. As before the simulated carrier frequency is 9.35-GHz and has a percent error of 0.58%. The measured signal had a carrier frequency of 9.434-GHz and a percent error of 0.36%. The peak voltage level of the simulated and measured signal is 0.32 and 0.42-V respectively. Using the measured signal amplitude as a reference, the percent error of the simulated signal is 21.88%. The nonideal rise and fall times of the measured signal are clearly noticeable.

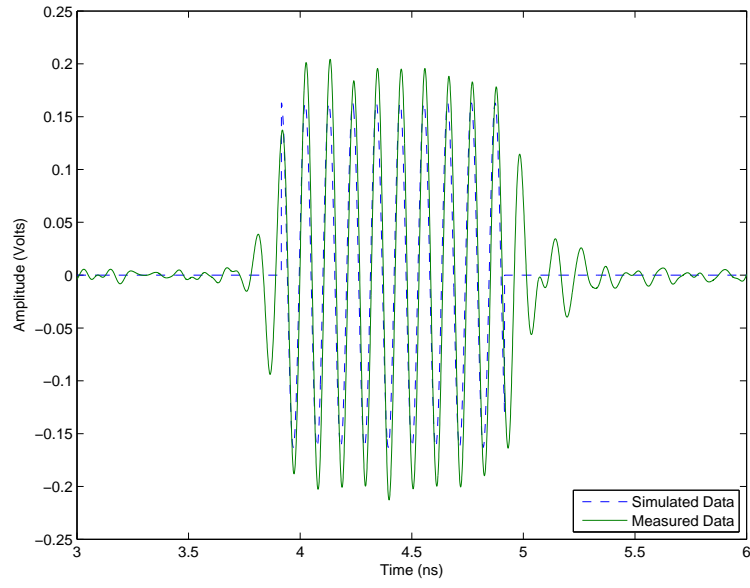


Figure 4.11: Comparison of simulated and measured signal at RF PAM output of transmitter.

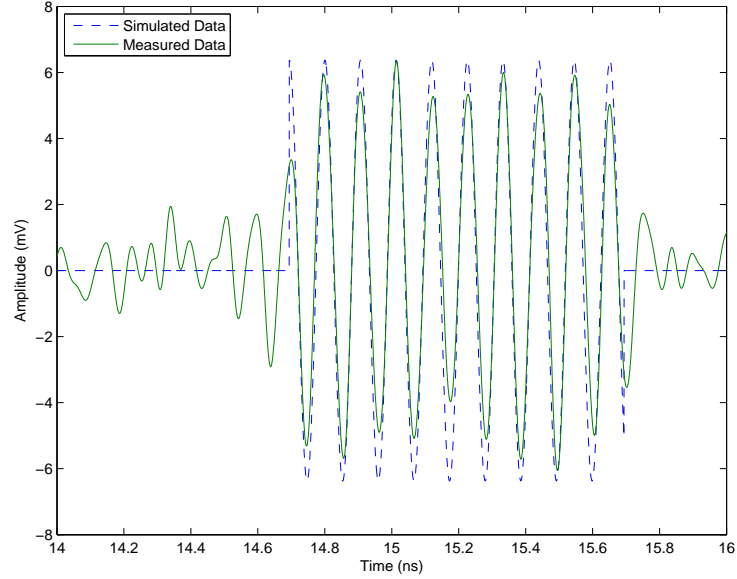
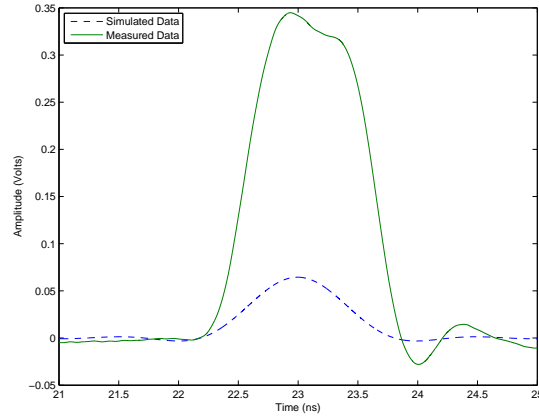
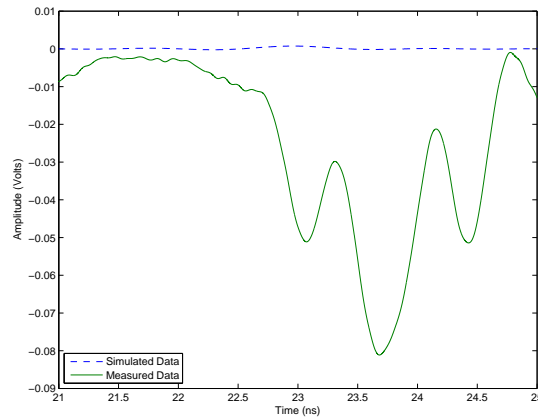


Figure 4.12: Comparison of simulated and measured signal RF output of antenna pedestal.

4.4.1.4 *Antenna Pedestal RF Output.* Figure 4.12 shows the simulated and measured output of the antenna pedestal. Both the measured and simulated signals have carrier frequencies of 10-GHz for an error of 6.383%. The simulated and measured signal have a peak-to-peak voltage of 12.4-mV and 12.4-mV for a percent error of 2.71%.



(a) I Channel.



(b) Q Channel.

Figure 4.13: Comparison of simulated and measured signal at PAM output of receiver.

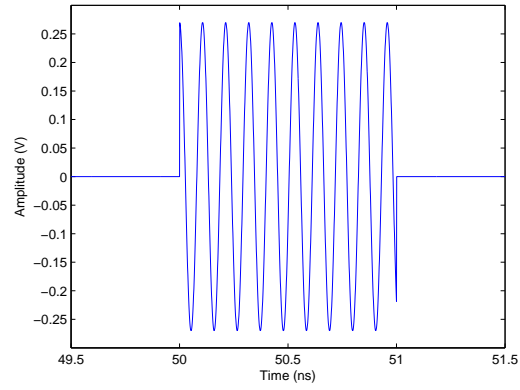
4.4.1.5 *PAM Output of Receiver Module.* Figure 4.13(a) and 4.13(b) respectively show I- and Q-channel PAM output of the Lab-Volt receiver module. Both Figure 4.13(a) and 4.13(b) show the simulated and measured data. For the simulated signal, a 90° phase shift is seen between the I and Q channel. For the simulated

data, Figure 4.13(a) shows the received signal on the I channel at a maximum while Figure 4.13(b) shows the received signal on the Q channel with a near zero amplitude. To stabilize the measured signal and eliminate much of the noise encountered, 5000 pulses were averaged on the oscilloscope. Because the signal is at baseband frequency analysis is not necessary. The maximum amplitude of the simulated I and Q channel is 64.5-mV and 7.36- μ V respectively. The maximum magnitude of the measured I and Q channel is 344.8 and 81.1-mV respectively. Using the measured signal as a baseline, the percent error on the I and Q channel is 81.30% and 100.91% respectively. The Q-channel error may appear extreme, but it should be noted that the Q channel signal is shifted ninety degrees compared to the I channel. Since the I channel is modeled at a maximum amplitude, the Q-channel amplitude should be zero. Any amplitude deviation away from zero would appear to have a large percent error. It is unsure why the measured I-channel signal is so much larger than the simulated. It should be noted that the difference is not extreme. The measured and received I-channel signals are within one order of magnitude.

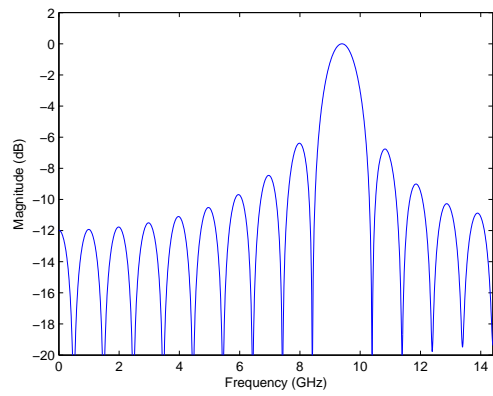
4.4.2 Integration of Antenna Characterization into Lab-Volt Simulation.

Prior to the transmit antenna, all data is simulated under ideal conditions. The signal in the time domain, Figure 4.14(a), has a 1-ns pulse with a 9.4-GHz carrier. The frequency domain plot, Figure 4.14(b), has a sinc function centered at 9.4-GHz with a 2-GHz mainlobe bandwidth. Anticipated results occur prior to the transmit antenna. These signals serve as a basis for comparison for signals after the transmit antenna.

Figure 4.15(a) and 4.15(b) show the signal in the time and frequency domain respectively just after the transmit antenna. The frequency domain plot shows how the bandwidth of the transmitted signal is limited by the transmit antenna. The antenna transfer function behaves like a band pass filter. A band pass filter incorporates the effects of a low pass filter and a high pass filter. The reciprocal spreading theorem states that decreasing the bandwidth causes the signal to widen in the temporal

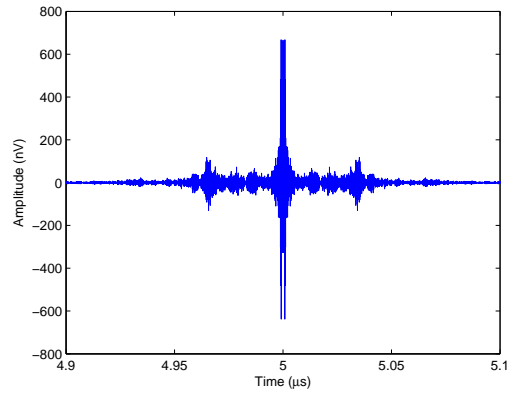


(a) Time domain.

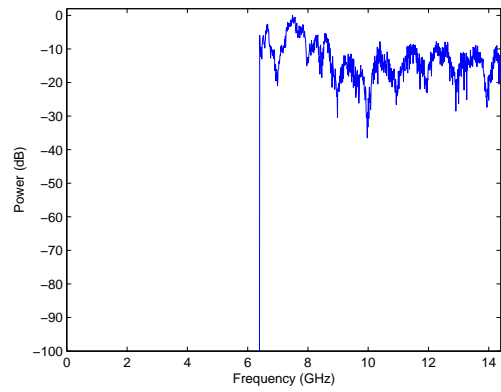


(b) Frequency domain.

Figure 4.14: Signal prior to transmit antenna.



(a) Time domain.



(b) Frequency domain.

Figure 4.15: Signal after transmit antenna.

domain [23]. Signal processing fundamentals state a high pass filter produces sharp edges in the temporal domain. Though not perfect in shape the time domain signal's envelope has anticipated signal spreading and sharp edges.

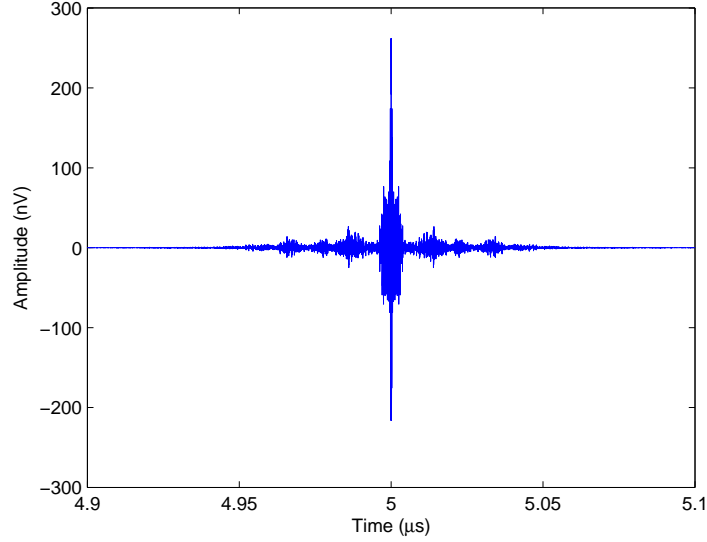


Figure 4.16: After reflection time domain.

Signal loss as governed by the Friis transmission equation occurs from the transmit antenna to the target. Beyond amplitude reduction, no figure is presented due to a lack of significant changes. Figure 4.16 shows the resulting signal after reflection off the small rectangular target previously discussed. Once again signal loss as governed by the Friis transmission equation occurs from the target to the receive antenna. Beyond amplitude reduction, no figure is presented due to a lack of significant changes.

Before entering the receiver module, the signal must pass through the receive antenna. Figure 4.17 shows the signal in the time domain after being filtered a second time by the transmit antenna. Once again signal widening and sharp edges occur.

As discussed in the Methodology of this chapter, receiver power dividers are assumed ideal and lossless in that they equally split signal levels. Beyond amplitude reduction, no figure is presented because no significant changes occur following the

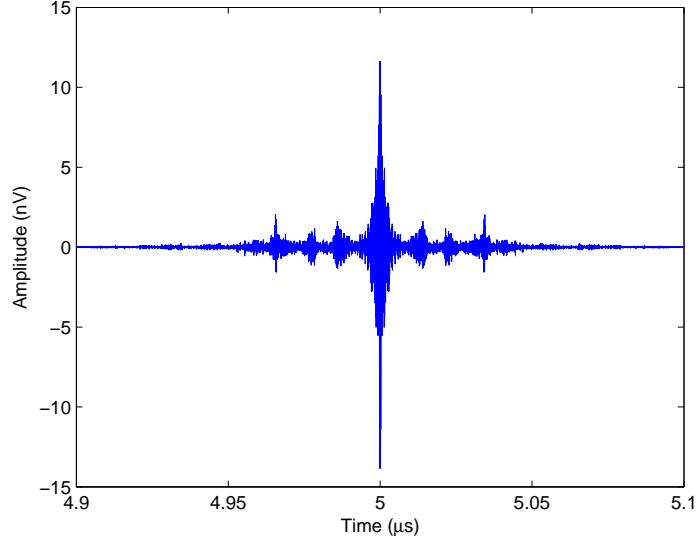
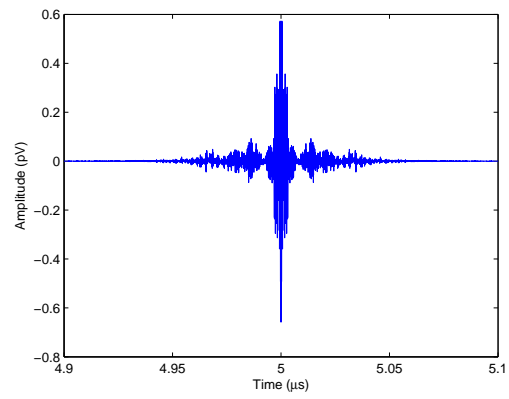


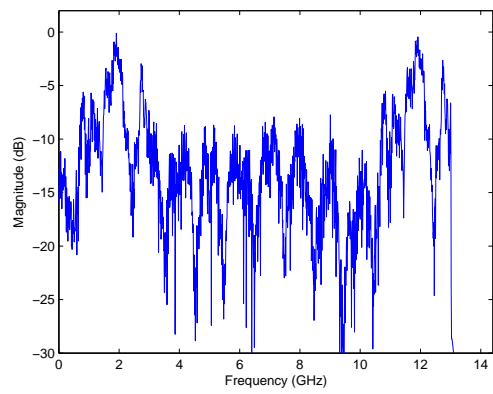
Figure 4.17: Time domain signal after receiver antenna.

receive antenna and power divider. Figure 4.18(a) and 4.18(b) show the signal in the time and frequency domain respectively after demodulation within the Lab-Volt receiver module. Comparing the pulse width of the time domain transmitted and demodulated signals, Figure 4.14(a) and 4.18(a) respectively, the demodulated signal has approximately twice the envelope of the transmitted signal. Following demodulation, both I and Q channels are split again; however, due to a lack of significant change a figure is not included.

Figure 4.19(a) and 4.19(b) show the I- and Q-channel signals after the wideband filter on the PAM channels. These output signals represent the final product of the Lab-Volt simulation. When compared to the envelope of the simulated ideal signal seen in Figure 4.14(a), a large degree of signal widening occurs. When compared to the original signal, it is unsure why the I- and Q-channel signals have large oscillations and peaks outside the main pulse.

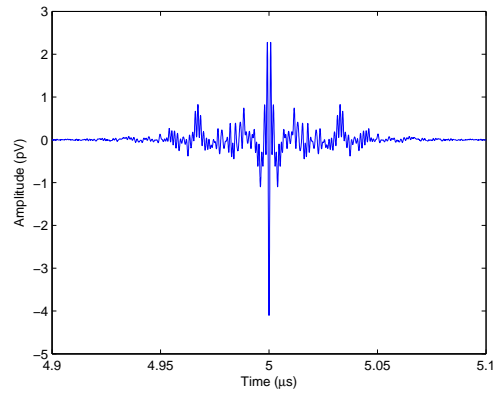


(a) Time domain.

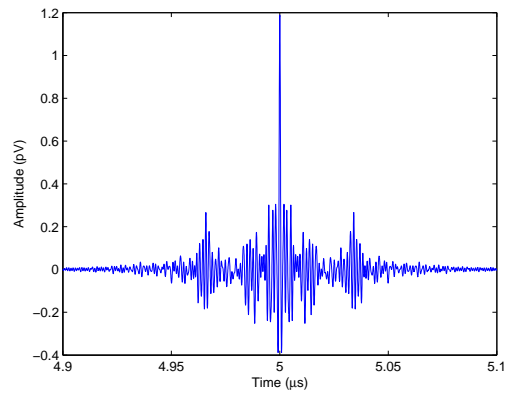


(b) Frequency domain.

Figure 4.18: Signal after demodulation.



(a) I-Channel signal.



(b) Q-Channel signal.

Figure 4.19: Signal in time domain after wideband amplifier.

V. Extension of Lab-Volt Characterization to Hardware in the Loop Simulation

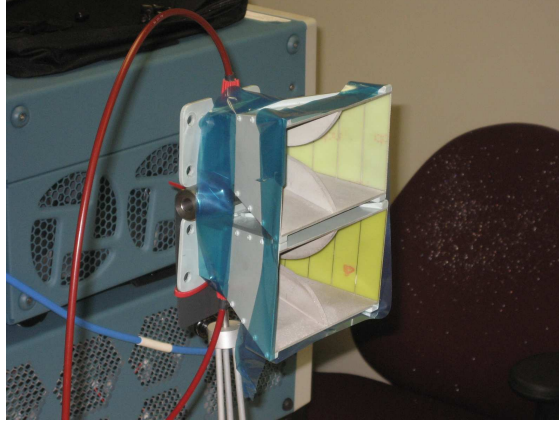
The final goal in this thesis is to integrate the Lab-Volt system in an elementary HILS configuration. The equipment used to produce the HILS configuration is introduced in the beginning of Section 5.1.1 followed by the various attempts to integrate the Lab-Volt system into a HILS configuration in Section 5.1.2. The successful HILS configuration is presented in Section 5.2 to include a thorough analysis of signals at each stage.

5.1 Methodology

5.1.1 Equipment . The Tektronix AWG7000 Arbitrary Waveform Generator generates signals that were injected into the Lab-Volt system. The AWG is capable of generating 10-Gsample/sec signals. The AWG technical manual [24] states that the AWG produces signals with a maximum frequency of 3.5-GHz and a maximum amplitude of $1-V_{PP}$. Options within the AWG selection menu allow a maximum carrier frequency of 5-GHz. The oscilloscope presented in Chapter III captured and analyzed received signals. Phase matched cables were used to connect the various components of the Lab-Volt system in the HILS configuration. Various other components were attempted; they are introduced and described as their need is discovered.

5.1.2 Unsuccessful Attempts At HILS Configuration . As discussed the AWG is incapable of generating a signal within the Lab-Volt, parabolic antenna's 8-10-GHz operating bandwidth. To overcome this problem, two American Electric Laboratories H-1498 860 2-18-GHz horn antennas were configured in a transmit and receive setup. Figure 5.1(a) shows a close-up of the transmit and receive horn antenna setup and Figure 5.1(b) shows the horn setup oriented towards the large reflective target.

From basic antenna properties presented by Balanis [1] the horn antenna setup will have a significantly less directivity than the Lab-Volt parabolic reflector. From



(a) Close-up of transmit and receive horn antenna setup.



(b) Horn antenna setup and large reflective target.

Figure 5.1: Horn antenna setup.

the RADAR range equation, Equation (2.14), the received power for the horn antenna setup will be significantly less. A larger antenna beamwidth will also be more susceptible to clutter and multipath. To increase signal strength a Hewlett Packard 8349B Microwave Amplifier was incorporated prior to the transmit antenna.

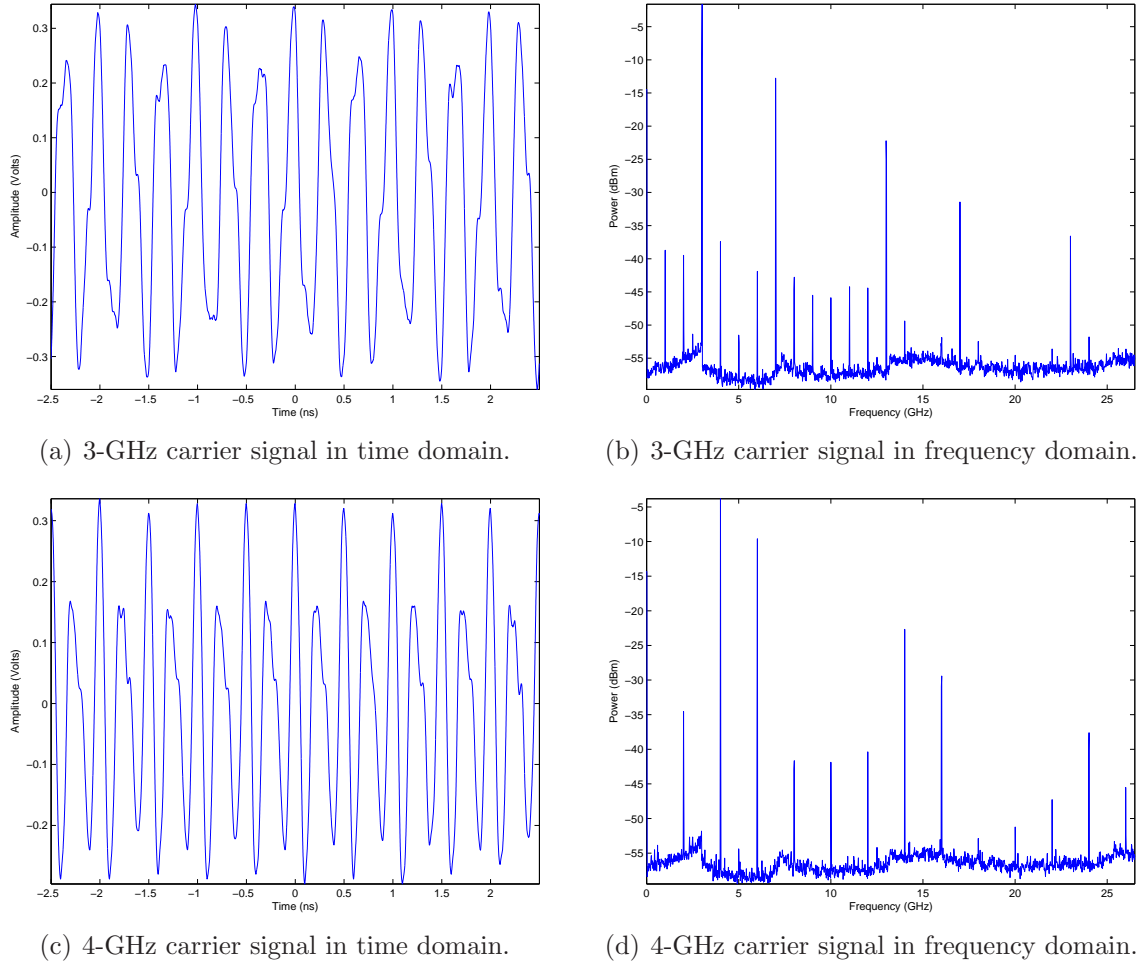


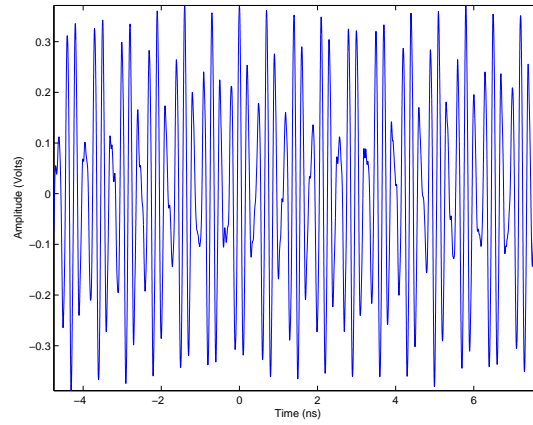
Figure 5.2: Various carrier signals out of the AWG.

The lowest allowable carrier frequency was limited to 2-GHz by the amplifier and horn antenna. The highest carrier frequency was limited to 5-GHz by the AWG. The AWG digitally generates all signals. As the carrier frequency approached the AWG's limit the signal became less smooth due to a lower sampling rate relative to the carrier frequency. Figure 5.2(a) and 5.2(b) show a 3-GHz signal in the time and frequency domains respectively. Figure 5.2(c) and 5.2(d) show a 4-GHz signal

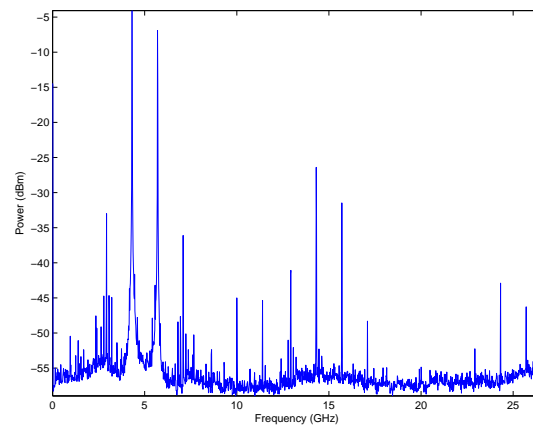
in the time and frequency respectively. Anticipated higher harmonics as a result of the digitally generated signals are seen in the frequency domain plots. For reasons discussed later, a 4.30625-GHz carrier is chosen. A carrier close to 4-GHz is chosen because it is well above the horn antenna's 2-GHz cutoff frequency and produces a quality sinusoidal signal within the AWG's limitations.

Two signals were produced by the AWG: a 4.30625-GHz, PAM signal with a 5-ns pulse width and a 4.30625-GHz CW signal. The PAM signal's PRF is 97-Hz. The CW signal served as the LO for the Lab-Volt receiver module. Using a Boonton 4300 RF Power Meter, the power out of the Lab-Volt transmitter module's LO output is 12.19-dBm. According to the Lab-Volt receiver module manual [14], the typical signal LO power is 13-dBm and the maximum input power is 23-dBm. The 4.30625-GHz CW LO signal from the AWG produces 2.42-dBm. Another amplifier could not be obtained to bring the measured power levels to the sufficient power levels. The signal directly from the AWG must suffice as the LO for the input signal to the Lab-Volt receive module. When both signals were used for their respective purposes, the final signal at the PAM output of the Lab-Volt receiver module produced a sinusoidal signal. A defined pulse could not be seen. It is believed that modulating the PAM and CW signal from the AWG caused the higher harmonics in both signals to be shifted to a frequency within the passband of the Lab-Volt receiver module's wideband amplifier where they were amplified and dominated the received pulse. To solve this problem both the PAM and CW signal are filtered so as to remove the higher harmonics.

To preserve the shape of the pulse, the pass band of the filter applied to the PAM signal should be larger than the pass band of the filter applied to the LO signal. Two filters were available in the AFIT microwave lab: a 11689A Hewlett-Packard LPF with a 4.4-GHz cutoff frequency and a 33941 K&L Microwave Incorporated BPF with a 4.30625-GHz center frequency. To remove higher harmonics from the PAM signal, the BPF was applied to the LO signal from AWG. The LO signal from AWG is below the typical levels presented in the Lab-Volt receiver manual and measured amounts. To insure maximum signal preservation, the carrier frequency was set to the center



(a) Time domain.



(b) Frequency domain.

Figure 5.3: Unfiltered 4.30625-GHz CW LO signal.

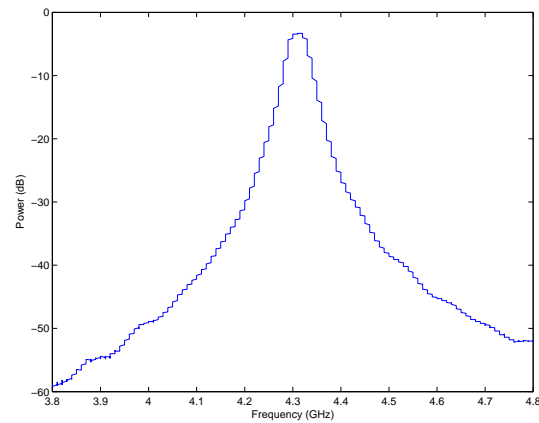
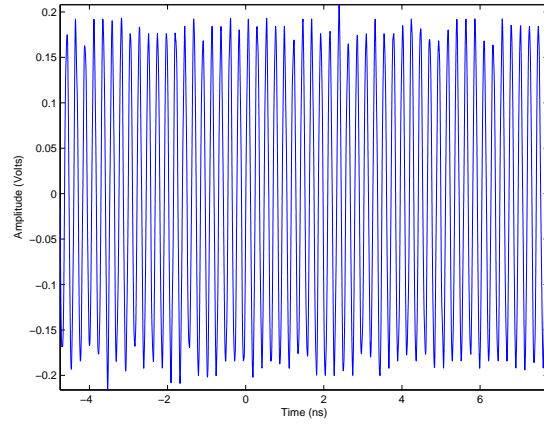
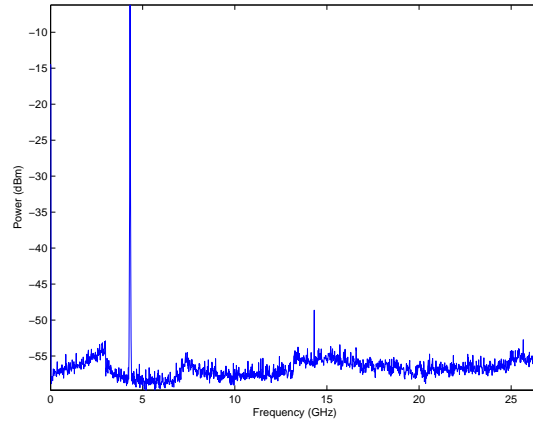


Figure 5.4: BPF response.



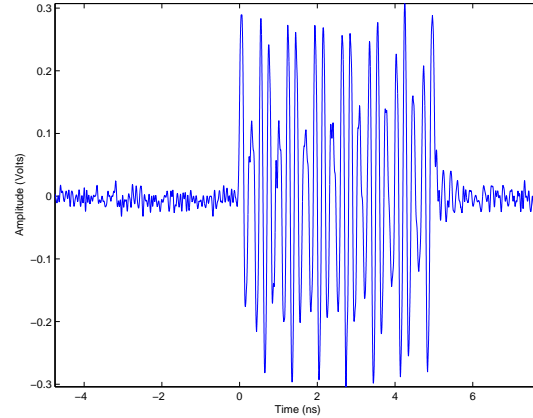
(a) Time domain.



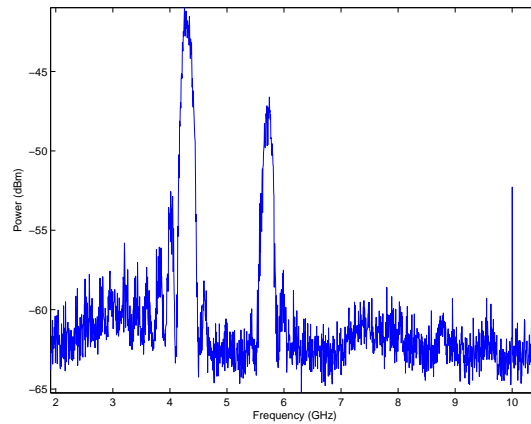
(b) Frequency domain.

Figure 5.5: Filtered 4.30625-GHz CW LO signal.

frequency of the bandpass filter. Figure 5.3(a) and 5.3(b) show the unfiltered CW signal in the time and frequency domain respectively. Figure 5.5(a) and 5.5(b) show the LO signal after filtering. In the frequency domain, the higher harmonics are greatly reduced and the effects are clearly seen in the time domain by a smoother signal.



(a) Time domain.



(b) Frequency domain.

Figure 5.6: Unfiltered 4.30625-GHz PAM transmitted signal.

As previously discussed the large pass band of the LPF was preferred for the 4.30625-GHz PAM signal so as to preserve the sinc envelope. Figure 5.6(a) and 5.6(b) show the unfiltered 4.30625-GHz PAM signal in the time and frequency domain respectively. Higher harmonics are observed in the frequency domain and their effects are evident in the time domain just as with the LO signal. The response of the LPF applied to the PAM signal is seen in Figure 5.7. The filtered PAM signal in the time

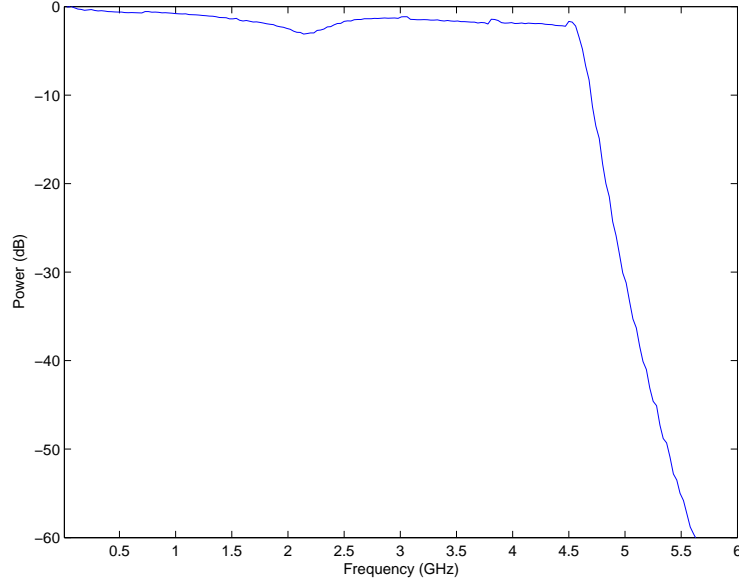
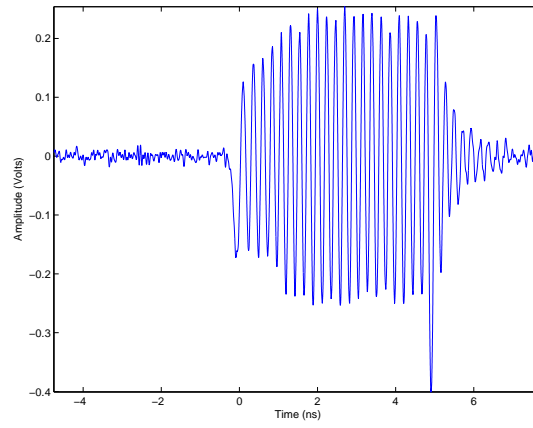


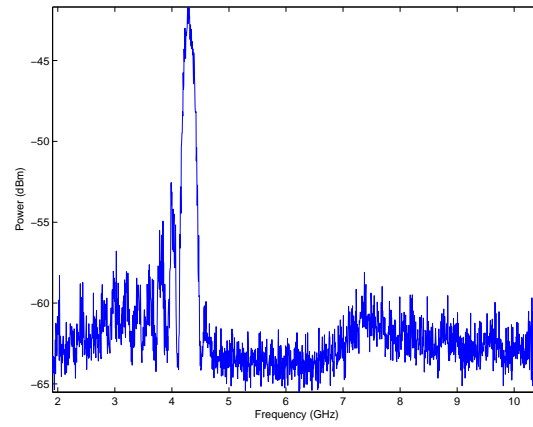
Figure 5.7: LPF response.

and frequency domain are seen in Figure 5.8(a) and 5.8(b) respectively. The higher harmonics have been removed and as a result the envelope of the received signal is wider.

With the previously discussed PAM signal, no components of the Lab-Volt transmitter module are included. It is the author's opinion that including more Lab-Volt modules in the HILS configuration increases the authenticity of the system being developed. Instead of using a digitally generated PAM signal from the AWG, an attempt was made to pass a 4.30625-GHz CW signal into the CW RF input, port J in Figure 3.3(b). When the CW signal from the AWG was injected into port J, no input was seen at the final output, port I. Upon closer examination of the Lab-Volt manual [15], port J can only accept frequencies in the 6 to 12.5-GHz bandwidth. The 4.30625-GHz signal from the AWG is unacceptable for injection into port J of the Lab-Volt transmitter module. The Lab-Volt transmitter module is hence eliminated from the HILS configuration all together.



(a) Time domain.



(b) Frequency domain.

Figure 5.8: Filtered 4.30625-GHz PAM transmitted signal.

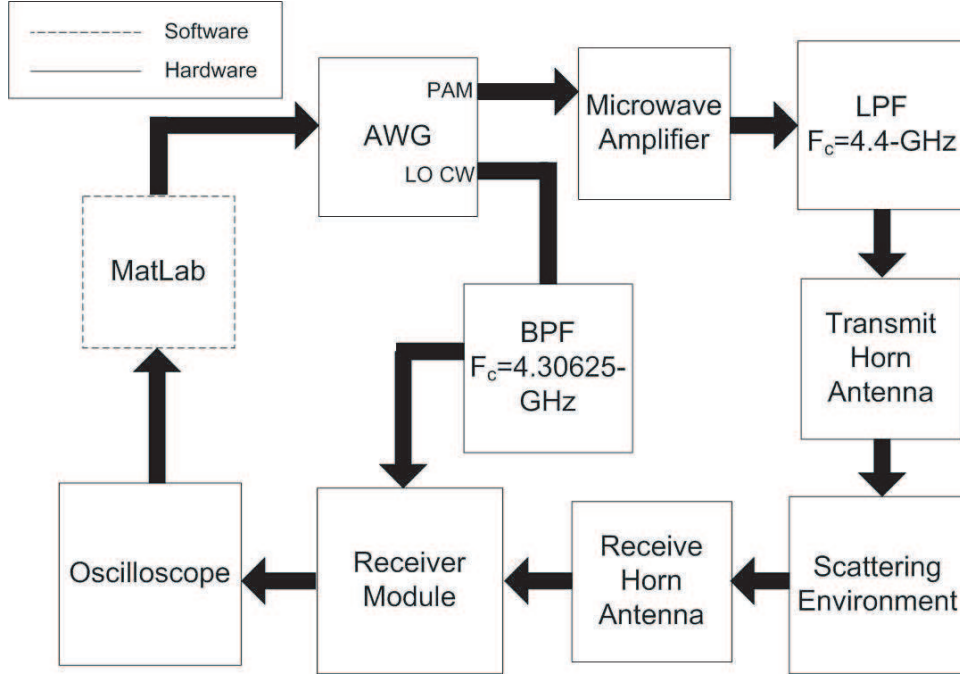


Figure 5.9: Lab-Volt integration into a HILS configuration

5.2 Successful HILS Configuration

Figure 5.9 shows a block diagram of the final successful HILS configuration. As previously discussed, the AWG produced a 4.30625-GHz CW signal shown in Figure 5.3(a) and 5.3(b) and a 4.30625-GHz PAM signal shown in Figure 5.6(a) and 5.6(b). The CW signal was filtered as shown in Figure 5.5(a) and 5.5(b) and injected into the input of the receiver modules LO. The PAM signal was filtered as shown in Figure 5.8(a) and 5.8(b) and injected into the amplifier. It should be noted that the MatLab connection between the oscilloscope and the AWG is a manual connection; the user must manually transfer information files from the oscilloscope to the AWG.

As shown in Figure 5.9, the filtered 4.30625-GHz PAM signal shown in Figures 5.8(a) and 5.5(a) are respectively fed into the amplifier and LO input of Lab-Volt receiver module. Figure 5.10 shows the amplifier output. The amplitude was increased to $4.928\text{-}V_p$.

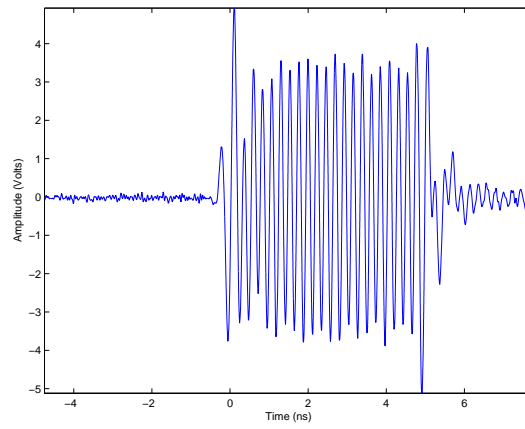


Figure 5.10: PAM signal following amplifier and LPF as seen in Figure 5.9.

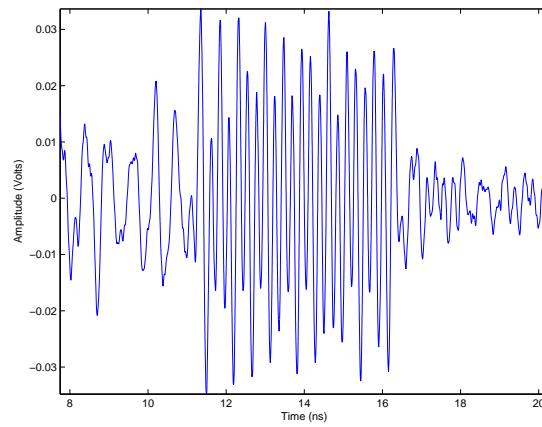
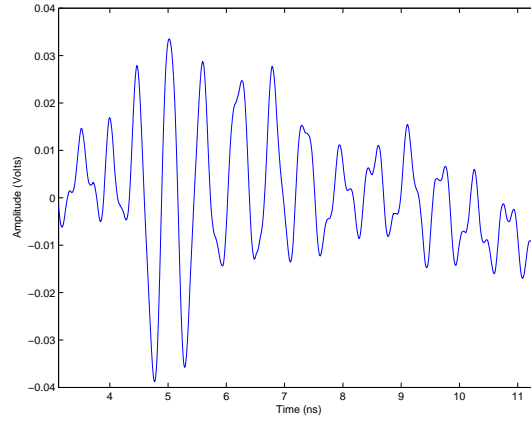
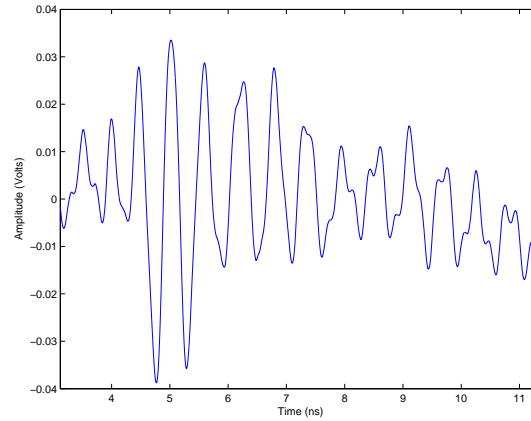


Figure 5.11: PAM signal following receive horn receive antenna as seen in Figure 5.9.

Figure 5.11 shows the received signal at the output of the receive antenna. The received signal amplitude is 33.64-mV_p . Though large amounts of noise are present, the original pulse shape in Figure 5.11 is predominately preserved.



(a) Receiver PAM output.



(b) Zoomed-in view of PAM output.

Figure 5.12: Received signal at PAM output of receiver module as seen in Figure 5.9.

Figure 5.12(a) shows the received signal at the PAM output of the Lab-Volt receiver module. Figure 5.12(b) zooms in on the received pulse in Figure 5.12(a). Due to the presence of a sinusoidal signal the microwave filters did not fully remove all harmonics, but the pulse width is comparable to the pulse width in Figure 5.11.

VI. Conclusion and Future Extent to this Work

The ability to accurately represent RADAR signals in software allows for the integration of RADAR simulations and hardware so as to achieve a HILS configuration. This work explored three areas: characterization of the Lab-Volt transmitter module, antenna, receiver module, and DCS module; creation of a static Lab-Volt simulation for comparison of the captured signals and with prospect of integration with RADAR hardware; and finally the Lab-Volt system was integrated in a HILS configuration. The degrees of success in each area is presented as well as potential areas of future exploration.

6.1 *Lab-Volt Characterization*

It should be noted that the characterization process performed is only for the Lab-Volt system. If another RADAR system is to be characterized, a characterization process tailored to that system and the hardware components within it must be developed so as to fully understand how the signal and error cascade through the RADAR system. If the Lab-Volt system in the HILS configuration presented in Chapter V were to be characterized, each additional hardware component to include the filters, microwave amplifier, and antennas would need to be characterized. Future efforts could be directed towards generating a template in which to guide the creation of a characterization process for any RADAR system. At the a minimum the template must contain the following:

- Measure all signals within the RADAR system to include frequency and modulation scheme parameters.

Determine the percent error between the specified and measured signal parameters.

- Identify all major hardware components within each module of the RADAR system.

Understand signal variations between the input and output for each hardware component in both the time and frequency domain.

- Statistically place numerical values on the manner in which adjustments effect the RADAR signal.

6.1.1 Transmitter Module. The Lab-Volt transmitter module was successfully characterized by capturing signals at various outputs so as to understand the signals at each output, the rise and fall times, and the manner in which the various adjustments affect the signal out of the transmitter.

6.1.2 Antenna Transfer Function. To simulate a received RADAR signal, signal variations introduced by the transmit and receive antenna must be fully understood. This research explores producing an empirical antenna transfer function that when applied to a simulated signal would produce an accurate output signal. It was anticipated that the antenna transfer function would band limit the signal in the frequency domain and produce signal spreading in the time domain. Uncalibrated antenna data produced an antenna pattern with dual lobes as anticipated for a tracking antenna. Gain calibration techniques presented by Balanis [1] produced desirable results. The main beam narrowed and the backlobe was omitted. The experimental phase calibration technique did not produce a desirable time domain signal and was not implemented in the Lab-Volt simulation. Reasons for phase calibration failure are unsure. The signal widening from the antenna transfer function was not as defined as expected. Gain calibrated antenna patterns produced anticipated results for a tracking antenna. It is believed the transfer function was flawed in that it did not correctly calibrate the phase. To produce an antenna transfer function with the correct phase response, future efforts should be directed at implementing the phase calibration method presented by Balanis [1].

6.1.2.1 Receiver and DCS Module. Signals out of the PAM I- and Q-channel outputs for the receiver and DCS module were captured at various pulse

widths and carrier frequencies. The DCS gain and offset adjustments were characterized. Q-channel offset and gain adjustments behaved as expected; the variance was large for both a quarter and three-quarter rotation. A large variance was experienced out of the I-channel offset and gain adjustments. All captured signals not presented in Chapter III and Chapter IV are presented in Appendix B. Future work could focus on characterizing the roll off of the WB amplifiers, LPF, and HPF and thoroughly understanding how demodulated signals are affected.

6.2 *Lab-Volt Simulation*

The Lab-Volt simulation was successfully integrated with the signals captured in the characterization process. Percent errors were established between the captured and simulated signals. Varying degrees of error were experienced at various locations of the Lab-Volt system. Future work can improve upon the Lab-Volt simulation by making it more real time and integrating it with the RADAR hardware in a HILS configuration. One potential for producing a real time simulation would be to explore the implementation in simulink.

6.3 *HILS Configuration*

After performing various modifications to the Lab-Volt system, the AWG, transmit and receive horn-antenna setup, Lab-Volt receiver module, and oscilloscope were integrated into a HILS configuration. Though low frequency harmonics appeared at the final output, the PAM output of the Lab-Volt receiver module showed a vague pulse waveform. The quality of the HILS configuration was greatly limited by the available microwave components available in the AFIT microwave lab. It is important to include as many Lab-Volt modules in the HILS configuration as possible so as introduce as much of the error encountered throughout the RADAR system as possible. The carrier frequency generated by the AWG prevented the use of the transmitter module and Lab-Volt parabolic antenna. Efforts should be taken to obtain mixers and filters that would produce signals at the standard Lab-Volt operating frequency.

If higher frequency signals can be generated, injection at various locations beyond the front panel of the various Lab-Volt modules can be explored. The faults inside the various modules are a potential for signal injection.

If individual components within the receiver or transmitter module are replaced with corresponding simulation files, it may be advantageous to explore approaching HILS from a controls perspective so as to insure various simulation files and hardware components correctly communicate and interface between one another.

The current HILS configuration presented in Figure 5.9 has a manual connection between the oscilloscope and the AWG. Future research could focus on connecting the oscilloscope and the AWG across an ethernet such that captured signals could be captured real time, analyzed, and the transmitted signal adjusted to exploit a desired effect. Future research can also explore the implementation of advanced RADAR processing techniques presented by Levanon [16] in a HILS configuration in an attempt to exploit target detection.

Appendix A. Matlab Code

Initialization_Overhead.m

```
0001 %Author: 2Lt Oscar Mayhew
0002 %Date working: 30 July 2007
0003 %Description: Overhead control for initialization of all parameters
0004 %           throughout the Lab Volt System. The following is intialized:
0005 %           1) Lab-Volt system parameters
0006 %           2) Target_Initialize
0007 %           3) Target Parameters
0008 %           4) Universal Data
0009 %Inputs: none
0010 %Outputs: none
0011 %Options:
0012 %Date editted:
0013 %Editions made:
0014
0015 close all
0016 clear all
0017
0018 Master_Directory=cd;
0019
0020 Intialization=strcat(Master_Directory,'\Intialization');
0021 cd(Intialization);
0022
0023 [f_car]=Lab_Volt_Initialize(Master_Directory);
0024 %once Lab-Volt system is initialized, the carrier frequency is known and
0025 %the antenna pattern that needs to be plotted can be determined
0026
0027 [azimuth,target_dim]=Target_Initialize(Master_Directory);
0028 %once the azimuth target location relative to boresight is known the angle
```

```

0029 %in angle to pick off the frequency response is known
0030
0031 %now go to the folder that initializes the parameters that the user has no
0032 %control over
0033 No_Control_Folder=strcat(Intialization,'\User Non Control');
0034 cd(No_Control_Folder);
0035
0036 %set whether the empirically derived antenna parameter will be used or the
0037 %standard gain given in the
0038 [f_min,f_max,f_step]=Antenna_Initialize(Master_Directory);
0039
0040 %once the important information from the antenna pattern plot is obtained
0041 %the time and frequency vectors can be defined
0042 Universal_Initialize(Master_Directory,f_min,f_max,f_step);
0043
0044 Receiver_Initialize(Master_Directory)

```

Lab_Volt_Initialize.m

```
0001 %Author: 2Lt Oscar Mayhew
0002 %Date working: 30 July 2007
0003 %Description: This function initializes the Lab-Volt system- based on the
0004 %assumptions made only the transmitter module is pertinent
0005 %Inputs: none
0006 %Outputs: none
0007 %Options:
0008 %Date editted:
0009 %Editions made:
0010
0011 function [f_c]=Lab_Volt_Initializes(Master_Directory)
0012
0013 %ALL KNOBS are on a scale from 0 to 10, with 0 turned all the way to the
0014 %left and 10 turned all the way to the right
0015
0016 INITIALIZE_FILE=cd;
0017
0018 %%%%%%%%%%%%%%%%%%%%%%%%%%%%%%%%%%%%%%%%%%%%%%%%%%%%%%%%%%%%%%%TRANSMITTER MODULE%%%%%%%%%%%%%%%%%%%%%%%%%%%%%%%%%%%%%%%%%%%%%%%%%%%%%%%%%%%%%%
0019 %OUTPUT LOCATION- based on where the signal is sent to the antenna
0020 %1: corresponds to CW/FM-CW RF OUTPUT
0021 %2: corresponds to PULSED RF OUTPUT
0022 OUTPUT_LOCATION=2;
0023
0024 %%%%%%%%%%%%%%%%%%%%%%%%%%%%%%%%%%%%%%%%%%%%%%%%%%%%%%%%%%%%%%%TRANSMITTER MODULE%%%%%%%%%%%%%%%%%%%%%%%%%%%%%%%%%%%%%%%%%%%%%%%%%%%%%%%%%%%%%%
0025 %TRANSMITTER BUTTONS- each variable corresponds to a pyhsical button on the
0026 %transmitter
0027 FREQUENCY_BUTTON=2; %can be 1,2,3- 1 is variable carrier frequency,
0028 %2 is for standard 9.4 GHz, 3 is for FM modulation
```

```

0029 FREQUENCY_KNOB=10; %this knob controls the variable carrier frequency
0030 FM_FREQUENCY_KNOB=2;%this knob controls the FM modulating frequency
0031 FM_DEVIATION_KNOB=10;%this knob controls the FM deviation
0032 PW_BUTTON=1; %can be 1,2,3,4- controls pulse width
0033 PW_KNOB=0; %only adjust if PW_BUTTON=4; controls variable pulse width
0034 %%%%%%%%%%%%%%%%%%%%%%%%%%%%%%%%%%%%%%%%%%%%%%%%%%%%%%%%%%%%%%%%%%%%%%%%%
0035
0036 %3 options are possible for the selection of the carrier frequency:
0037 %variable
0038 %between 8-12GHz, 9.4 GHz, FM modulation with 9.4GHz carrier
0039 switch FREQUENCY_BUTTON
0040     case 1
0041         f_c=(10e9-8e9)/10*FREQUENCY_KNOB+8e9;
0042         f_mod=0;
0043         f_dev=0;
0044     case 2
0045         f_c=9.4e9;
0046         f_mod=0;
0047         f_dev=0;
0048     case 3
0049         f_c=9.4e9;
0050         f_mod=(2.5e3-.1e3)/10*FM_FREQUENCY_KNOB+.1e3;
0051         f_dev=(500e6-0)/10*FM_DEVIATION_KNOB;
0052 end
0053
0054 %4 options are possible for the selection of the pulse width: 1ns, 2ns, 5ns,
0055 %or variable between 1ns and 5ns
0056 switch PW_BUTTON
0057     case 1

```

```

0058         tau=1e-9;
0059     case 2
0060         tau=2e-9;
0061     case 3
0062         tau=5e-9;
0063     case 4
0064         tau=(5e-9-1e-9)/10*FM_DEVIATION_KNOB+1e-9;
0065 end
0066
0067 %save the operating parameters to the transmitter folder
0068 TRANSMITTER_FOLDER=strcat(Master_Directory,'\Transmitter');
0069 cd(TRANSMITTER_FOLDER);
0070 save('Lab_Volt_Param.mat','f_c','f_mod','f_dev','tau','OUTPUT_LOCATION')
0071
0072 %save the operating paramters to the user non control folder
0073 INIT_FOL_NO_CON=strcat(Master_Directory,'\Intialization\User Non Control');
0074 cd(INIT_FOL_NO_CON);
0075 save('Lab_Volt_Param.mat','f_c','f_mod','f_dev','tau','OUTPUT_LOCATION')
0076
0077 cd(INITIALIZE_FILE);

```

Target_Initialize.m

```
0001 %Author: 2Lt Oscar Mayhew
0002 %Date working: 30 July 2007
0003 %Description: This function defines the range, azimuth and elevation
0004 %location relative to boresight, target velocity, target dimension for a
0005 %square target
0006 %Inputs: none
0007 %Outputs: none
0008 %Options:
0009 %Date edited:
0010 %Editions made:
0011
0012 function [azimuth,target_dim]=Target_Initialize(Master_Directory)
0013
0014 %define the elevation and azimuth location, simplest case is boresight
0015 azimuth=0;
0016 elevation=0;
0017
0018 %define target range from the receiver and transmitter, for a monostatic
0019 %system such as the Lab Volt system the distances are the same
0020 range_tx=1.5;
0021 range_rx=1.5;
0022
0023 %target velocity
0024 target_vel=0;
0025
0026 %define the dimensions of the target as .25 m- assumes a square target
0027 target_dim=.25;
0028
```

```
0029 No_Control_Folder=cd;
0030 %save parameters to the space enviroment folder
0031 Space_Enviro_Folder=strcat(Master_Directory,'\Space Environment');
0032 cd(Space_Enviro_Folder);
0033 save('target_param.mat','range_tx','range_rx','target_dim')
0034
0035 cd(No_Control_Folder)
0036 save('target_param.mat','range_tx','range_rx','target_dim')
```

Antenna_Initialize.m

```
0001 %Author: 2Lt Oscar Mayhew
0002 %Date working: 30 July 2007
0003 %Description: This function combines the raw antenna pattern data into
0004 %                something the RADAR model can effectively use.
0005 %Inputs: the master directory folder
0006 %Outputs: minimum, maximum, center, and step frequency for the antenna
0007 %response, the minimum, maximum, and stepped azimuth angles
0008 %Options:
0009 %Date edited:
0010 %Editions made:
0011
0012 function [f_min,f_max,f_step]=Antenna_Initialize(Master_Directory)
0013
0014 %save the current directory so we can return to it in the end
0015 No_Control_Folder=cd;
0016
0017 %go to the file where the RAW antenna data is stored
0018 RAW_DATA_FILE=strcat(No_Control_Folder,'\Raw Data Files');
0019 cd(RAW_DATA_FILE);
0020
0021 %grab the measurement PARAMETERS for the upper and lower bandwidths
0022 parameters_lower=dlmread('pattern3.spread','\t',[0 0 1 3]);
0023 parameters_upper=dlmread('pattern4.spread','\t',[0 0 1 3]);
0024
0025 f_min=parameters_lower(1,1)*1e9;
0026 f_cent=parameters_lower(1,2)*1e9;
0027 f_max=parameters_upper(1,2)*1e9;
0028 freq_point=parameters_lower(1,3);
```

```

0029 f_step=(f_cent-f_min)/(freq_point-1);
0030
0031 %define deg step information
0032 deg_point=parameters_lower(2,3);
0033 deg_min=-(deg_point-1)/2;
0034 deg_max=(deg_point-1)/2;
0035 deg_step=(deg_max-deg_min)/(deg_point-1);
0036
0037
0038 %grab the raw antenna DATA from the lower bandwidth
0039 data=dlmread('pattern3_spread','\t',2,0);
0040
0041 azimuth_slice1=zeros(freq_point,deg_point);
0042 %pick off all frequencies per each degree
0043 index=1;
0044 for index=1:1:deg_point
0045     %define frequencies
0046     azimuth_slice1(:,index)=data(freq_point*(index-1)+1:freq_point*...
0047         index,3)+i*data(freq_point*(index-1)+1:freq_point*index,4);
0048 end
0049
0050 %grab and the raw antenna data from the upper bandwidth
0051 data=dlmread('pattern4_spread','\t',2,0);
0052
0053 azimuth_slice2=zeros(freq_point,deg_point);
0054 %pick off all frequencies per each degree
0055 index=1;
0056 for index=1:1:deg_point
0057     %define frequencies

```

```

0058     azimuth_slice2(:,index)=data(freq_point*(index-1)+1:freq_point*...
0059         index,3)+i*data(freq_point*(index-1)+1:freq_point*index,4);
0060 end
0061
0062 %combine the upper and lower bandwidths of the antenna pattern, remember
0063 %that the center frequency is counted twice
0064 azimuth_slice=[azimuth_slice1(1:freq_point-1,:); azimuth_slice2];
0065
0066 %implement gain transfer method with the standard gain antenna
0067 cd(No_Control_Folder);
0068 [azimuth_slice]=Gain_Calibrate(azimuth_slice,freq_point,f_min,f_max);
0069 save('Azimuth_Slice.mat','azimuth_slice')
0070
0071 freq_point=2*freq_point-1;
0072 Antenna_Pattern(Master_Directory,f_min,f_max,freq_point,deg_max,deg_min,...
0073     deg_point,deg_step,azimuth_slice)

```

Antenna_Pattern.m

```
0001 %Author: 2Lt Oscar Mayhew
0002 %Date working: 1 May 2007
0003 %Description: This function defines parameters that are universal accross
0004 %               the Lab Volt system: speed of light, time vector and
0005 %               frequency vector as governed by the measured antenna pattern
0006 %               data
0007 %Inputs: the master directory folder, the minimum, maximum, and stepped
0008 %frequency, the carrier frequency; the index value for the minimum, center,
0009 %and max frequency; the antenna azimuth slice (dB vs frequency) and
0010 %minimum, maximum and stepped azimuth angle and stepped frequency points
0011 %Outputs: none
0012 %Options:
0013 %Date editted:
0014 %Editions made:
0015
0016 function Antenna_Pattern(Master_Directory,f_min,f_max,freq_point,...
0017     deg_max,deg_min,deg_point,deg_step,azimuth_slice)
0018
0019 load -mat azimuth_slice
0020 load -mat constants
0021
0022 azimuth=0;
0023 f_car=9.8e9;
0024
0025 %determine what index in the antenna pattern matrix that coresponds to the
0026 %desired carrier frequency and azimuth angle
0027 f_index=(f_car-f_min)*(freq_point-1)/(f_max-f_min)+1;
0028 deg_index=(azimuth-deg_min)*(deg_point-1)/(deg_max-deg_min)+1;
```

```

0029
0030 deg=deg_min:deg_step:deg_max;
0031
0032 %plot the antenna pattern
0033 figure(1)
0034 antenna_mag=abs(azimuth_slice(f_index,:));
0035 polar(deg*pi/180,antenna_mag/max(antenna_mag))
0036
0037 %determine the frequency step and the index in which the minimum frequency
0038 %is would occur if the frequency started at zero
0039 f_step=(f_max-f_min)/(freq_point-1);
0040 f_min_index=f_min/f_step;
0041
0042 %define a vector that is the same length as the frequency vector in
0043 %constants.mat, this will be the antenna filter response, add the antenna
0044 %response to the last part
0045 f_response=[zeros(1,f_min_index) azimuth_slice(:,deg_index)'];
0046
0047 %take the conjugate and mirror over the center frequency insuring not to
0048 %count the center frequency twice
0049 f_response=[f_response fliplr(conj(f_response(2:length(f_response))))];
0050
0051 figure(2)
0052 plot(f*1e-9,10*log10(abs(f_response)/max(abs(f_response))))
0053 xlabel('Frequency (GHz)')
0054 ylabel('Magnitude (dB)')
0055
0056 INITIALIZE_FILE=cd;
0057 ANTENNA_FOLDER=strcat(Master_Directory,'\Antenna');

```

```
0058 cd(ANTENNA_FOLDER);  
0059 f_sweep=f_response;  
0060 save('Antenna_Filter.mat','f_sweep')  
0061 cd(INITIALIZE_FILE);
```

Gain_Calibrate.m

```
0001 %Author: 2Lt Oscar Mayhew
0002 %Date working: 30 July 2007
0003 %Description: This function applies the gain transfer method as presented
0004 %by Balanis from the standard gain antenna
0005 %Inputs: the RAW parabolic antenna data accross the bandwidth at the
0006 %desired azimuth angle, the minimum and maximum value of the bandwidth and
0007 %the number of stepped frequency points
0008 %Outputs: gain calibrated antenna data in the form of azimuth angle by
0009 %degree step
0010 %Options:
0011 %Date edited:
0012 %Editions made:
0013
0014 function [antenna_data]=Gain_Calibrate(antenna_data,freq_point,f_min,f_max)
0015
0016 %save the current directory so we can return to it in the end
0017 No_Control_Folder=cd;
0018
0019 %go to the file where the RAW antenna data is stored
0020 RAW_DATA_FILE=strcat(No_Control_Folder,'\Raw Data Files');
0021 cd(RAW_DATA_FILE);
0022
0023 %Grab the calibrated antenna pattern and bandwidth for the FIRST range of
0024 %data
0025 data=dlmread('patter3_cal_spread','\t',2,0);
0026 [freq_point,ele]=size(data);
0027 freq_point=freq_point/361;
0028
```

```

0029 azimuth_slice1=zeros(freq_point,361);
0030 %pick off all frequencies per each degree
0031 index=1;
0032 for index=1:1:361
0033     %define frequencies
0034     azimuth_slice1(:,index)=data(freq_point*(index-1)+1:freq_point*...
0035         index,3)+i*data(freq_point*(index-1)+1:freq_point*index,4);
0036 end
0037
0038 %%%%%%%%%%%%%%%%%%%%%%%%%%%%%%%%%%%%%%%%%%%%%%%%%%%%%%%%%%%%%%%%%%%%%%%%%
0039 %Grab the calibrated antenna pattern and bandwidth for the SECOND range of
0040 %data
0041 data=dlmread('patter4_cal_spread','\t',2,0);
0042
0043 azimuth_slice2=zeros(freq_point,361);
0044 %pick off all frequencies per each degree
0045 index=1;
0046 for index=1:1:361
0047     %define frequencies
0048     azimuth_slice2(:,index)=data(freq_point*(index-1)+1:freq_point*...
0049         index,3)+i*data(freq_point*(index-1)+1:freq_point*index,4);
0050 end
0051
0052 %combine the upper and lower bandwidths of the antenna pattern
0053 [row,col]=size(azimuth_slice1);
0054 azimuth_slice=[azimuth_slice1(1:row-1,:); azimuth_slice2];
0055
0056 %convert the calibrated data to dB
0057 azimuth_slice=10*log10(abs(azimuth_slice));

```

```
0058
0059 %convert the antenna under test data to dB
0060 antenna_data=10*log10(abs(antenna_data));
0061
0062 %combine the calibrated and antenna under test data
0063 antenna_data=azimuth_slice+antenna_data;
0064
0065 %convert back to non dB
0066 antenna_data=10.^(antenna_data/10);
0067
0068 %back out the space loss
0069 cen_ped2base=23;
0070 wall2ped=290.5-cen_ped2base;
0071 space_loss=4*pi/wall2ped^2;
0072 antenna_data=space_loss^-1*antenna_data;
0073
0074 cd(No_Control_Folder)
```

Universal_Initialize.m

```
0001 %Author: 2Lt Oscar Mayhew
0002 %Date working: 1 May 2007
0003 %Description: This function defines parameters that are universal accross
0004 %               the Lab Volt system: speed of light, time vector and
0005 %               frequency vector as governed by the measured antenna pattern
0006 %               data
0007 %Inputs: the master directory folder, the minimum, maximum, and step
0008 %frequency
0009 %Outputs: none
0010 %Options:
0011 %Date editted:
0012 %Editions made:
0013
0014 function Universal_Initialize(Master_Directory,f_min,f_max,f_step)
0015
0016 c=3e9;
0017
0018 load -mat Lab_Volt_Param
0019
0020 f=0:f_step:2*f_max;
0021 t_step=1/2/f_max;
0022 t_max=1/f_step;
0023 t=0:t_step:t_max;
0024
0025 record_len=length(t);
0026 NON_CONTROL_FOLD=cd;
0027
0028 %save the basic files to the master directory
```

```

0029 cd(Master_Directory);
0030 save('Constants.mat','t','f','c','record_len')
0031
0032 %save the basic files to the transmitter folder
0033 TRANSMITTER_FOLDER=strcat(Master_Directory,'\Transmitter');
0034 cd(TRANSMITTER_FOLDER);
0035 save('Constants.mat','t','f','c','record_len')
0036
0037 %save the basic files to the receiver folder
0038 RECEIVER_FOLDER=strcat(Master_Directory,'\Receiver');
0039 cd(RECEIVER_FOLDER);
0040 save('Constants.mat','t','f','c','record_len')
0041
0042 %save the basic files to the antenna folder
0043 ANTENNA_FOLDER=strcat(Master_Directory,'\Antenna');
0044 cd(ANTENNA_FOLDER);
0045 save('Constants.mat','t','f','c','record_len')
0046
0047 %save the basic files to the space environment folder
0048 SPACE_FOLDER=strcat(Master_Directory,'\Space Environment');
0049 cd(SPACE_FOLDER);
0050 save('Constants.mat','t','f','c','record_len')
0051
0052 %save the basic files to the non control folder
0053 cd(NON_CONTROL_FOLD);
0054 save('Constants.mat','t','f','c','record_len')

```

Controller.m

```
0001 %Author: 2Lt Oscar Mayhew
0002 %Date working: 30 July 2007
0003 %Description: Top level control of emulation of Lab Volt radar system.
0004 %Designed for general bystatic case. "Initialization_Overhead.m" must be
0005 %before "Controller.m" in order to set up all the operating parameters .mat
0006 %file
0007 %Inputs: none
0008 %Outputs: none
0009 %Options: all operating options are adjusted in the initialization file
0010 %Date edited:
0011 %Editions made:
0012
0013 close all
0014 clear all
0015
0016 load -mat constants
0017
0018 fig_num=1; %keep track of the figures generated in each subprogram
0019 master_folder=cd;
0020
0021 %TRANSMITTER STAGE
0022 %for organizational purposes, all transmitter files are kept within the
0023 %\Transmitter directory
0024 transmitter_folder=strcat(master_folder,'\Transmitter');
0025 cd(transmitter_folder);
0026 [fig_num,signal,L0]=transmitter(fig_num,master_folder);
0027
0028 figure(fig_num)
```

```

0029 fig_num=fig_num+1;
0030 plot(t*1e9,signal)
0031 title('Final Output of Transmitter vs. Time')
0032 xlabel('Time (ns)')
0033 ylabel('Amplitude (V)')
0034 TX_OUTPUT=signal;
0035
0036 %{
0037 figure(fig_num)
0038 fig_num=fig_num+1;
0039 plot(f,10*log10(abs(fft(signal))/max(abs(fft(signal))))))
0040 xlabel('Frequency (GHz)')
0041 ylabel('Magnitude')
0042 title('Final Output of Transmitter vs. Frequency')
0043 %}
0044
0045 %TRANSMIT ANTENNA STAGE
0046 %the antenna has a finite band width- acts as a band pass filter
0047 %could apply a band pass filter to model this
0048 trans_ant_folder=strcat(master_folder,'\Antenna');
0049 cd(trans_ant_folder);
0050 [signal,fig_num]=ANTENNA_CONTROLLER(fig_num,signal);
0051 cd(master_folder);
0052 %{
0053 figure(fig_num)
0054 fig_num=fig_num+1;
0055 plot(t*1e9,signal)
0056 title('Output of Transmit Antenna vs. Time')
0057 xlabel('Time (ns)')

```

```

0058 ylabel('Amplitude (V)')
0059 %}
0060 %{
0061 figure(fig_num)
0062 fig_num=fig_num+1;
0063 plot(f,10*log10(abs(fft(signal))/max(abs(fft(signal))))))
0064 xlabel('Frequency (GHz)')
0065 ylabel('Magnitude')
0066 title('Output of Transmit Antenna vs. Frequency')
0067 %}
0068 %SCATTER STAGE
0069 %for organizational purposes, all scatter files are kept within a scatter
0070 %folder
0071 radiation_folder=strcat(master_folder,'\Space Environment');
0072 cd(radiation_folder);
0073 [signal,fig_num]=Radiation_Enviro(signal,fig_num,master_folder);
0074
0075
0076 %RECEIVE ANTENNA STAGE
0077 %the antenna has a finite band width- acts as a band pass filter
0078 %could apply a band pass filter to model this
0079 %for organizational purposes, all antenna files are kept within an antenna
0080 %folder
0081 trans_ant_folder=strcat(master_folder,'\Antenna');
0082 cd(trans_ant_folder);
0083 [signal,fig_num]=ANTENNA_CONTROLLER(fig_num,signal);
0084 cd(master_folder);
0085
0086 figure(fig_num)

```

```

0087 fig_num=fig_num+1;
0088 plot(t*1e9,signal)
0089 title('Output of Receive Antenna vs. Time')
0090 xlabel('Time (ns)')
0091 ylabel('Amplitude (V)')
0092 AN_OUTPUT=signal;
0093 %{
0094 figure(fig_num)
0095 fig_num=fig_num+1;
0096 plot(f,10*log10(abs(fft(signal))/max(abs(fft(signal)))))
0097 xlabel('Frequency (GHz)')
0098 ylabel('Magnitude')
0099 title('Output of Receive Antenna vs. Frequency')
0100 %}
0101 %RECEIVER
0102 %for organizational purposes, all receiver files are kept within a
0103 %receiver folder
0104 receiver_folder=strcat(master_folder,'\Receiver');
0105 cd(receiver_folder);
0106 [signal_I,signal_Q,CW_DOP_Out,FMCW_OUT,fig_num]=receiver(signal,L0,...
0107     master_folder,fig_num);
0108
0109 %MTI
0110 %[signal]=MTI(signal_I,signal_Q,master_folder)

```

Transmitter.m

```
0001 function [fig_num,out_signal,L0]=transmitter(fig_num,master_folder)
0002 %Author: 2Lt Oscar Mayhew
0003 %Date working: 27 March 2007
0004 %Description: Controls basic components of the transmitter.
0005 %Inputs: next figure number, loads the basic pre defined operating
0006 %parameters
0007 %Outputs: Local Oscillator and transmitted signal
0008 %Options: all options are defined within the parameters file
0009 %Date edited:
0010 %Editions made:
0011
0012 load -mat Lab_Volt_Param
0013 load -mat constants
0014
0015 %RF OSCILLATOR
0016 [signal,fig_num]=RF_OSCILLATOR(fig_num,master_folder);
0017
0018 figure(fig_num)
0019 fig_num=fig_num+1;
0020 plot(t*1e9,signal)
0021 title('Carrier Signal vs. Time')
0022 xlabel('Time (ns)')
0023 ylabel('Amplitude (V)')
0024
0025 %ISCOLATOR
0026 %assumed ideal so nothing additional provided
0027
0028 %DIRECTIONAL COUPLER
```

```

0029 %The stalo and coho are included incase this model were to be extended to
0030 %a real world large scale RADAR system
0031 [LO,signal,fig_num]=DIRECTIONAL_COUPLER(fig_num,signal);
0032 [STALO,CW_OUTPUT,fig_num]=STALO_DIRECTIONAL_COUPLER(fig_num,signal);
0033 [COHO,CW_OUTPUT,fig_num]=COHO_DIRECTIONAL_COUPLER(fig_num,signal);
0034
0035 %for CW/FM-CW RF OUTPUT the signal can be sent to the transmit antenna
0036 if OUTPUT_LOCATION==1
0037     out_signal=signal;
0038 end
0039
0040 %Generate the pulse train
0041 [pulse_train,fig_num]=PULSE_GEN(fig_num,master_folder);
0042
0043 %Modulate the pulse train with CW signal
0044 [signal,fig_num]=MOD_PULSE(pulse_train,signal,fig_num,master_folder);
0045
0046 %for PM RF OUTPUT the signal can be sent to the transmit antenna
0047 if OUTPUT_LOCATION==2
0048     out_signal=signal;
0049 end
0050
0051 %amplifier
0052 [signal]=AMPLIFIER(fig_num,signal);

```

RF_Oscillator.m

```
0001 function [signal,fig_num]=RF_OSCILLATOR(fig_num,master_folder)
0002 %Author: 2Lt Oscar Mayhew
0003 %Date working: 27 March 2007
0004 %Description: generates the carrier signal, calls the frequency modulation
0005 %function (if frequency modulation is selected it will be specified within
0006 %'parameters.mat')
0007 %Inputs: next figure to be outputted, loads basic operating parameters from
0008 %'parameters.mat'
0009 %Outputs: carrier signal, the next figure to be outputted
0010 %Options:
0011 %Date editted:
0012 %Editions made:
0013
0014 load -mat Lab_Volt_Param
0015 load -mat constants
0016
0017 [fm_mod_sig,fig_num]=FREQUENCY_MODULATION(fig_num);
0018
0019 P_osc =2.7564;
0020 Amp=sqrt(P_osc);
0021 signal=Amp*cos(2*pi*f_c*t+fm_mod_sig);
0022
0023 CW_OUTPUT=signal;
0024 save('CW_OUTPUT','CW_OUTPUT')
0025 save('TIME','t')
```

Frequency_Modulation.m

```
0001 function [fm_mod_sig,fig_num]=FREQUENCY_MODULATION(fig_num)
0002 %Author: 2Lt Oscar Mayhew
0003 %Date working: 14 May 2007
0004 %Description: generates the FM modulating signal, Lab-Volt paramaters that
0005 %govern this are contained in 'Lab-Volt.mat' and the time vector is
0006 %contained in 'constants.mat'
0007 %Inputs: number of the current figure to be created,
0008 %Outputs: number of the next figure to be created, FM modulating signal
0009 %Options: operating options can be varied in the 'LAB_VOLT_INITIALIZE.m'
0010 %Date editted:
0011 %Editions made:
0012
0013 load -mat Lab_Volt_Param
0014 load -mat constants
0015
0016 fm_mod_sig=f_dev*sin(2*pi*f_mod*t);
0017 %{
0018 figure(fig_num)
0019 fig_num=fig_num+1;
0020 plot(t*1e9,fm_mod_sig)
0021 title('Frequency Modulating vs. Time')
0022 xlabel('Time (ns)')
0023 ylabel('Amplitude (V)')
0024 %}
```

Directional_Coupler.m

```
0001 function [LO,CW_OUTPUT,fig_num]=DIRECTIONAL_COUPLER(fig_num,signal)
0002 %Author: 2Lt Oscar Mayhew
0003 %Date working: 14 March 2007
0004 %Description: Divides the signal from the oscillator between the Local
0005 %Oscillator and transmitted signal
0006 %Inputs: next figure number, signal
0007 %Outputs: Local Oscillator, signal
0008 %Options:
0009 %Date editted:
0010 %Editions made:
0011
0012 load -mat Lab_Volt_Param
0013 load -mat constants
0014
0015 %i need to go back and switch this to a power
0016 div_LO=0.8679;
0017 div_CW=0.1321;
0018
0019 sig_sign=sign(signal);
0020 signal=signal.^2;
0021 CW_OUTPUT=div_CW*signal;
0022 LO=div_LO*signal;
0023 CW_OUTPUT=sqrt(CW_OUTPUT).*sig_sign;
0024 LO=sqrt(LO).*sig_sign;
0025
0026 figure(fig_num)
0027 fig_num=fig_num+1;
0028 plot(t*1e9,CW_OUTPUT)
```

```
0029 %axis([5.413e-6 5.415e-6 -1.2 1.2])
0030 xlabel('Time (ns)')
0031 ylabel('Amplitude')
0032 title('CW Output')
0033
0034 figure(fig_num)
0035 fig_num=fig_num+1;
0036 plot(t*1e9,L0)
0037 %axis([5.413e-6 5.415e-6 -1.2 1.2])
0038 xlabel('Time (ns)')
0039 ylabel('Amplitude')
0040 title('Local Oscillator')
```

Coho_Directional_Coupler.m

```
0001 function [COHO,CW_OUTPUT,fig_num]=COHO_DIRECTIONAL_COUPLER(fig_num,signal)
0002 %Author: 2Lt Oscar Mayhew
0003 %Date working: 27 March 2007
0004 %Description: Divides the signal from the oscillator into the Cohierent
0005 %Oscillator and transmitted signal. Though the Lab Volt system does not
0006 %have a cohierent oscillator, a general radar system does therefore it must
0007 %be included for the most general purpose system.
0008 %Inputs: next figure number, signal
0009 %Outputs: Cohierent Oscillator, signal
0010 %Options:
0011 %Date editted:
0012 %Editions made:
0013
0014 %i need to go back and switch this to a power
0015 COHO=signal;
0016 CW_OUTPUT=signal;
```

Stalo_Directional_Coupler.m

```
0001 function [STALO,CW_OUTPUT,fig_num]=STALO_DIRECTIONAL_COUPLER...  
0002     (fig_num,signal)  
0003 %Author: 2Lt Oscar Mayhew  
0004 %Date working: 14 March 2007  
0005 %Description: Divides the signal from the waveform generator between the  
0006 %Stable Local Oscillator and transmitted signal. The Lab Volt system does  
0007 %this in an 8 to 1 ratio  
0008 %Inputs: next figure number, signal  
0009 %Outputs: Local Oscillator, signal  
0010 %Options:  
0011 %Date editted:  
0012 %Editions made:  
0013  
0014 %i need to go back and switch this to a power  
0015 CW_OUTPUT=signal;  
0016 STALO=signal;
```

Pulse_Gen.m

```
0001 function [pulse_train,fig_num]=PULSE_GEN(fig_num,master_folder)
0002 %Author: 2Lt Oscar Mayhew
0003 %Date working: 14 March 2007
0004 %Description: generates a pulse for amplitude/pulse modulation. The time
0005 %vector is 10 pulses in length. The pulse is placed half way through the
0006 %time vector.
0007 %Inputs: time vector
0008 %Outputs: modulating signal
0009 %Options: range resolution and max unambiguous range
0010 %Date editted:
0011 %Editions made:
0012
0013 load -mat Lab_Volt_Param
0014 load -mat constants
0015
0016 %determine the length and maximum value of t
0017 max_index=length(t);
0018 t_max=t(max_index);
0019
0020 %define the pulse and index in which the pulse goes low, circle shift so
0021 %the pulse is in the middle
0022 pulse_train=zeros(1,max_index);
0023 index_low=round(tau/t_max*max_index);
0024 pulse_train(1:index_low)=.27;
0025 pulse_train=circshift(pulse_train,[0 round(max_index/2)]);
0026
0027 figure(fig_num)
0028 fig_num=fig_num+1;
```

```
0029 plot(t*1e9,pulse_train)
0030 title('Pulse Envelope vs. Time')
0031 xlabel('Time (ns)')
0032 ylabel('Amplitude (V)')
```

Mod_Pulse.m

```
0001 function [signal,fig_num]=MOD_PULSE(pulse_train,signal,fig_num,...
0002     master_folder)
0003 %Author: 2Lt Oscar Mayhew
0004 %Date working: 7 March 2007
0005 %Description: modulates the pulse train with the CW signal
0006 %Inputs:
0007 %Outputs:
0008 %Options:
0009 %Date edited:
0010 %Editions made:
0011
0012 load -mat Lab_Volt_Param
0013 load -mat constants
0014
0015 signal=pulse_train.*signal;
```

Amplifier.m

```
0001 function [signal]=AMPLIFIER(fig_num,signal)
0002 %Author: 2Lt Oscar Mayhew
0003 %Date working: 27 March 2007
0004 %Description: Though not present in the Lab Volt system an amplifier my be
0005 %present in a real world system to achieve appropriate power levels
0006 %Inputs: next figure number, signal
0007 %Outputs: Local Oscillator, signal
0008 %Options:
0009 %Date editted:
0010 %Editions made:
```

Antenna_Controller.m

```
0001 %Author: 2Lt Oscar Mayhew
0002 %Date working: 30 July 2007
0003 %Description: Applies the measured antenna filter response to the signal.
0004 %Inputs: signal
0005 %Outputs: none
0006 %Options: the antenna response can be turned off by setting f_resp=0
0007 %Date edited:
0008 %Editions made:
0009
0010 function [signal,fig_num]=Ant_Control(fig_num,signal)
0011 current_directory=cd;
0012
0013 load -mat constants
0014 f_resp=0;
0015
0016 if f_resp==0
0017     %convert signal voltage to a power
0018     sig_sign=sign(signal);
0019     sig_power=signal.^2;
0020     %apply gain as described by MatLab Book
0021     G=10^(23/10);
0022     return_pow=G*sig_power;
0023     %convert back to a volatage
0024     signal=sqrt(return_pow).*sig_sign;
0025 elseif f_resp==1
0026     %plot the signal before the antenna
0027     figure(fig_num)
0028     fig_num=fig_num+1;
```

```

0029     plot(f*1e-9,10*log10(abs(fft(signal))/max(abs(fft(signal)))))
0030     xlabel('Frequency (GHz)')
0031     ylabel('Power (dB)')
0032     title('Signal in Frequency Domain, Pre-Antenna')
0033     figure(fig_num)
0034     fig_num=fig_num+1;
0035     plot(t*1e9,signal)
0036     xlabel('Time (ns)')
0037     ylabel('Amplitude (V)')
0038     title('Signal in Time Domain, Pre-Antenna')
0039
0040     %convert signal to frequency domain
0041     signal=fft(signal);
0042
0043     %strip the phase and magnitude from signal
0044     signal_mag=abs(signal);
0045     signal_phase=angle(signal);
0046
0047     %load antenna response and strip phase and magnitude
0048     load -mat Antenna_Filter
0049     antenna_mag=abs(f_sweep);
0050     antenna_phase=angle(f_sweep);
0051
0052     %apply antenna response to signal
0053     signal_mag=sqrt(signal_mag.^2.*antenna_mag);
0054     signal_phase=signal_phase+antenna_phase;
0055     signal=signal_mag.*exp(i*signal_phase);
0056     signal=ifft(signal);
0057

```

```

0058     %plot signal after antenna
0059     figure(fig_num)
0060     fig_num=fig_num+1;
0061     plot(f*1e-9,10*log10(abs(fft(signal))/max(abs(fft(signal))))))
0062     xlabel('Frequency (GHz)')
0063     ylabel('Power (dB)')
0064     title('Signal in Frequency Domain, Post-Antenna')
0065     figure(fig_num)
0066     fig_num=fig_num+1;
0067     plot(t*1e9,signal)
0068     xlabel('Time (ns)')
0069     ylabel('Amplitude (V)')
0070     title('Signal in Time Domain, Post-Antenna')
0071 end

```

Radiation_Enviro.m

```
0001 function [signal,fig_num]=Radiation_Enviro(signal,fig_num,master_folder)
0002 %Author: 2Lt Oscar Mayhew
0003 %Date working: 7 March 2007
0004 %Description: Controls the signal once it has left the transmit antenna.
0005 %Calls the space decay function for the signal from the transmitter to the
0006 %target and from the target to the receiver (assumes bystatic to ensure
0007 %general). Also calls the function for the scattering off the target. This
0008 %program also maintains a running tally of the number of figures outputted.
0009 %Inputs: RCS attributes, tranmitted signal,
0010 %Outputs: next figure number and the received signal
0011 %Options:
0012 %Date editted:
0013 %Editions made:
0014
0015 load -mat constants
0016 load -mat target_param
0017
0018 %SPACIAL DECAY/LOSS TO TARGET
0019 signal=Space_Decay(signal,range_tx,master_folder);
0020
0021 %REFLECTION OFF TARGET
0022 [signal,fig_num]=Reflection(signal,fig_num,master_folder);
0023
0024 %SPACIAL DECAY/LOSS TO RECEIVER
0025 signal=Space_Decay(signal,range_rx,master_folder);
0026 %{
0027 figure(fig_num)
0028 plot(t*1e9,signal)
```

```
0029 fig_num=fig_num+1;
0030 title('Transmitted Signal at Receive Antenna vs. Time')
0031 xlabel('Time (ns)')
0032 ylabel('Amplitude (V)')
0033 %}
```

Space_Decay.m

```
0001 function [signal]=Space_Decay(signal,range,master_folder)
0002 %Author: 2Lt Oscar Mayhew
0003 %Date working: 14 March 2007
0004 %Description: space decay proportional to  $1/(4\pi*r^2)$ 
0005 %Inputs: signal, range signal travels
0006 %Outputs: decayed signal after traveling range
0007 %Options:
0008 %Date edited:
0009 %Editions made:
0010
0011 load -mat constants
0012
0013 power_loss=1/(4*pi*range^2);
0014 signal=power_loss*signal;
```

Receiver.m

```
0001 function [signal_I,signal_Q,CW_DOP_Out,FMCW_OUT,fig_num]=receiver...
0002     (signal,L0,master_folder,fig_num)
0003 %Author: 2Lt Oscar Mayhew
0004 %Date working: 14 March 2007
0005 %Description: coordinates all actions within the receiver
0006 %Inputs: the input signal and Local Oscillator
0007 %Outputs: CW Doppler Output, FMCW Output, Pulsed Output (at baseband) for I
0008 %and Q channel
0009 %Options:
0010 %Date edited:
0011 %Editions made:
0012
0013 load -mat RECEIVER_PARAM
0014 load -mat constants
0015
0016 AN_OUTPUT=signal;
0017 save('AN_OUTPUT.mat','AN_OUTPUT')
0018
0019 %divide the received signal from the antenna into the I and Q channel
0020 [signal_I,signal_Q]=power_divider1(signal);
0021
0022 %divide the local oscillator signal to drive the mixer for the I and Q
0023 %channel. A 90 degree phase shift to the q channel
0024 [LO_I,LO_Q]=hybrid_junction(L0);
0025
0026 %modulate the received signal on both the I and Q channel- returns it to
0027 %base band and produces an image at twice the carrier frequency
0028 %assumes both the I and Q channel have the demodulator
```

```

0029 %Plot the I and Q channel signal prior to demodulation
0030 %{
0031 figure(fig_num)
0032 fig_num=fig_num+1;
0033 plot(t,signal_I)
0034 xlabel('Time (s)')
0035 ylabel('Amplitude')
0036 title('I Channel Signal, Pre Demodulation, Time Domain')
0037
0038 figure(fig_num)
0039 fig_num=fig_num+1;
0040 plot(f,10*log10(abs(fft(signal_I))/max(abs(fft(signal_I))))))
0041 xlabel('Frequency (Hz)')
0042 ylabel('Magnitude')
0043 title('I Channel Signal, Pre Demodulation, Frequency Domain')
0044
0045 figure(fig_num)
0046 fig_num=fig_num+1;
0047 plot(t,signal_Q)
0048 xlabel('Time (s)')
0049 ylabel('Amplitude')
0050 title('Q Channel Signal, Pre Demodulation, Time Domain')
0051
0052 figure(fig_num)
0053 fig_num=fig_num+1;
0054 plot(f,10*log10(abs(fft(signal_Q))/max(abs(fft(signal_Q))))))
0055 xlabel('Frequency (Hz)')
0056 ylabel('Magnitude')
0057 title('Q Channel Signal, Pre Demodulation, Frequency Domain')

```

```

0058 %}
0059 signal_I=demodulate(L0_I,signal_I);
0060 signal_Q=demodulate(L0_Q,signal_Q);
0061 %{
0062 figure(fig_num)
0063 fig_num=fig_num+1;
0064 plot(t,signal_I)
0065 xlabel('Time (s)')
0066 ylabel('Amplitude')
0067 title('I Channel Signal, Post Demodulation Pre Power Divide, Time Domain')
0068
0069 figure(fig_num)
0070 fig_num=fig_num+1;
0071 plot(f,10*log10(abs(fft(signal_I))/max(abs(fft(signal_I))))))
0072 xlabel('Frequency (Hz)')
0073 ylabel('Magnitude')
0074 title('I Channel Signal, Post Demodulation Pre Power Divide, ...
0075     Frequency Domain')
0076
0077 figure(fig_num)
0078 fig_num=fig_num+1;
0079 plot(t,signal_Q)
0080 xlabel('Time (s)')
0081 ylabel('Amplitude')
0082 title('Q Channel Signal, Post Demodulation Pre Power Divide, Frequency ...
0083     Domain')
0084
0085 figure(fig_num)
0086 fig_num=fig_num+1;

```

```

0087 plot(f,10*log10(abs(fft(signal_Q))/max(abs(fft(signal_Q)))))
0088 xlabel('Frequency (Hz)')
0089 ylabel('Magnitude')
0090 title('Q Channel Signal, Post Demodulation Pre Power Divide, Frequency ...
0091      Domain')
0092 %}
0093 [signal_I_CW_DOP,signal_I_PM]=power_divider2(signal_I);
0094 [signal_Q_FMCW,signal_Q_PM]=power_divider2(signal_Q);
0095
0096 %remove the higher frequency image that was introduced after mixing, only
0097 %signal at baseband will remain
0098 %assumes both the I and Q channel have the same WB Amp
0099 %{
0100 figure(fig_num)
0101 fig_num=fig_num+1;
0102 plot(t,signal_I)
0103 xlabel('Time (s)')
0104 ylabel('Amplitude')
0105 title('I Channel Signal, Post Demodulation Pre BPF, Time Domain')
0106
0107 figure(fig_num)
0108 fig_num=fig_num+1;
0109 plot(f,10*log10(abs(fft(signal_I))/max(abs(fft(signal_I)))))
0110 xlabel('Frequency (Hz)')
0111 ylabel('Magnitude')
0112 title('I Channel Signal, Post Demodulation Pre BPF, Frequency Domain')
0113
0114 figure(fig_num)
0115 fig_num=fig_num+1;

```

```

0116 plot(t,signal_Q)
0117 xlabel('Time (s)')
0118 ylabel('Amplitude')
0119 title('Q Channel Signal, Post Demodulation Pre BPF, Time Domain')
0120
0121 figure(fig_num)
0122 fig_num=fig_num+1;
0123 plot(f,10*log10(abs(fft(signal_Q))/max(abs(fft(signal_Q)))))
0124 xlabel('Frequency (Hz)')
0125 ylabel('Magnitude')
0126 title('Q Channel Signal, Post Demodulation Pre BPF, Frequency Domain')
0127 %}
0128 [signal_I_PM,fig_num]=WB_amp(signal_I_PM,fig_num);
0129 [signal_Q_PM,fig_num]=WB_amp(signal_Q_PM,fig_num);
0130
0131 figure(fig_num)
0132 fig_num=fig_num+1;
0133 plot(t*1e9,signal_I_PM)
0134 xlabel('Time (ns)')
0135 ylabel('Amplitude')
0136 title('I Channel Signal, Post WB Amplifier, Time Domain')
0137 RX_I_OUTPUT=signal_I_PM;
0138 save('RX_I_OUTPUT.mat','RX_I_OUTPUT')
0139 %{
0140 figure(fig_num)
0141 fig_num=fig_num+1;
0142 plot(f,10*log10(abs(fft(signal_I_PM))/max(abs(fft(signal_I_PM)))))
0143 xlabel('Frequency (Hz)')
0144 ylabel('Magnitude')

```

```

0145 title('I Channel Signal, Post WB Amplifier, Frequency Domain')
0146 %}
0147 figure(fig_num)
0148 fig_num=fig_num+1;
0149 plot(t*1e9,signal_Q_PM)
0150 xlabel('Time (ns)')
0151 ylabel('Amplitude')
0152 title('Q Channel Signal, Post WB Amplifier, Time Domain')
0153 RX_Q_OUTPUT=signal_Q_PM;
0154 save('RX_Q_OUTPUT.mat','RX_Q_OUTPUT')
0155 save('TIME.mat','t')
0156
0157 %{
0158 figure(fig_num)
0159 fig_num=fig_num+1;
0160 plot(f,10*log10(abs(fft(signal_Q_PM))/max(abs(fft(signal_Q_PM))))))
0161 xlabel('Frequency (Hz)')
0162 ylabel('Magnitude')
0163 title('Q Channel Signal, Post WB Amplifier, Frequency Domain')
0164 %}
0165 %later the LPF and HPF will be designed
0166 CW_DOP_Out=1;
0167 FMCW_OUT=1;
0168 %{
0169 %remove the higher frequency image that was introduced after mixing, only
0170 %signal at baseband will remain
0171 signal_I_CW_DOP=L_filter(signal_I_CW_DOP);
0172 signal_Q_FMCW=H_filter(signal_Q_FMCW);
0173 %}

```

Power_Divider1.m

```
0001 function [signal_I,signal_Q]=power_divider1(signal)
0002 %Author: 2Lt Oscar Mayhew
0003 %Date working: 14 March 2007
0004 %Description: generates the carrier signal
0005 %Inputs: received signal
0006 %Outputs: signal for the I and Q channel
0007 %Options:
0008 %Date edited:
0009 %Editions made:
0010
0011 signal_I=signal/2;
0012 signal_Q=signal/2;
```

Hybrid_Junction.m

```
0001 function [LO_I,LO_Q]=hybrid_junction(LO)
0002 %Author: 2Lt Oscar Mayhew
0003 %Date working: 14 March 2007
0004 %Description: divides the local oscillator into two and and applys a 90
0005 %phase shift to the Q channel local oscillator
0006 %Inputs: LO signal
0007 %Outputs: LO signal for I an Q channel
0008 %Options:
0009 %Date editted:
0010 %Editions made:
0011
0012 %strip the amplitude off the local oscillator signal
0013 Amp=max(LO);
0014
0015 %divide the I channel (in phase) by 1/2 to denote the splitting of the
0016 %local oscillator
0017 LO_I=.5*LO;
0018
0019 %strip off the amplitude of the local oscillator signal,apply the inverse
0020 %cosine to obtain just the arguement, apply a 90 degree face shift by
0021 %taking the sine, apply the amplitude and divide the signal by 2
0022 %this now denotes the Q Channel- 1/2 the power of the local oscillator with
0023 %a 90 degree phase shift
0024 LO_Q=.5*Amp*sin(acos(LO/Amp));
```

Power_Divider2.m

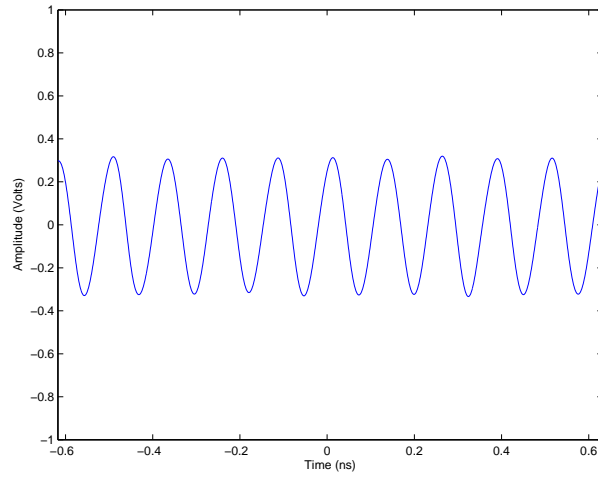
```
0001 function [signal_doppler,signal_PM]=power_divider2(signal)
0002 %Author: 2Lt Oscar Mayhew
0003 %Date working: 14 March 2007
0004 %Description: divides the power between Pulse Modulated port and the other
0005 %channel (the function of the other channel varies for the I and Q channel)
0006 %It is assumed that the power divider is the same for both I and Q channel
0007 %Inputs: signal (contains signals at base band and twice the carrier)
0008 %Outputs: CW output, Pulsed Output (at baseband)
0009 %Options:
0010 %Date editted:
0011 %Editions made:
0012 %
0013
0014 signal_doppler=signal/2;
0015 signal_PM=signal/2;
```

WB_amp.m

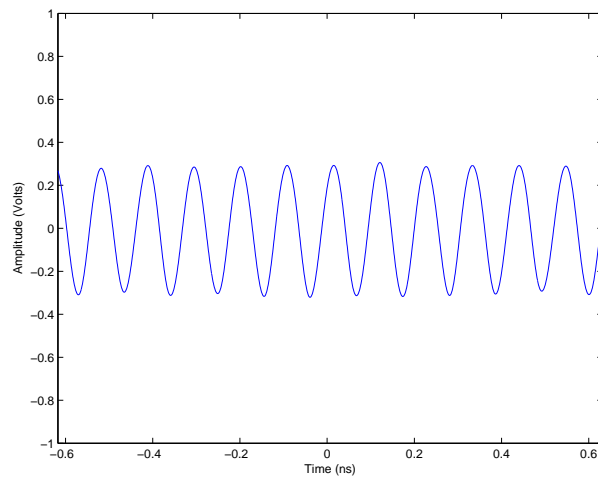
```
0001 function [signal,fig_num]=WB_amp(signal,fig_num)
0002 %Author: 2Lt Oscar Mayhew
0003 %Date working: 14 March 2007
0004 %Description: impliments a wideband amplifier to filter out the signal at
0005 %twice the carrier. Passband is from 100 kHz to 1 GHz with 45 dB of gain
0006 %Inputs: Pulse Modulated signal (contains signals at base band and twice
0007 %the carrier)
0008 %Outputs: Pulsed Output (at baseband)
0009 %Options:
0010 %Date editted:
0011 %Editions made:
0012 %
0013 load -mat RECEIVER_PARAM
0014 load -mat constants
0015 %{
0016 figure(fig_num)
0017 fig_num=fig_num+1;
0018 plot(f,10*log10(BPF))
0019 xlabel('Frequency (GHz)')
0020 ylabel('Magnititude')
0021 title('BPF Frequency Domain')
0022 %}
0023 max_gain=max(BPF);
0024 BPF=BPF/max_gain;
0025
0026 BPF_mag=abs(BPF);
0027 BPF_ang=angle(BPF);
0028
```

```
0029 signal=fft(signal);
0030 sig_mag=abs(signal);
0031 sig_ang=angle(signal);
0032
0033 mag=sqrt(sig_mag.^2.*BPF_mag);
0034 ang=sig_ang+BPF_ang;
0035
0036 signal=mag.*cos(ang)+mag.*sin(ang);
0037 signal=ifft(signal);
0038 signal=sqrt(max_gain)*signal;
```

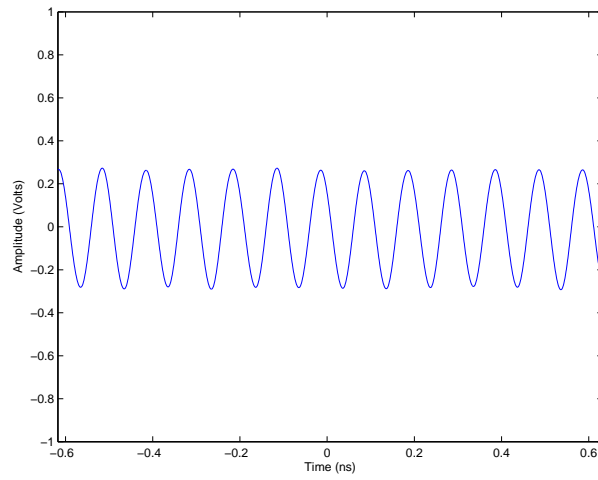
Appendix B. Lab-Volt Characterization



(a) 8-GHz Carrier Frequency.

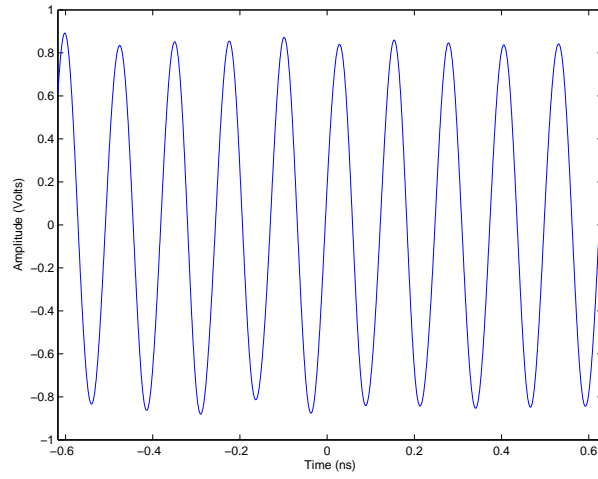


(b) 9.4-GHz Carrier Frequency.

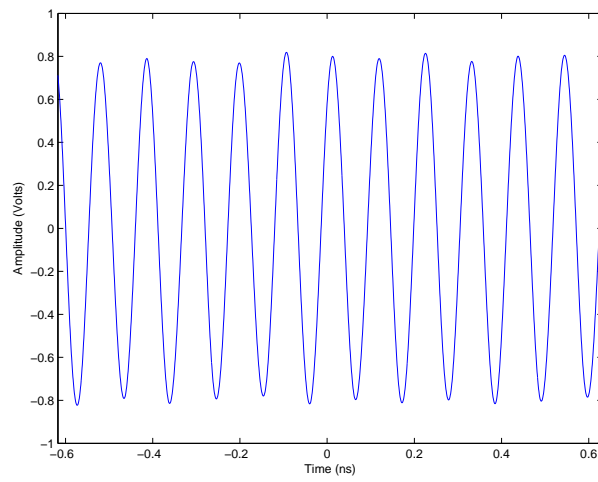


(c) 10-GHz Carrier Frequency.

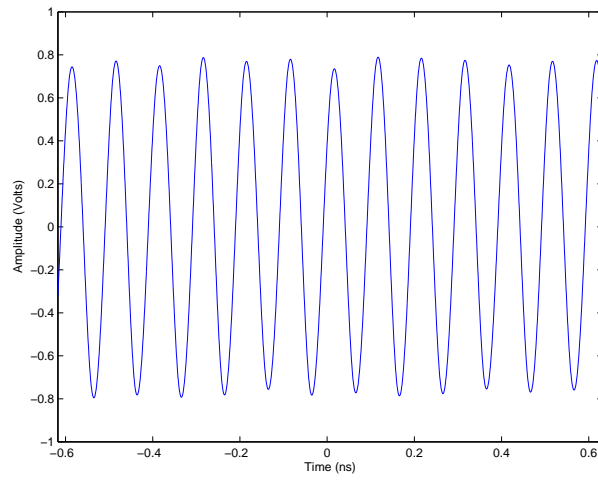
Figure B.1: Lab-Volt Transmitter CW Output.



(a) 8-GHz Carrier Frequency.

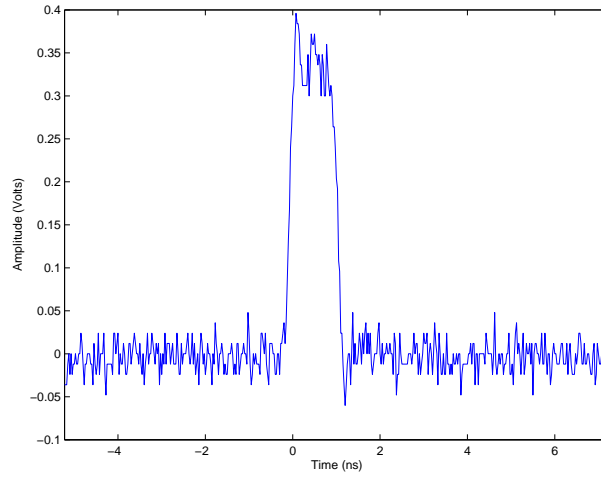


(b) 9.4-GHz Carrier Frequency.

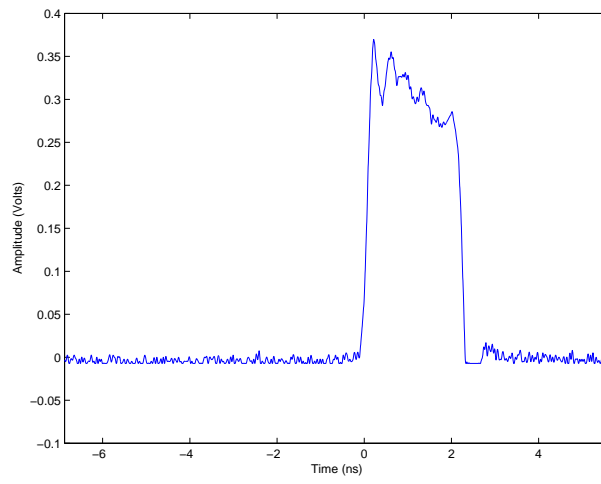


(c) 10-GHz Carrier Frequency.

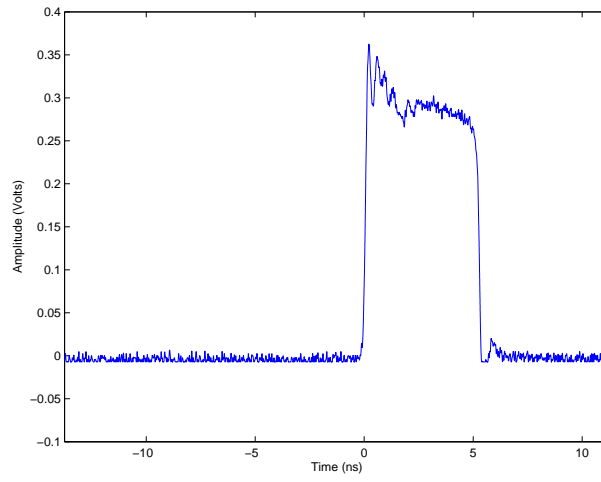
Figure B.2: Lab-Volt Transmitter LO Output.



(a) $\tau = 1$ -ns.

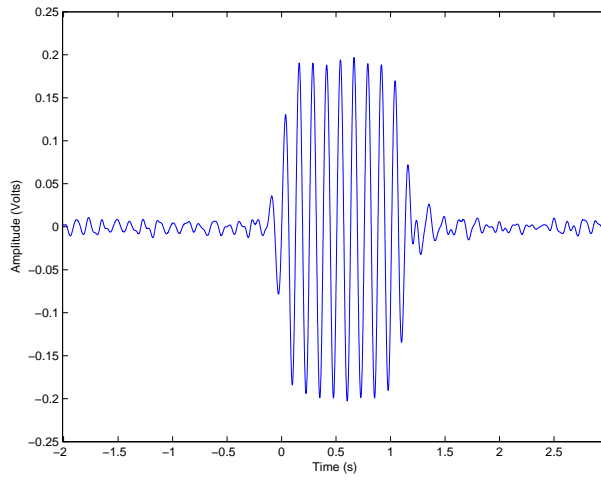


(b) $\tau = 2$ -ns.

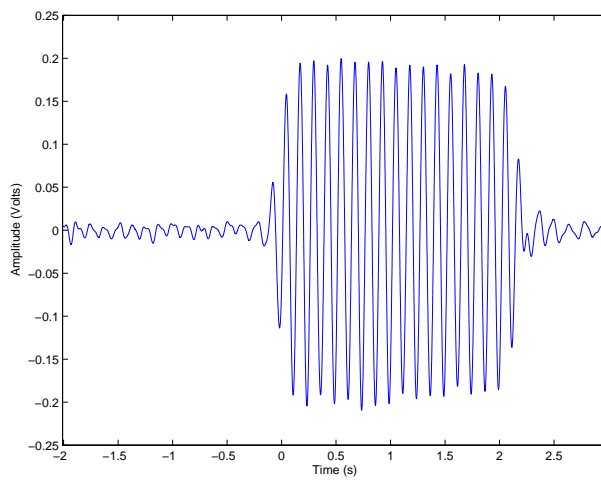


(c) $\tau = 5$ -ns.

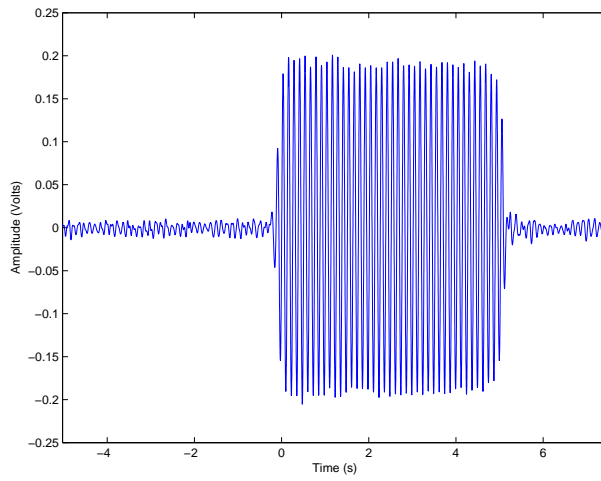
Figure B.3: Lab-Volt Transmitter Pulse Generator Output.



(a) $\tau = 1\text{-ns}$.

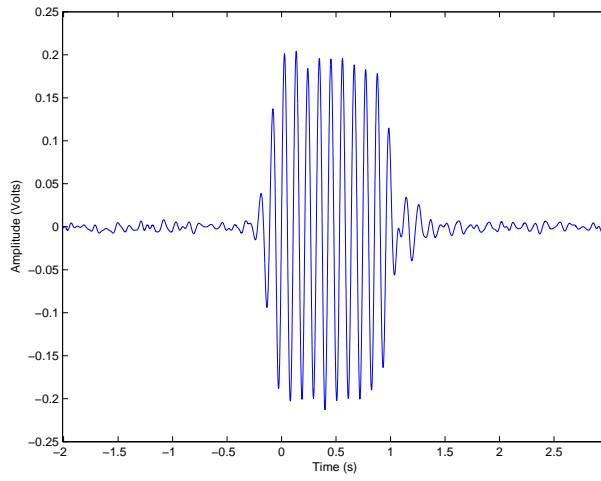


(b) $\tau = 2\text{-ns}$.

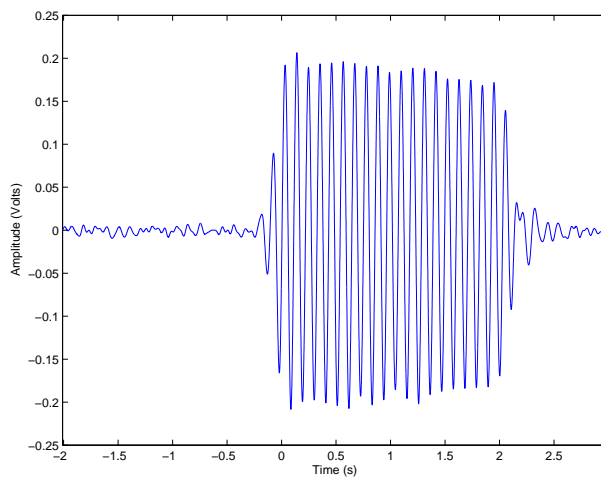


(c) $\tau = 5\text{-ns}$.

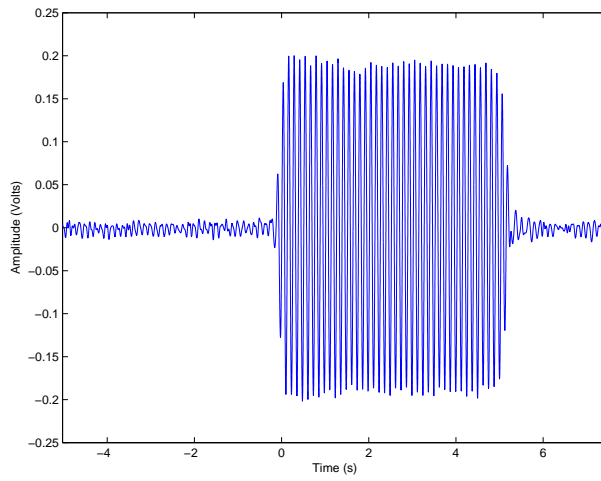
Figure B.4: Lab-Volt Transmitter Pulsed RF Output at 8-GHz Carrier Frequency.



(a) $\tau = 1\text{-ns}$.

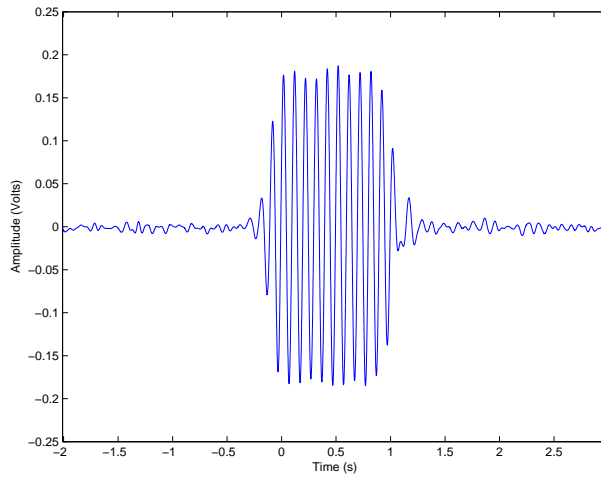


(b) $\tau = 2\text{-ns}$.

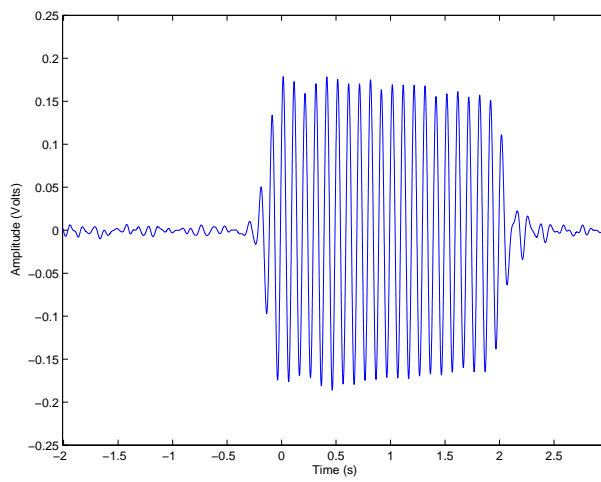


(c) $\tau = 5\text{-ns}$.

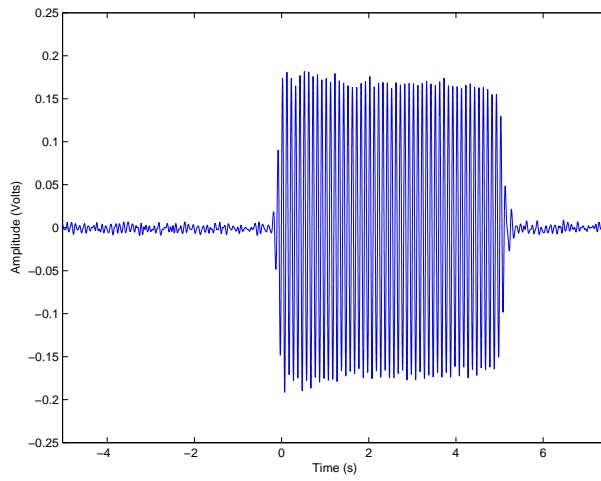
Figure B.5: Lab-Volt Transmitter Pulsed RF Output at 9.4-GHz Carrier Frequency.



(a) $\tau = 1\text{-ns}$.

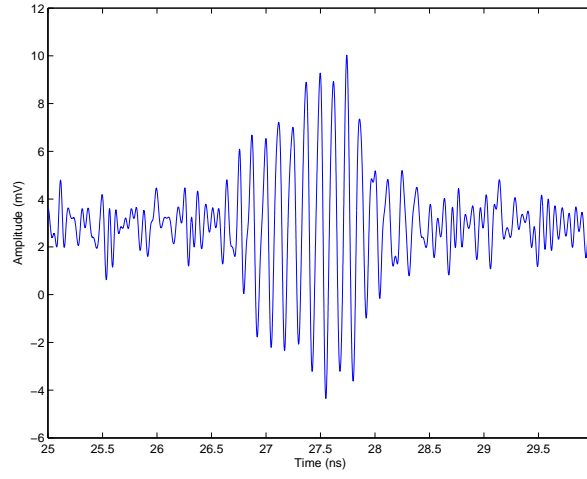


(b) $\tau = 2\text{-ns}$.

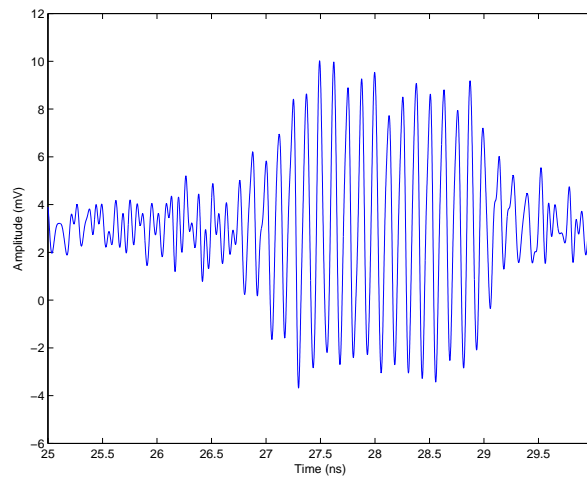


(c) $\tau = 5\text{-ns}$.

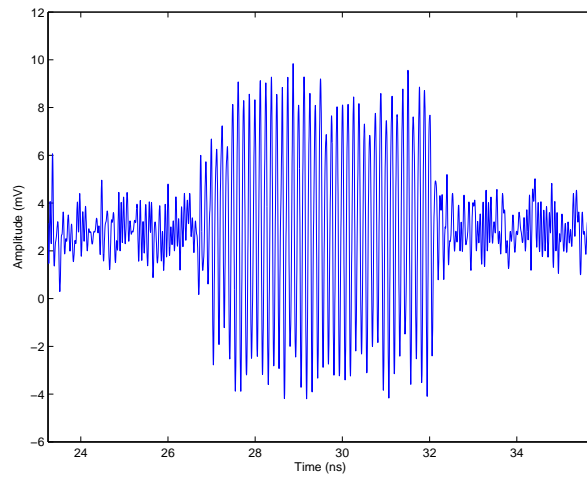
Figure B.6: Lab-Volt Transmitter Pulsed RF Output at 10-GHz Carrier Frequency.



(a) $\tau = 1\text{-ns}$.

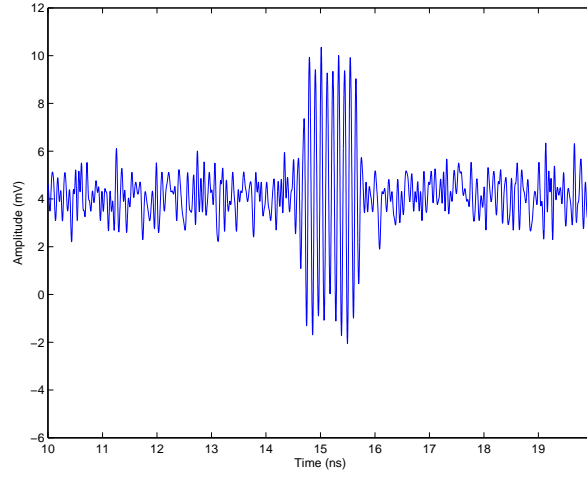


(b) $\tau = 2\text{-ns}$.

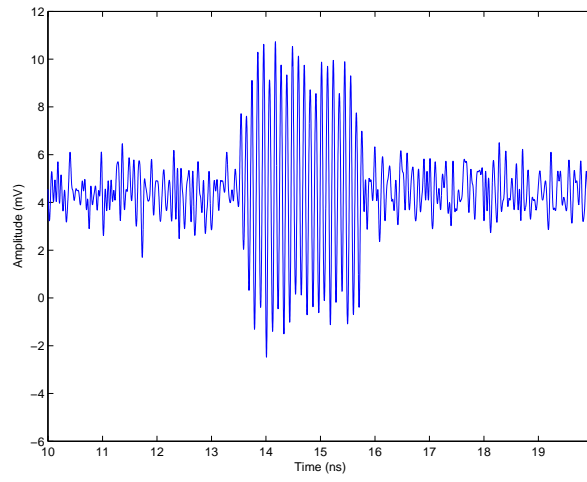


(c) $\tau = 5\text{-ns}$.

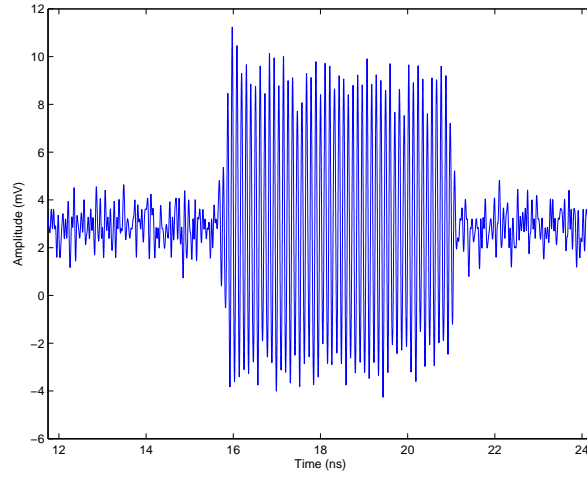
Figure B.7: RF Output at 8-GHz Carrier Frequency.



(a) $\tau = 1\text{-ns}$.

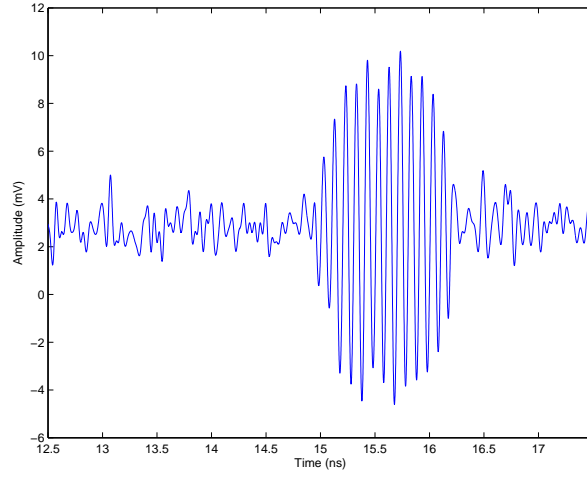


(b) $\tau = 2\text{-ns}$.

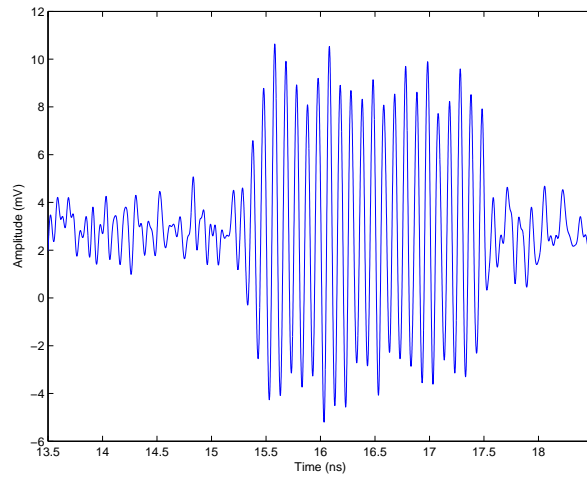


(c) $\tau = 5\text{-ns}$.

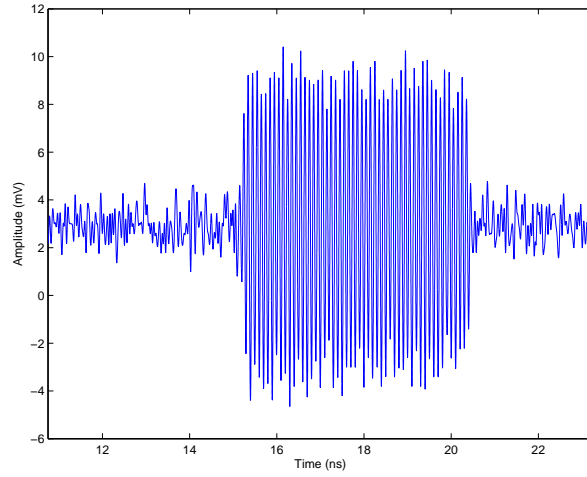
Figure B.8: Antenna Pedestal RF Output at 9.4-GHz Carrier Frequency.



(a) $\tau = 1\text{-ns}$.

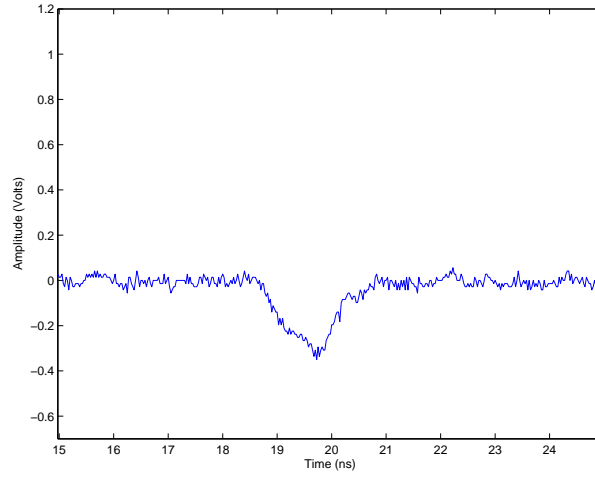


(b) $\tau = 2\text{-ns}$.

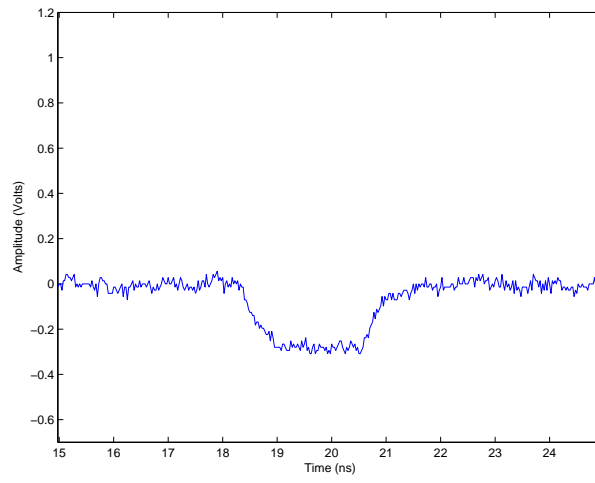


(c) $\tau = 5\text{-ns}$.

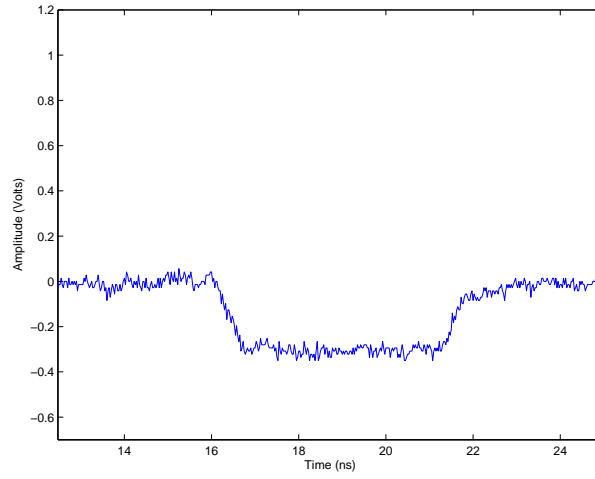
Figure B.9: Antenna Pedestal RF Output at 10-GHz Carrier Frequency.



(a) $\tau = 1\text{-ns}$.

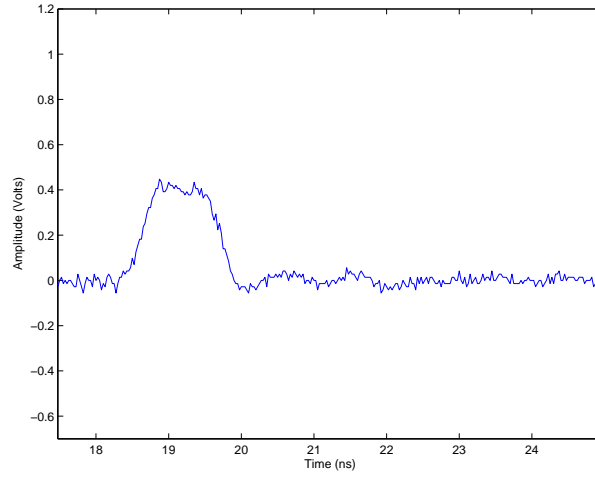


(b) $\tau = 2\text{-ns}$.

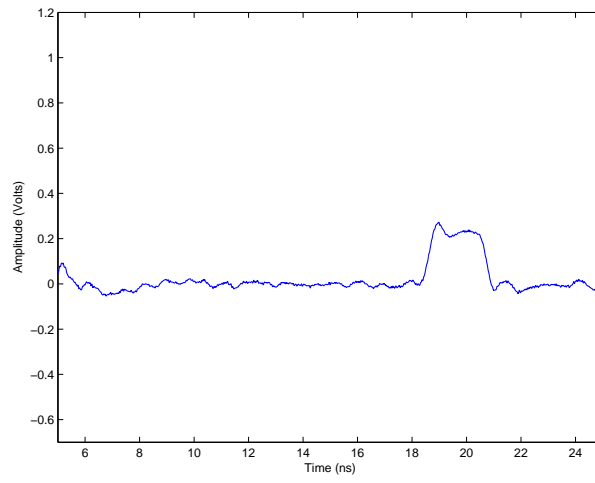


(c) $\tau = 5\text{-ns}$.

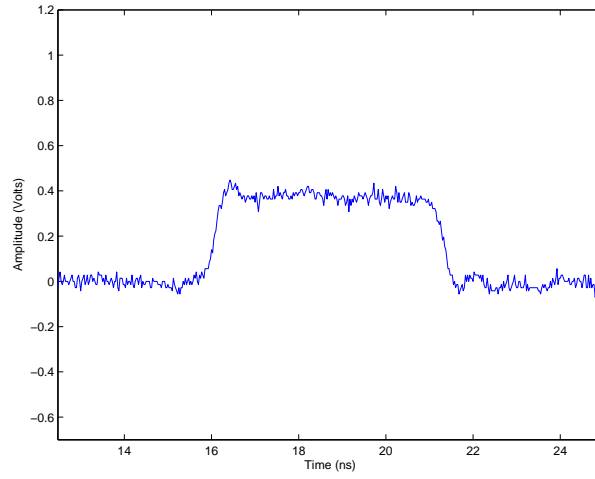
Figure B.10: Lab-Volt Receiver I-Channel Pulsed RF Output at 8-GHz Carrier Frequency.



(a) $\tau = 1\text{-ns}$.

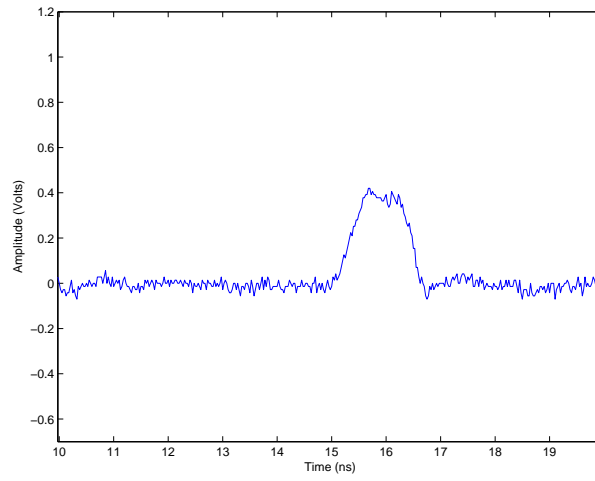


(b) $\tau = 2\text{-ns}$.

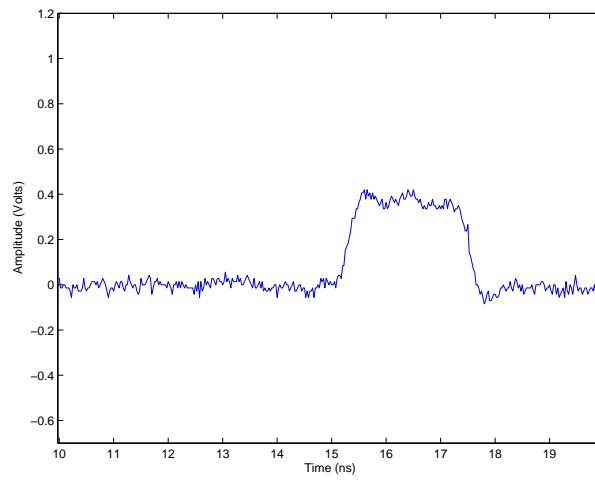


(c) $\tau = 5\text{-ns}$.

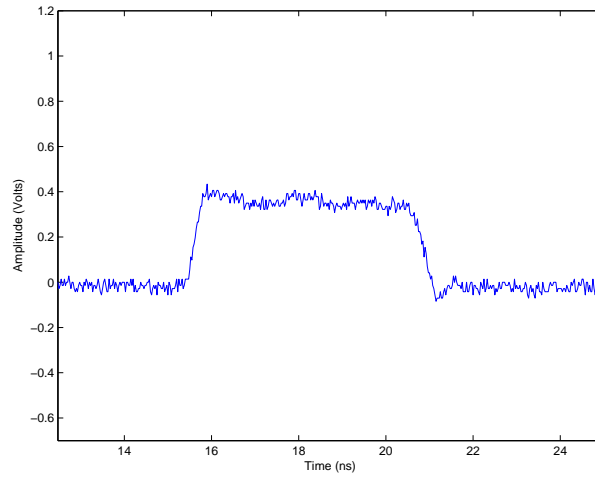
Figure B.11: Lab-Volt Receiver I-Channel RF Output at 9.4-GHz Carrier Frequency.



(a) $\tau = 1\text{-ns}$.

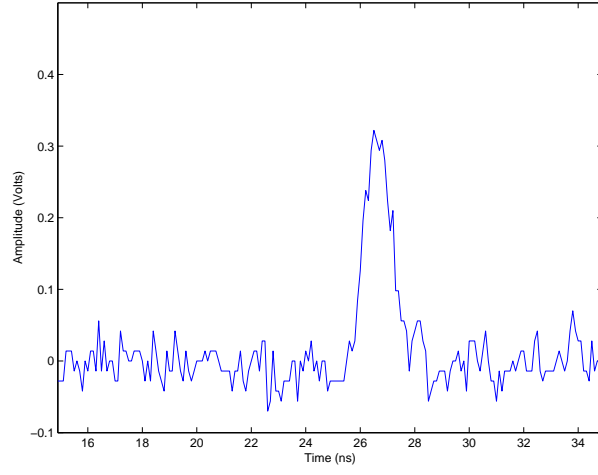


(b) $\tau = 2\text{-ns}$.

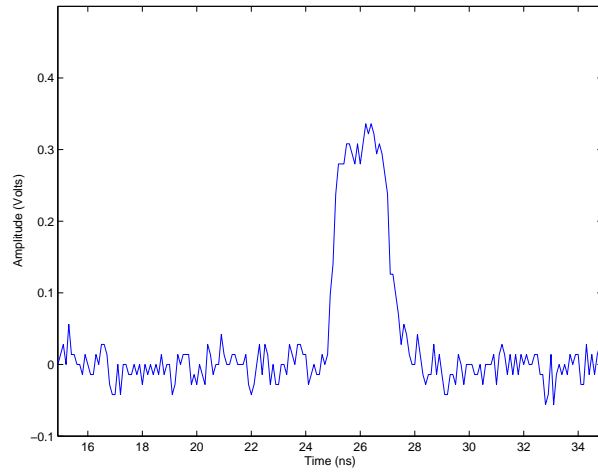


(c) $\tau = 5\text{-ns}$.

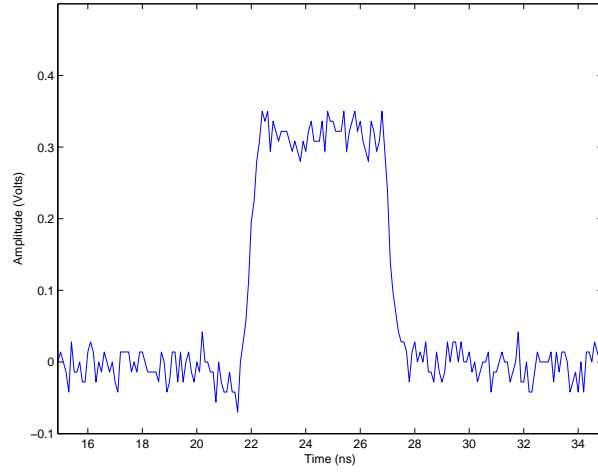
Figure B.12: Lab-Volt Receiver I-Channel RF Output at 10-GHz Carrier Frequency.



(a) $\tau = 1\text{-ns}$.

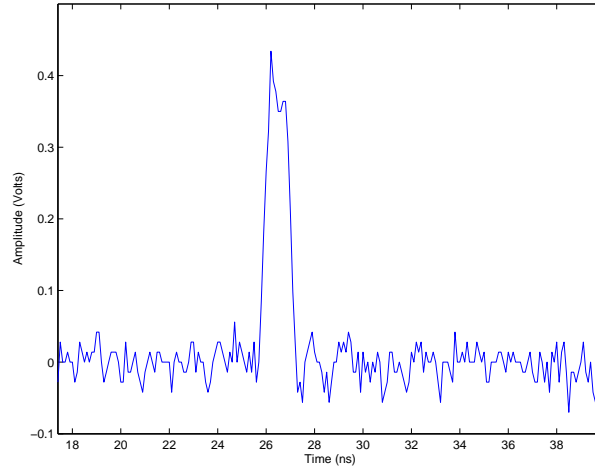


(b) $\tau = 2\text{-ns}$.

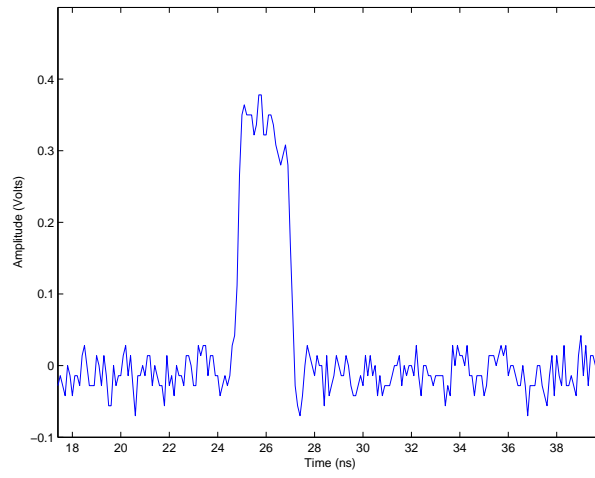


(c) $\tau = 5\text{-ns}$.

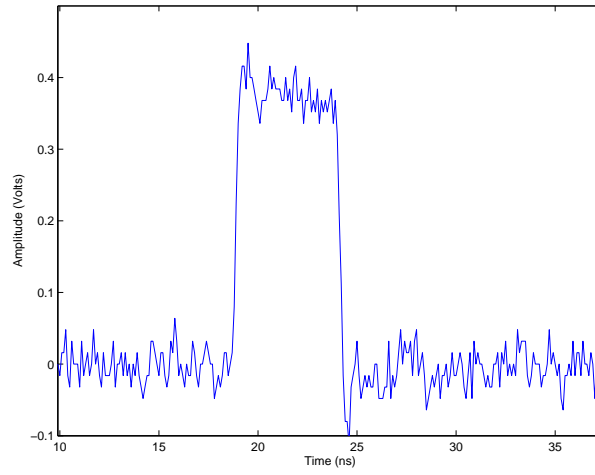
Figure B.13: Lab-Volt Receiver Q-Channel RF Output at 8-GHz Carrier Frequency.



(a) $\tau = 1\text{-ns}$.

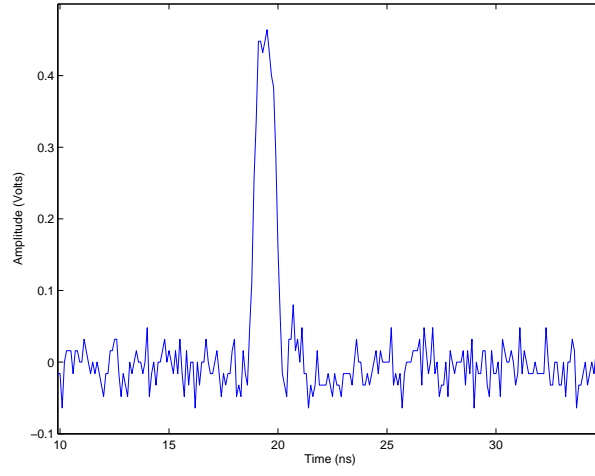


(b) $\tau = 2\text{-ns}$.

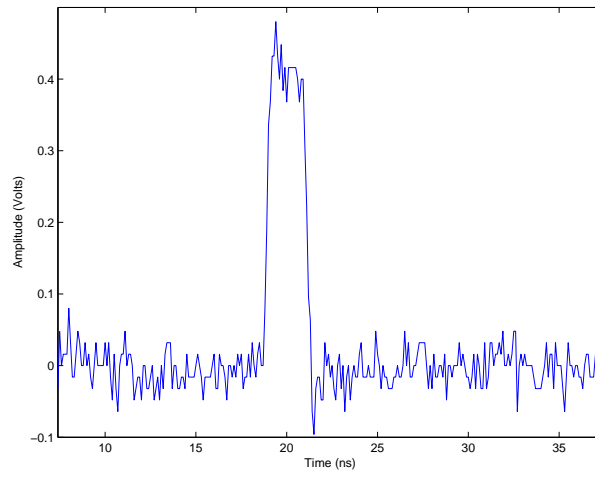


(c) $\tau = 5\text{-ns}$.

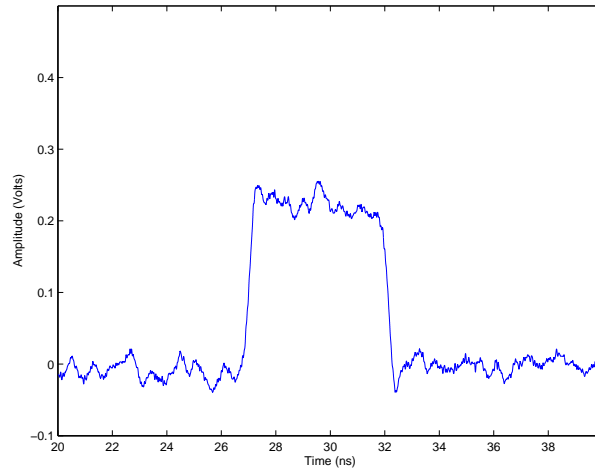
Figure B.14: Lab-Volt Receiver Q-Channel RF Output at 9.4-GHz Carrier Frequency.



(a) $\tau = 1\text{-ns}$.

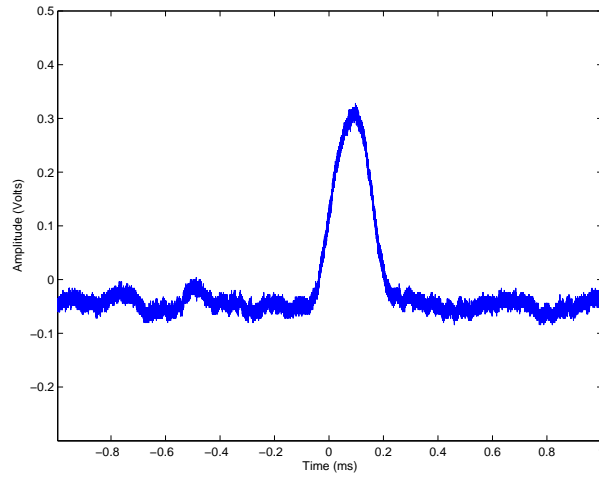


(b) $\tau = 2\text{-ns}$.

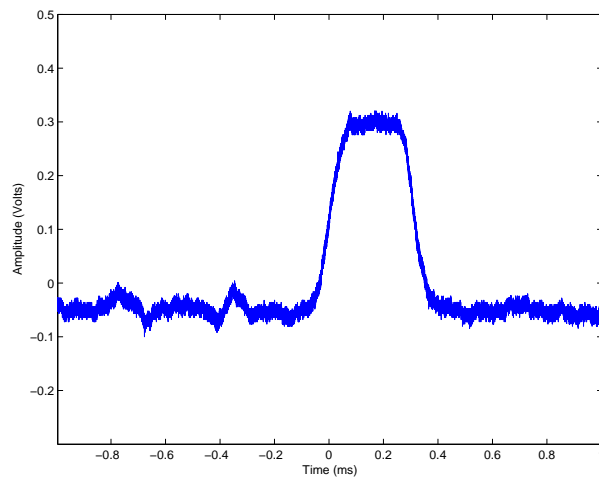


(c) $\tau = 5\text{-ns}$.

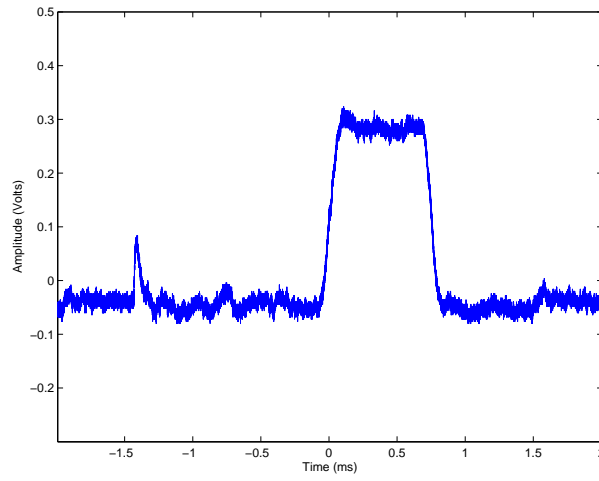
Figure B.15: Lab-Volt Receiver Q-Channel RF Output at 10-GHz Carrier Frequency.



(a) $\tau = 1\text{-ns}$.

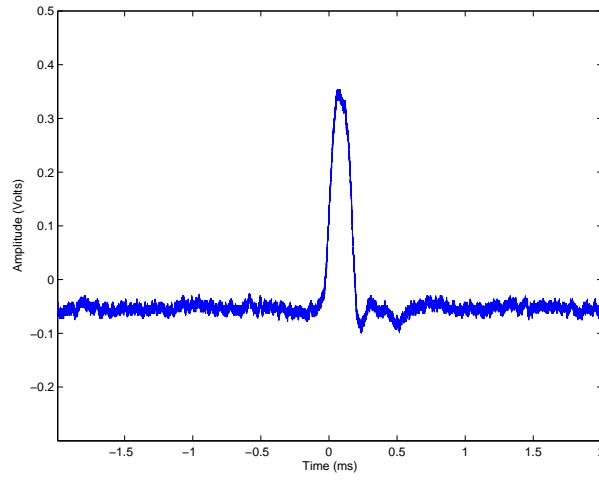


(b) $\tau = 2\text{-ns}$.

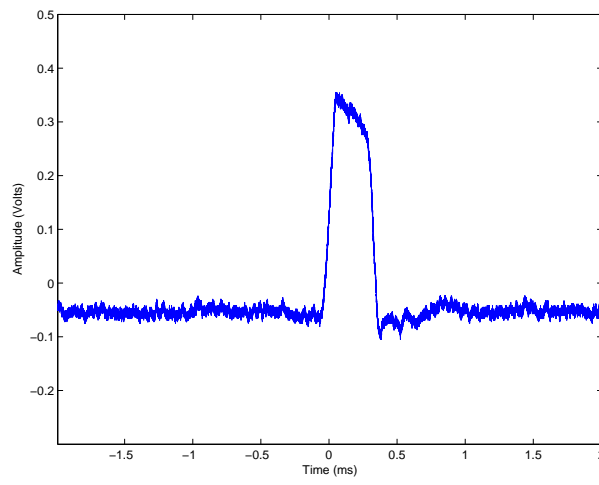


(c) $\tau = 5\text{-ns}$.

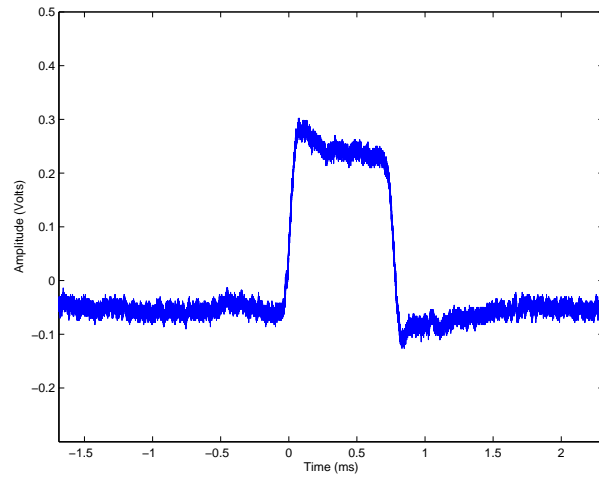
Figure B.16: Lab-Volt Dual Channel Sampler I-Channel RF Output at 8-GHz Carrier Frequency.



(a) $\tau = 1\text{-ns}$.

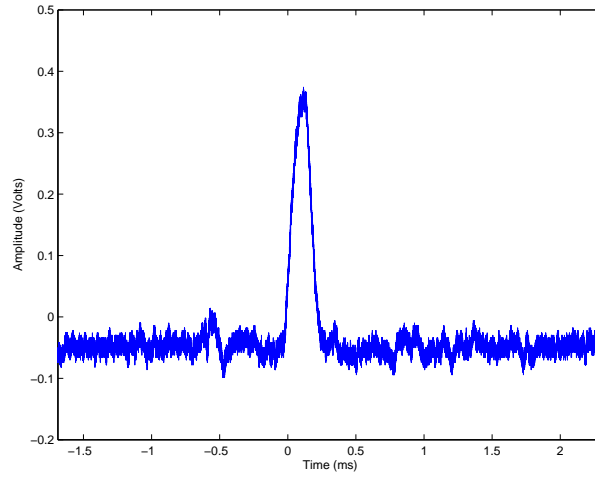


(b) $\tau = 2\text{-ns}$.

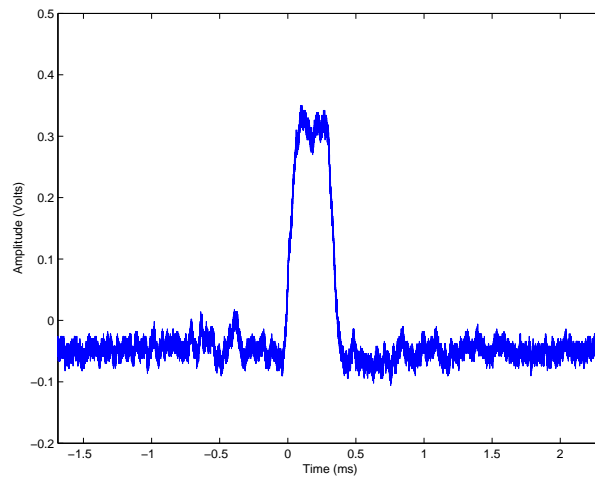


(c) $\tau = 5\text{-ns}$.

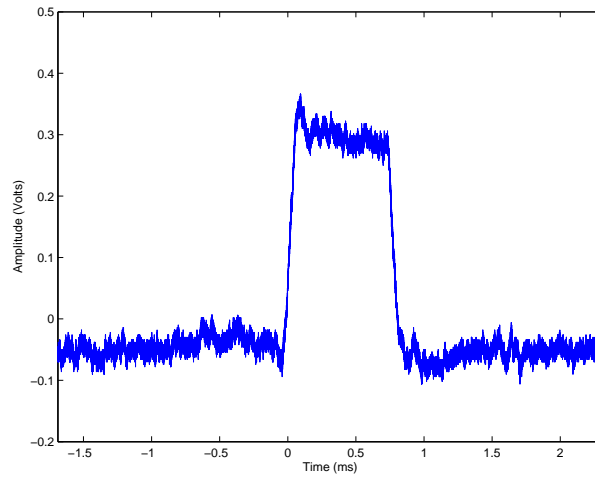
Figure B.17: Lab-Volt Dual Channel Sampler I-Channel RF Output at a 10-GHz Carrier Frequency.



(a) $\tau = 1$ -ns.

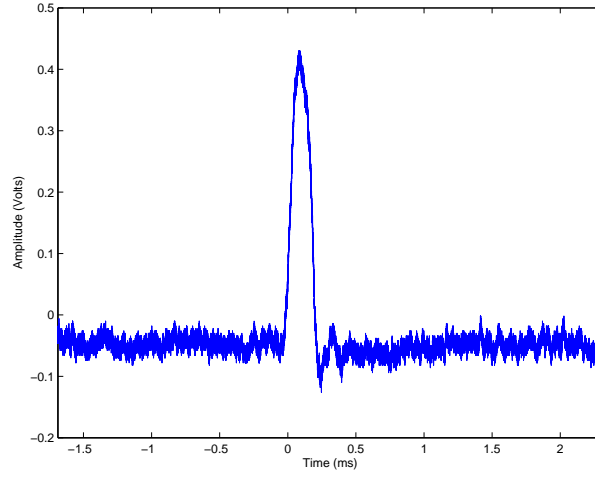


(b) $\tau = 2$ -ns.

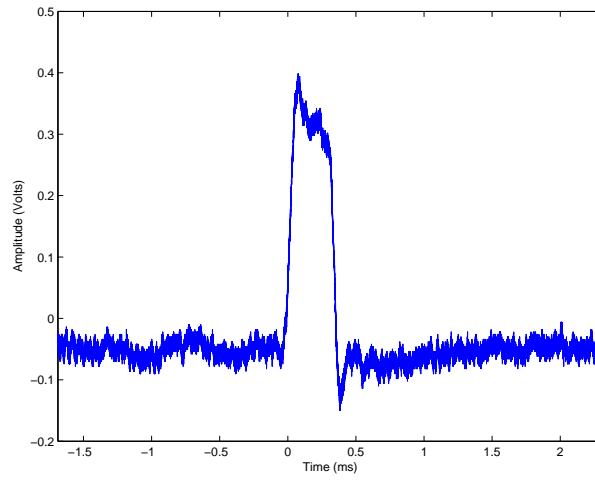


(c) $\tau = 5$ -ns.

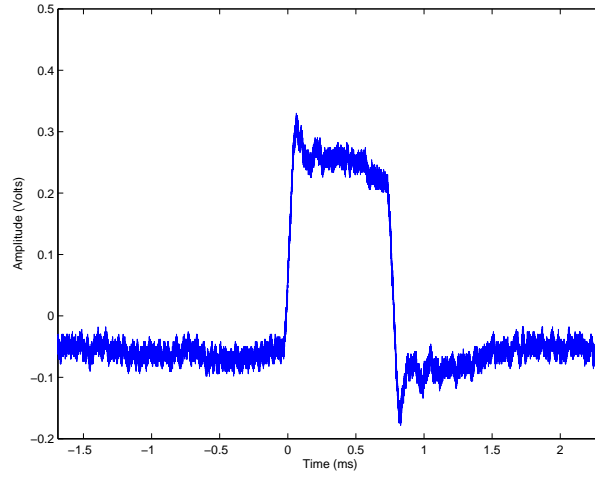
Figure B.18: Dual Channel Sampler Q-Channel at 8-GHz Carrier Frequency.



(a) $\tau = 1\text{-ns}$.

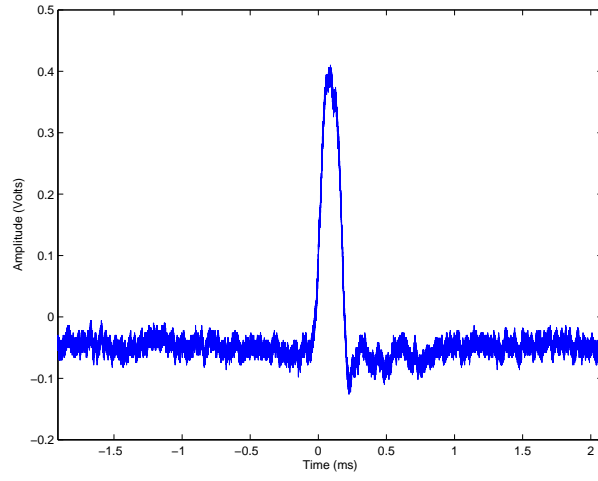


(b) $\tau = 2\text{-ns}$.

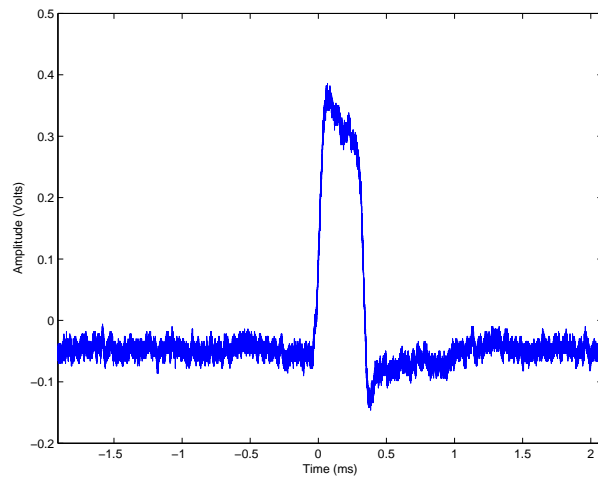


(c) $\tau = 5\text{-ns}$.

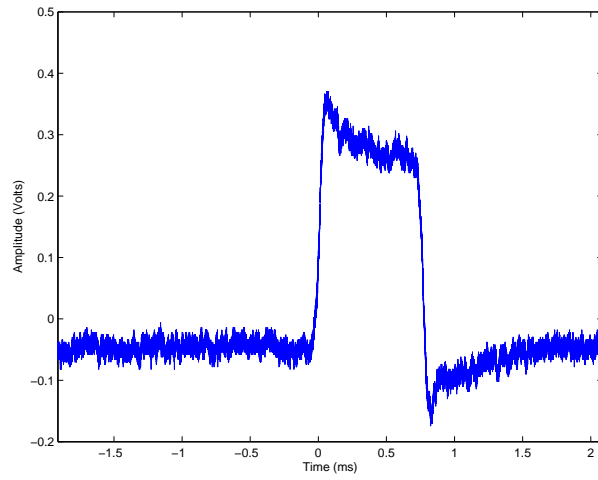
Figure B.19: Dual Channel Sampler Q-Channel at 9.4-GHz Carrier Frequency.



(a) $\tau = 1\text{-ns}$.

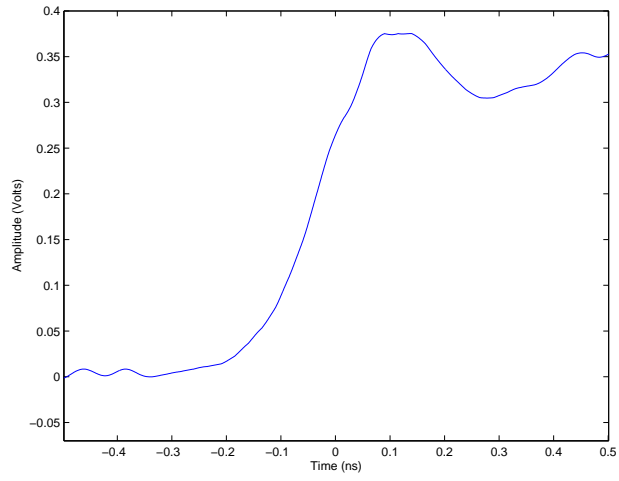


(b) $\tau = 2\text{-ns}$.

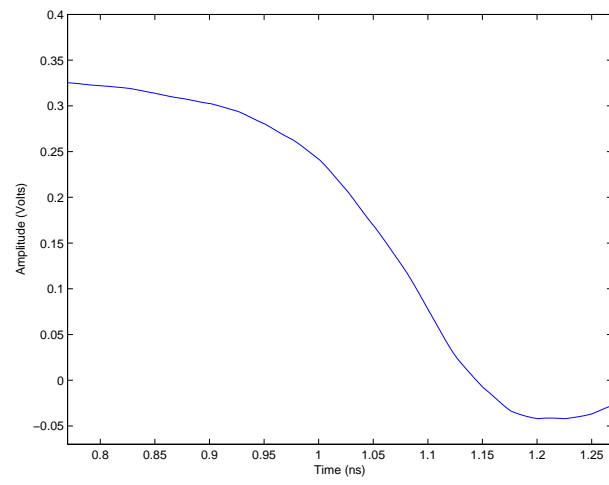


(c) $\tau = 5\text{-ns}$.

Figure B.20: Dual Channel Sampler Q-Channel at 10-GHz Carrier Frequency.

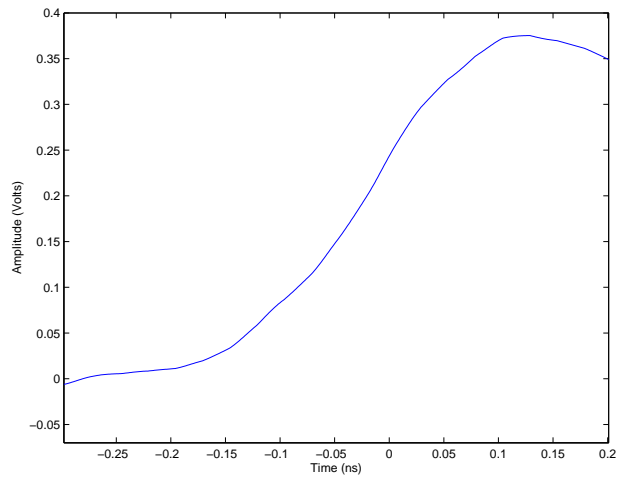


(a) Rise Time.

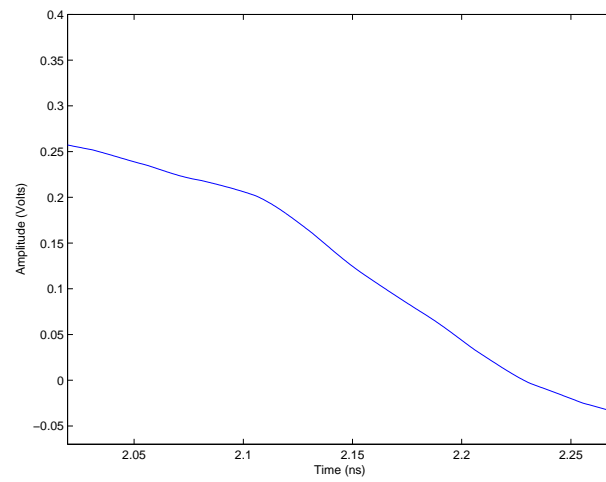


(b) Fall Time.

Figure B.21: Pulse Generator Output at $\tau = 1$ -ns.

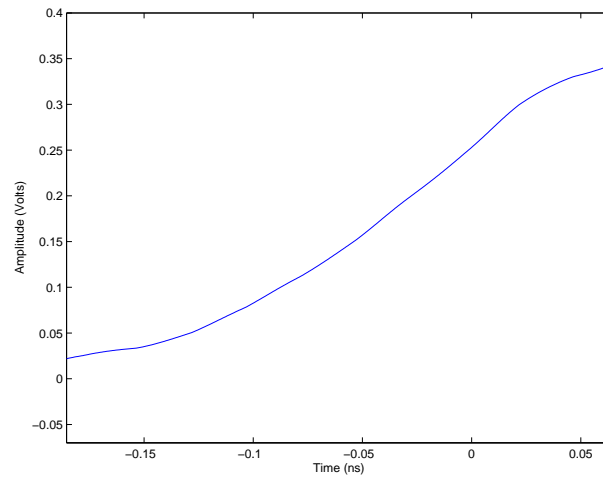


(a) Rise Time.

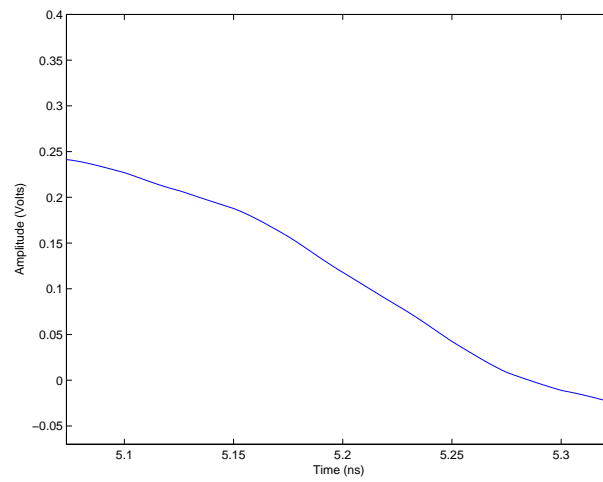


(b) Fall Time.

Figure B.22: Pulse Generator Output at $\tau = 2$ -ns.

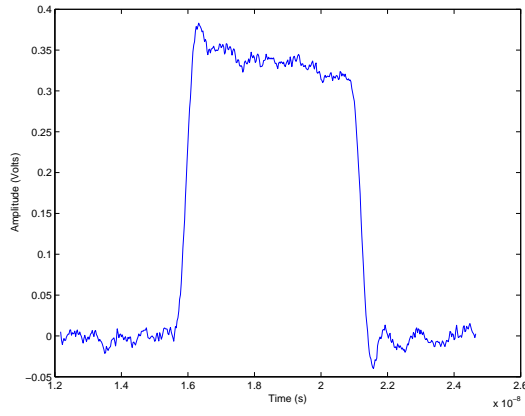


(a) Rise Time.

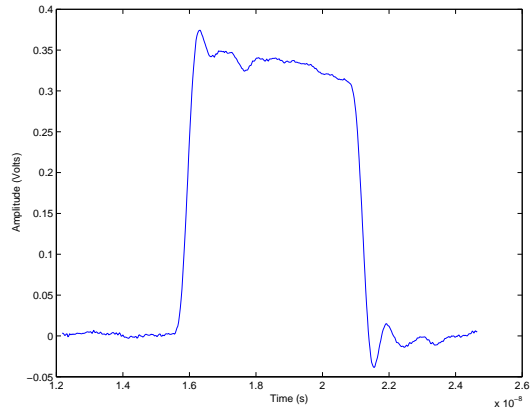


(b) Fall Time.

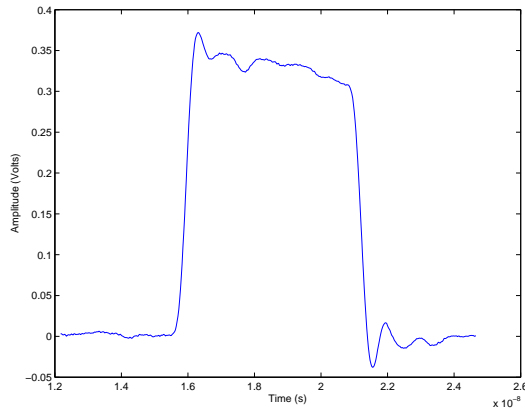
Figure B.23: Pulse Generator Output at $\tau = 5$ -ns.



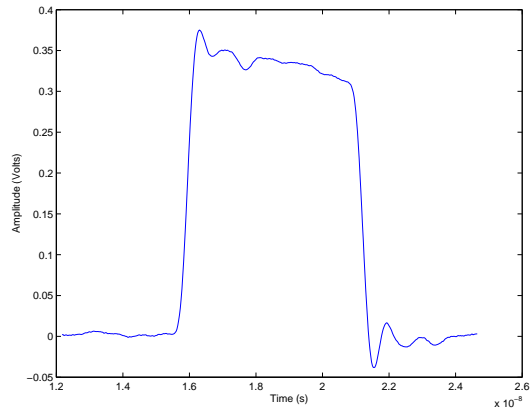
(a) 2 Pulses Integrated.



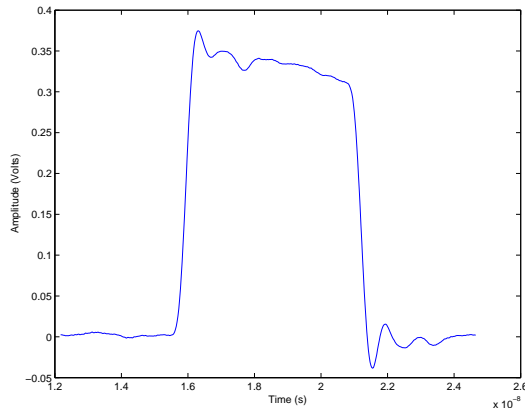
(b) 32 Pulses Integrated.



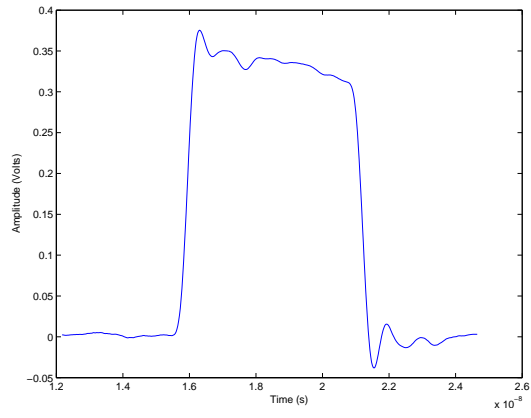
(c) 72 Pulses Integrated.



(d) 256 Pulses Integrated.

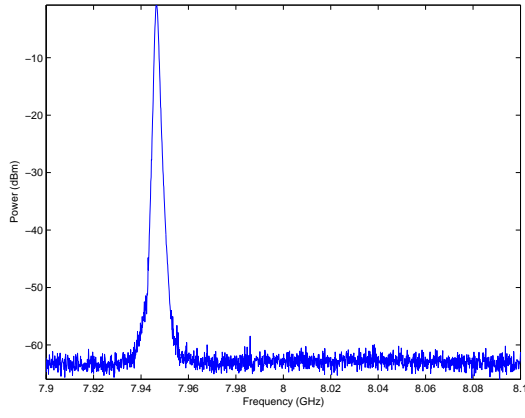


(e) 512 Pulses Integrated.

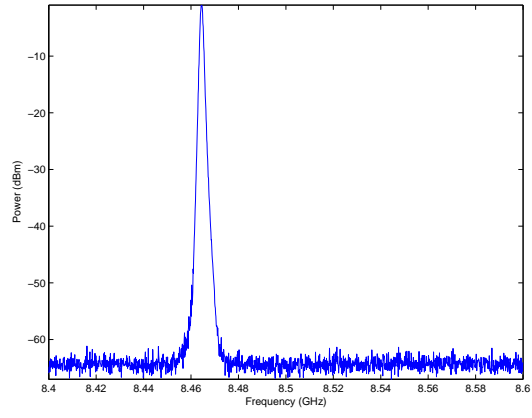


(f) 1,000,000 Pulses Integrated.

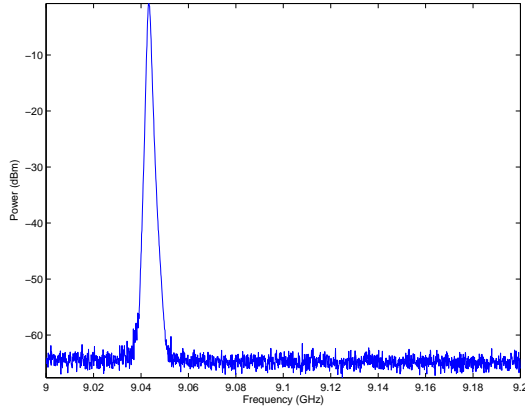
Figure B.24: Pulse Integration at Pulse Generator Output, $\tau = 1\text{-ns}$.



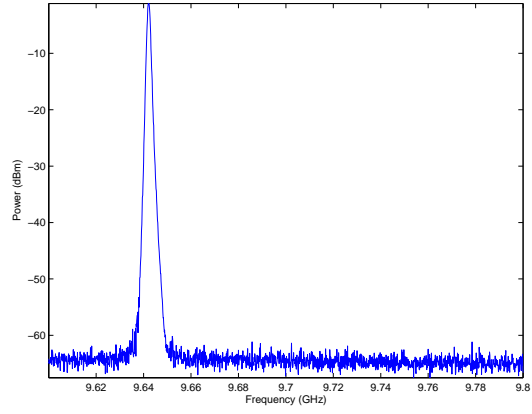
(a) 0% Rotation.



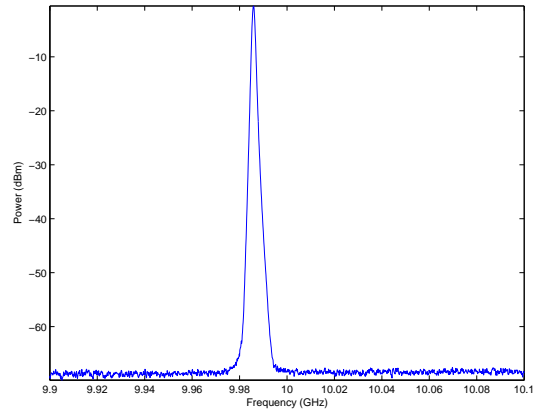
(b) 25% Rotation.



(c) 50% Rotation.

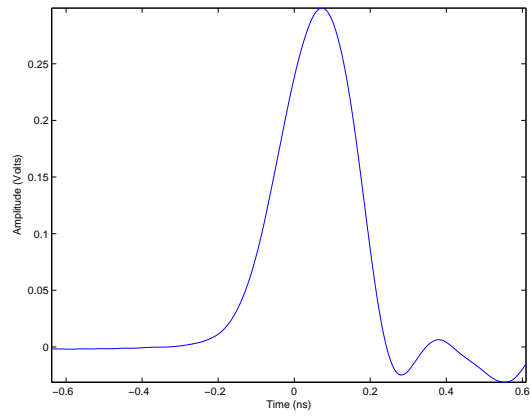


(d) 75% Rotation.

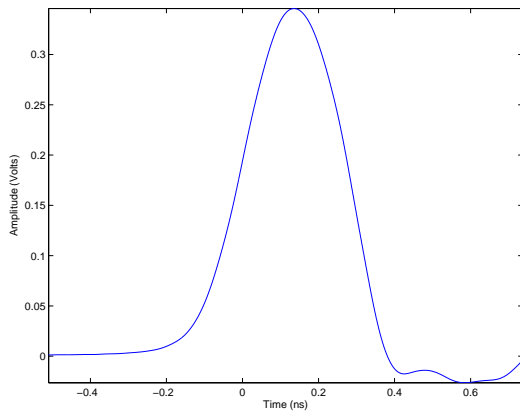


(e) 100% Rotation.

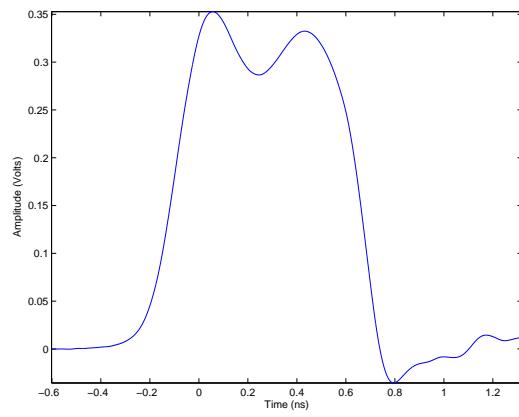
Figure B.25: Carrier Frequency Adjustment Characterization.



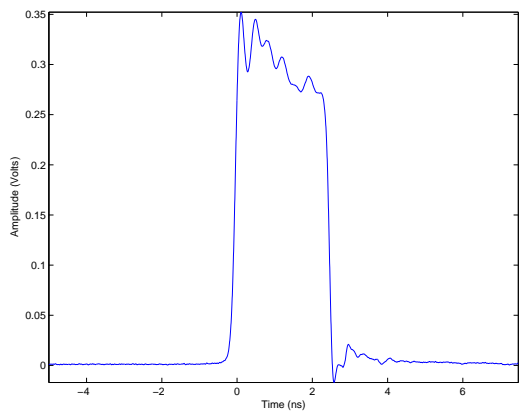
(a) 0% Rotation.



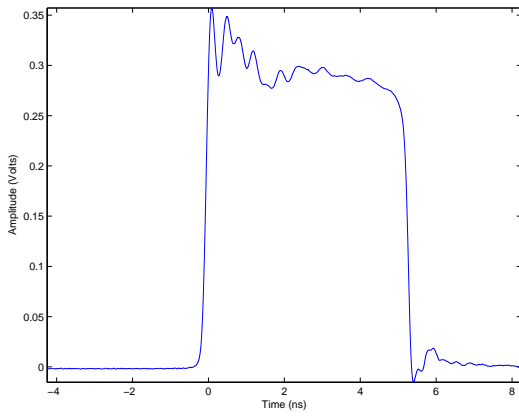
(b) 25% Rotation.



(c) 50% Rotation.

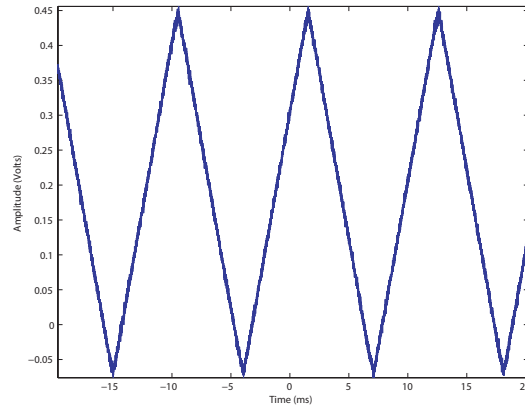


(d) 75% Rotation.

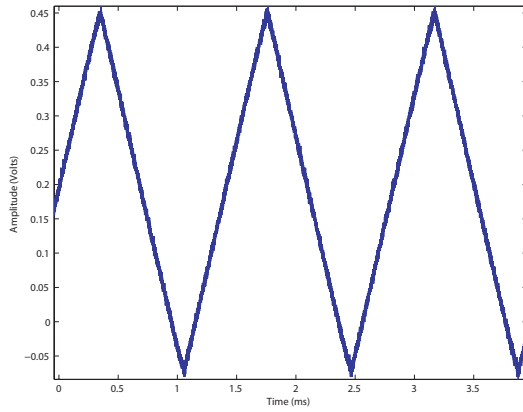


(e) 100% Rotation.

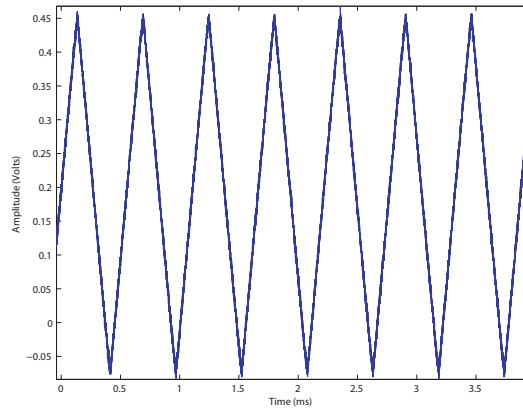
Figure B.26: Pulse Width Adjustment Characterization.



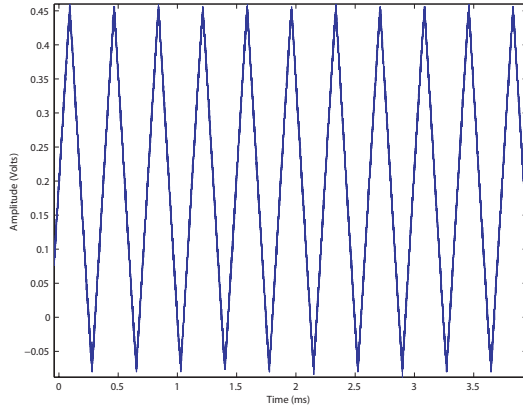
(a) Modulating Frequency: 0% Rotation, Frequency Deviation: 100% Rotation.



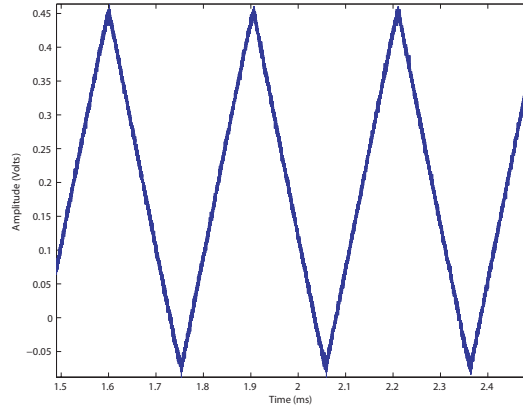
(b) Modulating Frequency: 25% Rotation, Frequency Deviation: 100% Rotation.



(c) Modulating Frequency: 50% Rotation, Frequency Deviation: 100% Rotation.

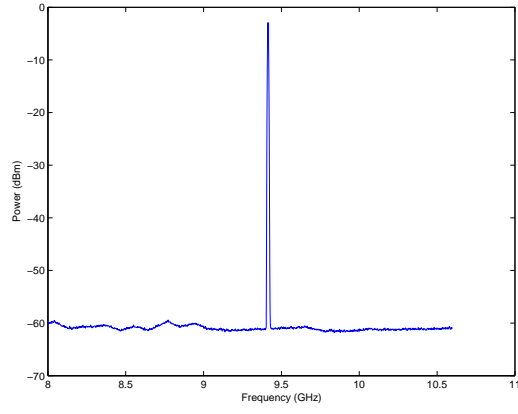


(d) Modulating Frequency: 75% Rotation, Frequency Deviation: 100% Rotation.

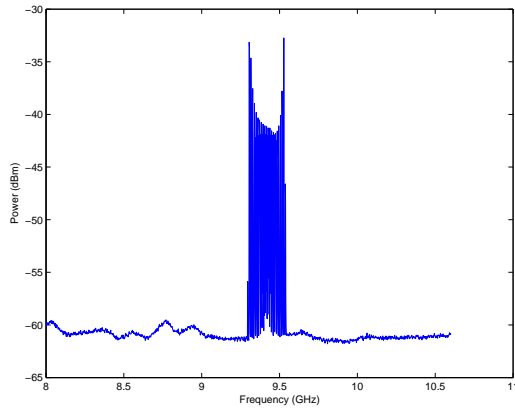


(e) Modulating Frequency: 100% Rotation, Frequency Deviation: 100% Rotation.

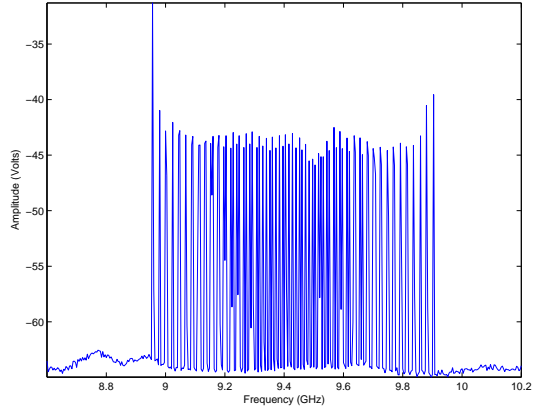
Figure B.27: Modulating Frequency Characterization.



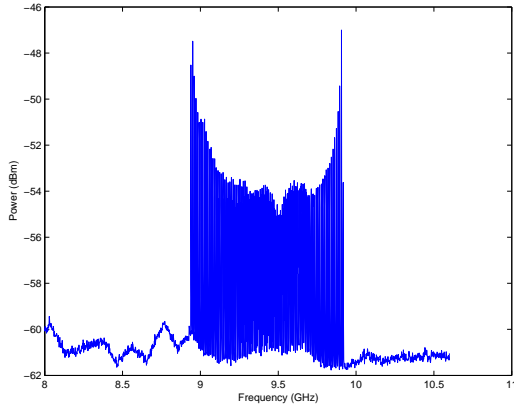
(a) Modulating Frequency: 50% Rotation, Frequency Deviation: 0% Rotation.



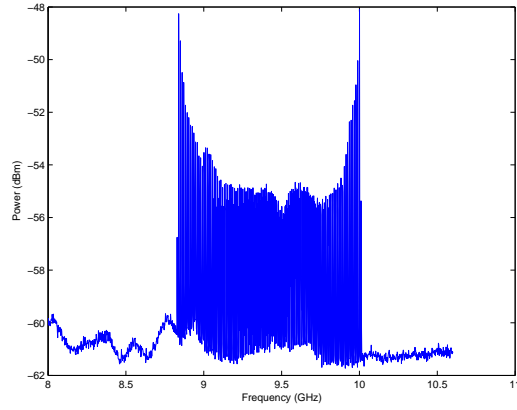
(b) Modulating Frequency: 50% Rotation, Frequency Deviation: 25% Rotation.



(c) Modulating Frequency: 50% Rotation, Frequency Deviation: 50% Rotation.

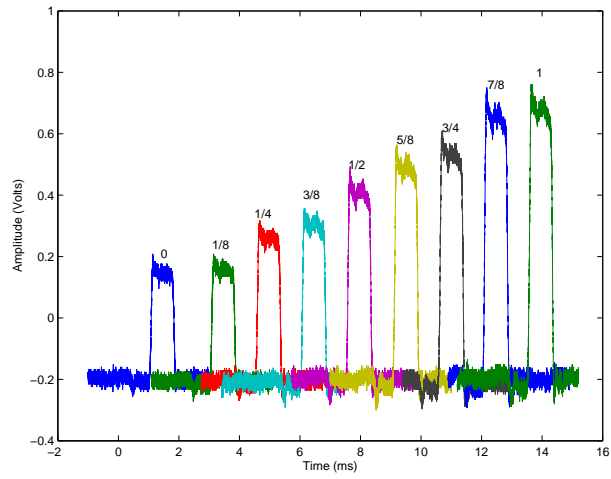


(d) Modulating Frequency: 50% Rotation, Frequency Deviation: 75% Rotation.

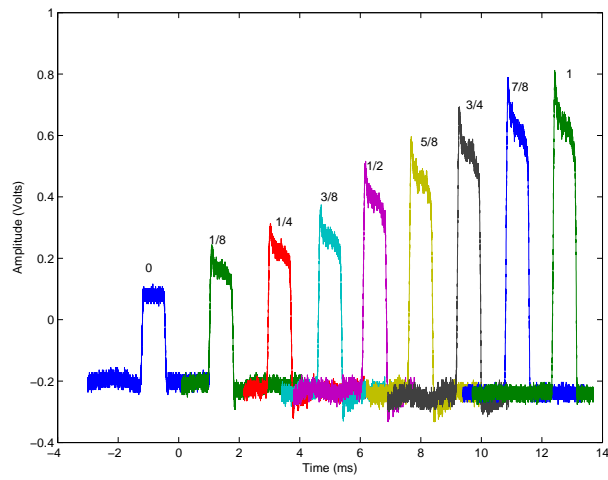


(e) Modulating Frequency: 50% Rotation, Frequency Deviation: 100% Rotation.

Figure B.28: Frequency Deviation Characterization.

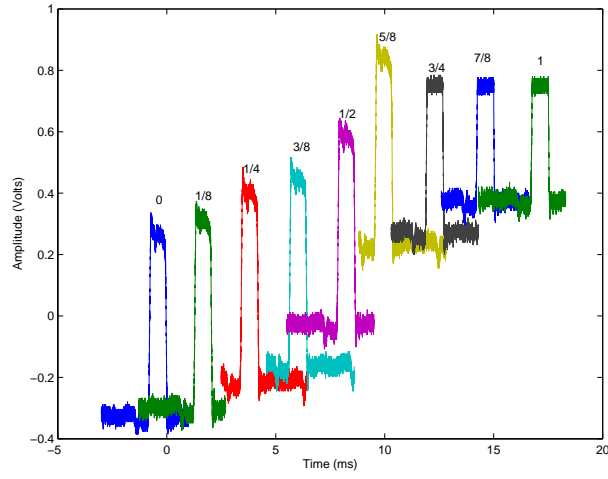


(a) I-Channel Gain Adjustment Output at Various Fractions of Rotation.

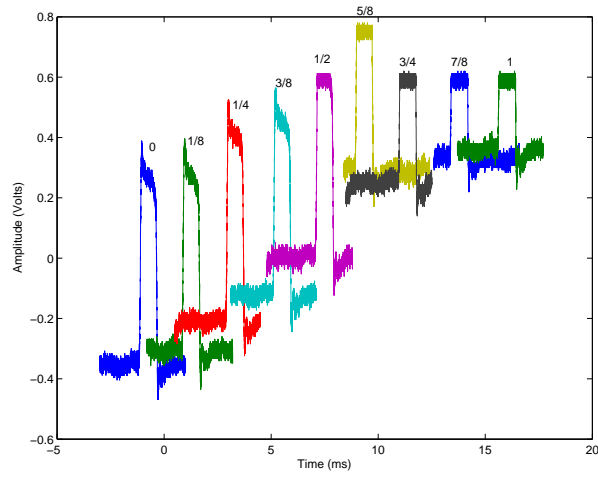


(b) Q-Channel Gain Adjustment Output at Various Fractions of Rotation.

Figure B.29: Dual Channel Sampler Gain Adjustment Characterization.



(a) I-Channel Dual Channel Sampler Output at Various Fractions of Rotation.



(b) Q-Channel Dual Channel Sampler Output at Various Fractions of Rotation.

Figure B.30: Offset Adjustment Characterization.

Bibliography

1. Balanis, Constantine A. *Antenna Theory Analysis and Design*. Wiley-Interscience, 111 River Street, Hoboken, NJ, 3 edition, 2005. ISBN 0-471-66782.
2. Carlos A. Coello Coello, David A. Van Veldhuizen and Gary B. Lamont. *Evolutionary Algorithms for solving Multi-Objective Problems*. Kluwer Academic Publishers, 233 Spring Street, New York, NY 10013, 2002.
3. Clarke, J. (editor). *Advancements in Radar Techniques*. Peter Peregrinus Ltd., 1985.
4. D. DiFilippo, G. Currie, G. Geling. "Simulator for Advanced Fighter RADAR EPM Development". *IEE Proc.-RADAR, Sonar Navig.*, 148(3):139–146, June 2001.
5. Darryl G. Huddleston, John R. Walker Jr., Keith D. Trott. "The Research and Seeker Emulation Radar (RASER)". *IEEE National Radar Conference*, 246–250, March 1994.
6. Devore, Jay L. *Probability and Statistics*. Thomson Brooks/Cole, 2004.
7. Dr. Russell Lefevre, Richard Scatterfield Vaughn Wright Richard DiDomizio, Eric Wilen. "Clutter Emulator for Radar Testing". *IEEE Systems Readiness Technology Conference*, 606–610, 1998.
8. Engelson, Morris. "Reciprocal Spreading Equals Spectrum Analysis Minus Math". *EDN Europe*, 113–116, May 1999.
9. Estep, Gu Zu-Han, Jeff. "LADAR Signature Simulation". *Automatic Object Recognition*, 1700:120–130, April 1992.
10. Fan BangKui, Han YueQiu Zeng YiFang, Mao ErKe. "A Real-Time Radar Video Signal Simulator". *3rd International Conference on Signal Processing*, 2:1101–1105, 1996.
11. the Staff of Lab-Volt (Quebec) Ltd. *Dual Channel Sampler Model 9605 Instruction Manual*. Telecommunications Radar, 1990.
12. the Staff of Lab-Volt (Quebec) Ltd. *Radar Analog MTI Processor Model 9622 Instruction Manual*. Telecommunications Radar, 1990.
13. the Staff of Lab-Volt (Quebec) Ltd. *Radar Antenna Model 9604 Instruction Manual*. Telecommunications Radar, 1990.
14. the Staff of Lab-Volt (Quebec) Ltd. *Radar Receiver Model 9621 Instruction Manual*. Telecommunications Radar, 1990.
15. the Staff of Lab-Volt (Quebec) Ltd. *Radar Transmitter Model 9620 Instruction Manual*. Telecommunications Radar, 1990.

16. Nadav Levanon, Eli Mozeson. *Radar Signals*. Wiley-Interscience, 2004.
17. Packer, R.J. "Computer Modelling of Advanced RADAR Techniques: The Advanced RADAR Simulator".
18. Pozar, David M. *Microwave Engineering*. John Wiley and Sons, Inc, 111 River Street, Hoboken, Ny, 3rd edition, 2005.
19. Seng Hong, Chad Simpson Patrick Marchall, Michael Saville. "Investigation of Genetic Algorithm for Countermeasure Technique Generator". *International Symposium on Signals, Systems, and Electronics (ISSE 2007)*, July 30- Aug 2 2007.
20. I. Skolnik, Merrill (editor). *Introduction to Radar Systems*. McGraw Hill, 3rd edition, 1988.
21. Stimson, Georger W. *Airborne Radar*. SciTech Publishing, Inc, 1998.
22. Stove, A. G. "A Software Simulator for Automotive RADAR". *IEEE Colloquium on Computer Modelling and Simulation of RADAR Systems*, 11/1–11/4, February 1993.
23. Stremmler, Ferrel G. *Introduction to Communication Systems*. Addison Wesley Longman, third edition, 1992.
24. Tektronix, Tektronix, Inc, 14200 SW Karl Braun Drive, P.O. Box 500, Beaverton, OR 97077. *AWG7000 Series Arbitrary Waveform Generators Quick Start User Manual*.
25. Tektronix, Tektronix, Inc, 14200 SW Karl Braun Drive, P.O. Box 500, Beaverton, OR 97077. *TDS6000B and TDS6000C Digital Storage Oscilloscope*.
26. Thomas Back, David B Fogel and Zbigniew Michalewicz (editors). *Evolutionary Computation 1: Basic Algorithms and Operators*. Institute of Physics Publishing, Ltd., The Public Ledger Building, Suite 1035, 150 South Independence Mall West, Philadelphia, PA 19106, 2000.
27. Van Blaricum, G. F. "Tactical Air Surveillance RADAR Netting (TASRAN) Simulator/Emulator". *Technical Reports*, 54, 1981.
28. Wesley D. True, David J. Krile, Kenneth W. Bauer. "Response Surface Methodology Applied to the Radar Range Equation". volume 3 of *IEEE Proceedings of the National Aerospace and Electronics Conference*, 960–966. IEEE, Piscataway, NJ, USA, May 1989.

Vita

Oscar Mayhew was born in Austin, Texas in 1981 and is the middle child among two sisters. After graduating from John B. Connelly High School in 2001, Oscar entered the United States Air Force Academy Preparatory School in Colorado Springs. Oscar proceeded to enter the United States Air Force Academy's class of 2006 where he was an active instructor in the Reconditioning program and received awards for the 2005 Global Engagement Outstanding Cadre Member and the Spring 2006 Outstanding Third Group Flight Commander Award. In May of 2006 Oscar graduated the United States Air Force Academy with a Bachelor of Science Degree in Electrical Engineering and was commissioned as a second lieutenant in the United States Air Force. Oscar entered the Air Force Institute of Technology in August of 2006 and completed the electromagnetics sequence with a focus in RADAR and antennas. Following graduation from the Air Force Institute of Technology, Oscar will attend Euro Nato Joint Jet Pilot Training at Sheppard Air Force Base, Texas.

REPORT DOCUMENTATION PAGE					Form Approved OMB No. 0704-0188	
<p>The public reporting burden for this collection of information is estimated to average 1 hour per response, including the time for reviewing instructions, searching existing data sources, gathering and maintaining the data needed, and completing and reviewing the collection of information. Send comments regarding this burden estimate or any other aspect of this collection of information, including suggestions for reducing this burden to Department of Defense, Washington Headquarters Services, Directorate for Information Operations and Reports (0704-0188), 1215 Jefferson Davis Highway, Suite 1204, Arlington, VA 22202-4302. Respondents should be aware that notwithstanding any other provision of law, no person shall be subject to any penalty for failing to comply with a collection of information if it does not display a currently valid OMB control number. PLEASE DO NOT RETURN YOUR FORM TO THE ABOVE ADDRESS.</p>						
1. REPORT DATE (DD-MM-YYYY)		2. REPORT TYPE		3. DATES COVERED (From — To)		
6-09-2007		Master's Thesis		Aug 2006 — Sept 2007		
4. TITLE AND SUBTITLE Radar System Characterization Extended to Hardware in the Loop Simulation for the Lab-Volt TM Training System				5a. CONTRACT NUMBER		
				5b. GRANT NUMBER		
				5c. PROGRAM ELEMENT NUMBER		
6. AUTHOR(S) Oscar C. Mayhew, 2dLt, USAF				5d. PROJECT NUMBER		
				5e. TASK NUMBER		
				5f. WORK UNIT NUMBER		
7. PERFORMING ORGANIZATION NAME(S) AND ADDRESS(ES) Air Force Institute of Technology Graduate School of Engineering and Management 2950 Hobson Way WPAFB OH 45433-7765				8. PERFORMING ORGANIZATION REPORT NUMBER AFIT/GE/ENG/07-29		
9. SPONSORING / MONITORING AGENCY NAME(S) AND ADDRESS(ES) Dr. Seng Hong AFRL/SNRA Bldg 620 2241 Avionics Circle WPAFB, 45433-7333 DSN 872-8876 x-3353				10. SPONSOR/MONITOR'S ACRONYM(S)		
				11. SPONSOR/MONITOR'S REPORT NUMBER(S)		
12. DISTRIBUTION / AVAILABILITY STATEMENT APPROVAL FOR PUBLIC RELEASE; DISTRIBUTION IS UNLIMITED						
13. SUPPLEMENTARY NOTES						
14. ABSTRACT Modeling RADAR signals in software allows the testing of potential electronic counter measures and electronic counter counter measures without the associated RADAR hardware and test facilities. Performing a characterization process on a real world RADAR system reveals all imperfections within the system. The Lab-Volt TM RADAR system served as the characterized real world RADAR system. The characterization process consisted of measurements at selected front panel locations on the Lab-Volt TM transmitter module, antenna pedestal, receiver module, and dual channel sampler module. Due to the overwhelming influence of antenna parameters on a received signal, the characterization process also attempted to derive an antenna transfer function that described how the antenna filters a signal that is passed through it. The characterization process also determined the manner in which different adjustments influenced the signal. A MatLab simulation modeled the Lab-Volt TM system operating under ideal conditions. Comparing measurements from the characterization process and the MatLab simulation placed numerical values on the imperfections in the Lab-Volt TM system. Finally, integration of the Lab-Volt TM system explored an elementary hardware-in-the-loop configuration.						
15. SUBJECT TERMS RADAR characterization, HILS, RADAR simulation, antenna characterization, RADAR						
16. SECURITY CLASSIFICATION OF:			17. LIMITATION OF ABSTRACT	18. NUMBER OF PAGES	19a. NAME OF RESPONSIBLE PERSON	
a. REPORT	b. ABSTRACT	c. THIS PAGE			Michael A. Saville, Maj, USAF (ENG)	
U	U	U	UU	184	19b. TELEPHONE NUMBER (include area code) (937) 255-3636, ext 4719	